UCRL-18143
Cy. 2

RECEIVED
LIBRARY AND
DOCUMENTS SEC

TWO-WEEK LOAN COPY

This is a Library Circulating Copy
which may be borrowed for two weeks.
For a personal retention copy, call
Tech. Info. Division, Ext. 5545

MEASUREMENT OF THE MUON POLARIZATION VECTOR IN $K^+ \to \pi^0 + \mu^+ + \nu$

David Cutts
(Ph.D. Thesis)

August 1968

UCRL-18143
Cy. 2

E,P

LAWRENCE RADIATION LABORATORY
UNIVERSITY of CALIFORNIA BERKELEY

DISCLAIMER

This document was prepared as an account of work sponsored by the United States Government. While this document is believed to contain correct information, neither the United States Government nor any agency thereof, nor the Regents of the University of California, nor any of their employees, makes any warranty, express or implied, or assumes any legal responsibility for the accuracy, completeness, or usefulness of any information, apparatus, product, or process disclosed, or represents that its use would not infringe privately owned rights. Reference herein to any specific commercial product, process, or service by its trade name, trademark, manufacturer, or otherwise, does not necessarily constitute or imply its endorsement, recommendation, or favoring by the United States Government or any agency thereof, or the Regents of the University of California. The views and opinions of authors expressed herein do not necessarily state or reflect those of the United States Government or any agency thereof or the Regents of the University of California.

UCRL-18143

UNIVERSITY OF CALIFORNIA

Lawrence Radiation Laboratory
Berkeley, California

AEC Contract No. W-7405-eng-48

MEASUREMENT OF THE MUON POLARIZATION VECTOR IN $K^+ \rightarrow \pi^0 + \mu^+ + \nu$

David Cutts
(Ph.D. Thesis)

August 1968

MEASUREMENT OF THE MUON POLARIZATION VECTOR IN $K^+ \rightarrow \pi^o + \mu^+ + \nu$

Table of Contents

Abstract v

I. Introduction 1

II. Method 6

III. Apparatus

A. Beam 13

B. Scintillation Counters and Spark Chambers 16

C. Experimental Technique 22

IV. Analysis Procedure

A. Selection of Events 27

B. Reconstruction of the $K_{\mu 3}$ Kinematics 31

C. Muon Polarization Analysis

1. Measurement of Polarization Components in K^+ Rest Frame 35

2. Determination of ξ 38

V. Known Sources of Error

A. Uncertainties in Analysis of $K_{\mu 3}$ Events 41

1. Study of $K_{\mu 2}$ Events 47

2. Study of $K_{\pi 2}$ Events 52

B. Presence of Background Events in the $K_{\mu 3}$ Data

1. Summary of Background Contributions 55

2. Study of $K_{\mu 3}$ events with Prompt μ-e Decay 57

3. Calculation of Background Contributions

$K_{\pi 2}$ Events 60

a) with π^+ decay-in-flight 61

b) with π^+-nuclear interaction. 68

τ' Background Calculation 71

$K_{\pi\pi\gamma}$ Background Calculation. 78

K_{e3} Background Calculation 83

VI. Results

A. Study of $K^+_{\mu 3}$ Decay 87

B. Measurement of K^+ Mean Life 100

VII. Discussion 104

Acknowledgments 111

Appendices

A. Solution of $K_{\mu 3}$ Kinematics 112

B. Calculation of Likelihood Normalizations. 115

C. Comparison of Prompt/Delayed $K_{\mu 3}$ Data 120

D. Depolarization by a Magnetic Field. 122

References 125

MEASUREMENT OF THE MUON POLARIZATION VECTOR IN $K^+ \to \pi^o + \mu^+ + \nu$

David Cutts

Lawrence Radiation Laboratory
University of California
Berkeley, California

September 1968

ABSTRACT

We have determined the parameter ξ in the decay $K^+ \to \pi^o + \mu^+ + \nu$ ($K_{\mu 3}$) from a muon polarization measurement carried out with spark chambers at the Bevatron. The parameter ξ, which may be complex and energy dependent, describes phenomenologically the manner in which the basic weak interaction responsible for the $K^+ \to \pi^o + \mu^+ + \nu$ decay is modified by the strong interactions of the K and π mesons. Because ξ is determined by the structure of the K and π mesons, it is frequently called a form factor.

The matrix element for $K_{\mu 3}$ decay is

$$\frac{G}{\sqrt{2}} \langle \pi^o \mu^+ \nu | \; J_\lambda^{\ell\dagger} J_\lambda^{h,\Delta s \neq 0} | K^+ \rangle$$

where $G/\sqrt{2}$ is the weak interaction coupling constant, $J_\lambda^{h,\Delta s \neq 0}$ the strangeness-changing hadronic current, and J_λ^ℓ the leptonic current. Summation over the index λ is assumed ($\lambda = 1,2,3,4$). The specific form of J_λ^ℓ is well known from beta decay and muon decay; the form of $J_\lambda^{h,\Delta s \neq 0}$ is unknown. We can, however, describe it phenomenologically using the fact that the whole matrix element must be a scalar. Since J_λ^ℓ has only vector and axial-vector terms, only the vector part of $J_\lambda^{h,\Delta s \neq 0}$ can contribute to the $K_{\mu 3}$ matrix element. (The axial-vector

term of $J_\lambda^{h,\Delta s\neq 0}$ does not contribute as the K and π have the same intrinsic parity.) These assumptions restrict its form to:

$$\langle \pi^o | J_\lambda^{h,\Delta s\neq 0} | K^+ \rangle = f_+(q^2)(p_K+p_\pi)_\lambda + f_-(q^2)(p_K-p_\pi)_\lambda .$$

Here p_K and p_π are the K and π four-momenta. $f_+(q^2)$ and $f_-(q^2)$ are unknown parameters which may be complex and dependent on the four-momentum transfer between the K and the π,

$$q^2 = (p_K - p_\pi)^2 .$$

In defining the parameters $f_+(q^2)$ and $f_-(q^2)$ we have written a general vector expression; there are two independent four-vectors in the K-π system, so there are two independent vector terms. The specific form of the expression is conventional. The direction of the muon polarization vector in $K_{\mu 3}$ decay is directly related to the value of the parameter $\xi(q^2)$, defined as the ratio of $f_-(q^2)/f_+(q^2)$:

$$\xi(q^2) \equiv f_-(q^2)/f_+(q^2) .$$

We have measured the muon polarization vector in $K_{\mu 3}$ decay and thereby determined ξ.

In the experiment K^+ mesons from a 500 MeV/c separated beam were brought to rest in a carbon stopper surrounded by lead-plate spark chambers to detect the two photons from the π^o. Muons were stopped in a magnetic-shielded aluminum-plate spark chamber. The data consist of 3133 events with μ-e decays and complete kinematics for $K^+_{\mu 3}$. From the angular distribution of the decay electrons we determined the vector giving the polarization and related this measurement to a determination of the parameter ξ. The data are statistically consistent with the assumption that ξ does not depend on momentum transfer.

Assuming ξ constant, our result is $\xi = (-0.9 \begin{smallmatrix}+0.5\\-0.4\end{smallmatrix}) + i(-0.3 \pm 0.5)$. This result is compatible with $\mathrm{Im}\xi = 0$ as would be required by time-reversal invariance. If we analyze the data imposing the constraint that ξ be real we find $\xi = -0.95 \pm 0.3$. The muon polarization along the direction predicted by these values for ξ is $+0.9 \pm 0.1$, in agreement with the value +1 required by theory. In a calibration experiment we find the muon longitudinal polarization in the decay $K^+ \rightarrow \mu^+ + \nu$ to be -1.0 ± 0.1. This result is evidence of the adequacy of our technique, as the polarization is known to be -1.

I. INTRODUCTION

The current phenomenological theory of weak interactions successfully describes μ-decay, a purely-leptonic process, as well as neutron β-decay and other strangeness-conserving semi-leptonic processes. We wish to test this description of weak interactions by studying strangeness-violating semi-leptonic processes. The most readily available examples of such processes, experimentally, are the $K_{\mu 3}$ and K_{e3} decay modes of the K meson:

$$K \rightarrow \pi + \mu + \nu \quad (K_{\mu 3})$$

and

$$K \rightarrow \pi + e + \nu \quad (K_{e3}).$$

This work is a study of the $K_{\mu 3}$ decay.

The basic idea of weak interaction theory is that the Hamiltonian for weak interactions is the product of a current with itself:

$$H_W = \frac{G}{\sqrt{2}} J_\lambda^\dagger J_\lambda \ .$$

In this equation $G/\sqrt{2}$ is the weak interaction coupling constant. The current J_λ is a four-vector, with $\lambda = 1, 2, 3, 4$; in the product $J_\lambda^\dagger J_\lambda$, the summation over the index λ is assumed. The current J_λ is the sum of a leptonic current, J_λ^ℓ, a strangeness-conserving hadronic current, $J_\lambda^{h,\Delta s=0}$, and a strangeness-violating hadronic current, $J_\lambda^{h,\Delta s\neq 0}$:

$$J_\lambda = J_\lambda^\ell + J_\lambda^{h,\Delta s=0} + J_\lambda^{h,\Delta s\neq 0}.$$

Separate terms in the product $J_\lambda^\dagger J_\lambda$ describe the different weak interaction processes. In this theory the leptonic current is a

combination of vector and axial-vector terms; specifically,

$$J_\lambda^\ell = \bar{\psi}_{\nu_\mu} \gamma_\lambda (1+i\gamma_5)\psi_\mu + \bar{\psi}_{\nu_e} \gamma_\lambda (1+i\gamma_5)\psi_e \qquad \text{(I-1)}$$

In Eq. I-1, ψ_μ and ψ_e are the muon and electron fields, respectively. $\bar{\psi}_{\nu_\mu}$ and $\bar{\psi}_{\nu_e}$ are related to the muon-neutrino and electron-neutrino fields, ψ_{ν_μ} and ψ_{ν_e}, by

$$\bar{\psi} = \psi^\dagger \gamma_4 \ .$$

The matrices γ_λ ($\lambda = 1,2,3,4$) are the standard 4×4 gamma-matrices; our convention is

$$\gamma_i = \begin{pmatrix} 0 & -\sigma_i \\ \sigma_i & 0 \end{pmatrix} \ , \qquad i = 1,2,3$$

$$\gamma_4 = \begin{pmatrix} 0 & 1 \\ 1 & 0 \end{pmatrix} \ .$$

Here $\sigma_i (i = 1,2,3)$ are the 2×2 Pauli matrices. The 4×4 matrix γ_5 is defined by $\gamma_5 \equiv \gamma_1\gamma_2\gamma_3\gamma_4$.

Experimental studies of both μ-decay, for which

$$H_w = \frac{G}{\sqrt{2}} J_\lambda^{\ell\dagger} J_\lambda^\ell \ ,$$

and semi-leptonic, strangeness-conserving processes with

$$H_w = \frac{G}{\sqrt{2}} J_\lambda^{\ell\dagger} J_\lambda^{h,\Delta s=0} \ ,$$

have established the specific form of the leptonic current as that given

by Eq. I-1. In the context of the present theory the same leptonic current J_λ^ℓ contributes to all leptonic weak interactions. We describe the strangeness-violating semi-leptonic processes by

$$H_w = \frac{G}{\sqrt{2}} J_\lambda^{\ell\dagger} J_\lambda^{h,\Delta s \neq 0}$$

where the current J_λ^ℓ is given by Eq. I-1.

This dissertation describes an experimental study of the $K_{\mu 3}^+$ decay, $K^+ \to \pi^0 + \mu^+ + \nu$. The Feynman diagram for $K_{\mu 3}^+$ is:

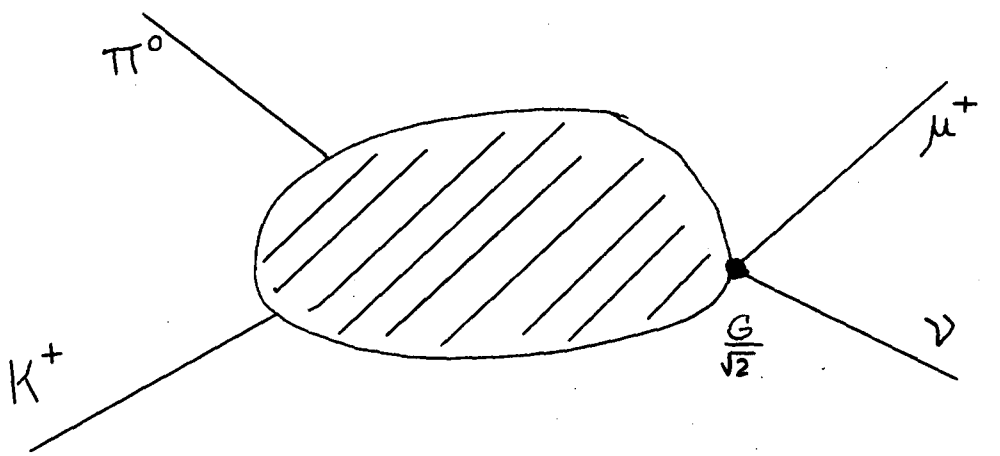

We describe the lepton vertex by the current J_λ^ℓ, with the weak coupling constant $G/\sqrt{2}$; the remainder of the diagram is unknown. We describe phenomenologically the contribution of the K^+ and the π^0 to the $K_{\mu 3}$ decay Hamiltonian with form factors, parameters to be experimentally measured. Since the Hamiltonian must be an invariant, the vector and axial-vector structure of the leptonic current J_λ^ℓ restricts the current $J_\lambda^{h,\Delta s \neq 0}$ to vector and axial-vector terms. For $K_{\mu 3}$ decay only vector terms are present, as the K and π have the same intrinsic parity. In the K-π system there are two independent four-vectors, the π and K four-momenta; we write, phenomenologically,

$$\langle\pi|J_\lambda^{h,\Delta s\neq 0}|K\rangle = f_+(q^2)(p_K + p_\pi)_\lambda + f_-(q^2)(p_K - p_\pi)_\lambda \ . \qquad \text{(I-2)}$$

Here f_+, f_- are form factors; and p_K, p_π are the K and π four-momenta. q^2 is the square of the four-momentum transfer between the K and the π:

$$q^2 = (p_K - p_\pi)^2 = (p_\mu + p_\nu)^2$$

with p_μ, p_ν the μ and ν four-momenta. The specific form of Eq. I-2 is conventional. The current-current formalism excludes any dependence of the form factors on the remaining scalar, $r^2 \equiv (p_\mu - p_\nu)^2$.

Assuming a current-current interaction, and using the currents given by Eqs. I-1 and I-2, the matrix element for $K_{\mu 3}$ decay becomes

$$\frac{G}{\sqrt{2}} f_+(q^2)[(p_K + p_\pi)_\lambda + \xi(q^2)(p_K - p_\pi)_\lambda]\cdot[\bar{U}_\mu \gamma_\lambda(1+i\gamma_5)U_{\nu_\mu}] \ , \qquad \text{(I-3)}$$

where U_μ and U_ν are the Dirac spinors for the fields ψ_μ and ψ_ν, respectively. We define the parameter $\xi(q^2)$ as the ratio of the form factors:

$$\xi(q^2) \equiv \frac{f_-(q^2)}{f_+(q^2)} \ .$$

In this study of the $K^+_{\mu 3}$ decay we measure directly the parameter $\xi(q^2)$. With this measurement we test the adequacy of the basic formalism to describe this strangeness-changing weak process. Additionally we investigate the q^2-dependence of this parameter; the range of momentum transfer is large

$$M_\mu^2 < q^2 < (M_K - M_\pi)^2$$

relative to that available in purely leptonic or other semi-leptonic decays, such as muon decay or neutron decay. The principle of time

reversal can be tested by measuring the phase of ξ. Time reversal invariance requires the form factors $f_+(q^2)$ and $f_-(q^2)$ to be relatively real, and consequently the phase of ξ to be 0° or 180°, for all values of q^2. (Final state interactions, which could introduce an imaginary part to ξ, have been shown to be negligible.[1]) By comparing this measurement of ξ in $K^+_{\mu 3}$ decay with the measurements of ξ in $K^o_{\mu 3}$ decay we can test the $\Delta I = 1/2$ rule, which requires ξ to be identical for both modes. The principle of universality of the muon and the electron requires that the form factors be the same for $K_{\mu 3}$ and K_{e3} decays. Our determination of ξ is independent of μ-e universality. To test this principle we can compare our measurement of ξ with the results for ξ of experiments which assume μ-e universality.

II. METHOD

In this experiment we determine the parameter $\xi(q^2)$ by measuring the muon polarization for completely reconstructed $K_{\mu 3}$ events. As noted by MacDowell[2] and by Werle,[3] the two component theory of the neutrino requires that for a specific kinematic configuration the muon be completely polarized in some direction. With the lepton current given by Eq. I-1, the neutrino in a given $K^+_{\mu 3}$ decay is completely left-handed (has helicity -1); since the π and K have zero spin, the μ, for the given decay, will itself be fully polarized. In a theoretical paper Cabibbo and Maksymowicz[4] observed that the direction of the muon polarization vector for specified kinematics was a sensitive function of the parameter $\xi(q^2)$. They suggested the experiment to measure the muon polarization in completely reconstructed $K_{\mu 3}$ events, and thus directly measure ξ. With the matrix element in $K_{\mu 3}$ decay given by Eq. I-3, Cabibbo and Maksymowicz derived the relation between $\xi(q^2)$ and the vector direction of the muon polarization:

$$\vec{P} = \frac{\vec{A}}{|\vec{A}|} \qquad \text{(II-1)}$$

where, in the K^+ rest frame,

$$\vec{A} = a_1(\xi)p_\mu - a_2(\xi)\left\{\frac{\vec{p}_\mu}{m_\mu}\left[(m_K - E_\pi) + (\vec{p}_\pi\cdot\vec{p}_\mu)\frac{(E_\mu - m_\mu)}{|\vec{p}_\mu|^2}\right] + \vec{p}_\pi\right\}$$

$$+ m_K(\vec{p}_\pi \times \vec{p}_\mu)\mathrm{Im}\ \xi(q^2). \qquad \text{(II-2)}$$

Here

$$a_1(\xi) = 2\frac{m_K^2}{m_\mu}[E_\nu + (E_\pi^{max} - E_\pi)\ \mathrm{Re}b(q^2)] \qquad \text{(II-3)}$$

$$a_2(\xi) = m_K^{\ 2} + 2m_K E_\mu \mathrm{Re}b(q^2) + m_\mu^2 |b(q^2)|^2 \qquad \text{(II-4)}$$

and

$$b(q^2) = \tfrac{1}{2}[\xi(q^2) - 1]$$

$$E_\pi^{max} = \frac{m_K^{\ 2} + m_\pi^{\ 2} - m_\mu^{\ 2}}{2m_K}$$

In these expressions $\vec{p}_\mu$ and $\vec{p}_\pi$ are the μ and π momenta; and E_μ, E_π, E_ν are the energies of the μ, π and ν in the K^+ rest system. m_K, m_π, and m_μ are the K^+, π^o, and μ^+ rest masses. For specified kinematics of the $K_{\mu 3}$ decay the vector muon polarization direction, given by Eq. II-1, is a function only of the parameter $\xi(q^2)$.

In our experiment we determined the complete kinematics for $K_{\mu 3}$ decays from K^+ mesons at rest. For each decay we defined a coordinate system relevant to that decay, a system to which we referred our measurement of the vector direction of the muon polarization. From the calculated kinematics we constructed for each $K_{\mu 3}$ event three orthogonal axes, longitudinal, transverse, and perpendicular, given by:

$$\hat{\epsilon}_L = \vec{p}_\mu / |\vec{p}_\mu|$$

$$\hat{\epsilon}_T = \frac{\vec{p}_\pi \times \vec{p}_\mu}{|\vec{p}_\pi \times \vec{p}_\mu|} \qquad \text{(II-5)}$$

$$\hat{\epsilon}_\perp = \frac{\vec{p}_\mu}{|\vec{p}_\mu|} \times \frac{\vec{p}_\pi \times \vec{p}_\mu}{|\vec{p}_\pi \times \vec{p}_\mu|}$$

In this coordinate system, the muon polarization direction is given by Eq. II-1, which becomes

$$\vec{P} = (A_L \hat{\epsilon}_L + A_T \hat{\epsilon}_T + A_\perp \hat{\epsilon}_\perp)/|\vec{A}| \qquad \text{(II-6)}$$

where

$$A_L = a_1(\xi)|\vec{p}_\mu| - \frac{a_2(\xi)|\vec{p}_\mu|}{m_\mu}\left[m_K - E_\pi + \frac{|\vec{p}_\pi|}{|\vec{p}_\mu|}(E_\mu - m_\mu)\cos\theta_{\pi\mu}\right]$$

$$- a_2(\xi)|\vec{p}_\pi| \cos\theta_{\pi\mu} \qquad \text{(II-7)}$$

$$A_T = |\vec{p}_\pi||\vec{p}_\mu| m_K \sin\theta_{\pi\mu} \operatorname{Im}\xi(q^2) \qquad \text{(II-8)}$$

$$A_\perp = -a_2(\xi)|\vec{p}_\pi| \sin\theta_{\pi\mu} \qquad \text{(II-9)}$$

The functions $a_1(\xi)$ and $a_2(\xi)$ are given by Eqs. II-3 and II-4. The principle of time reversal invariance requires that ξ be real and, consequently, that the component of muon polarization transverse to the decay plane be zero, as shown by Eq. II-8. The transverse polarization is proportional to a quantity like $\vec{\sigma}_\mu \cdot (\vec{p}_\pi \times \vec{p}_\mu)$ which is odd under the operation of time reversal; so that for invariance this term must vanish.

Figure 1 illustrates the coordinate system which we constructed for each $K_{\mu 3}$ event. The momenta $\vec{p}_\mu$ and $\vec{p}_\pi$ define the plane of the decay; in this plane we defined the axis $\hat{\epsilon}_L$ along $\vec{p}_\mu$, and the axis $\hat{\epsilon}_\perp$ orthogonal to $\vec{p}_\mu$ and towards $\vec{p}_\pi$. We constructed also the axis $\hat{\epsilon}_T$, transverse to the $K_{\mu 3}$ decay plane in the sense $\vec{p}_\pi \times \vec{p}_\mu$. In Fig. 1 we have drawn for illustration a polarization vector $\vec{\sigma}_\mu$ and the components $(\sigma_\mu)_L$, $(\sigma_\mu)_T$, $(\sigma_\mu)_\perp$ in this coordinate system (Eq. II-5).

Figure 2 shows the muon polarization direction at various positions in the $K_{\mu 3}$ Dalitz plot, as predicted by Eq. II-6. The solid and dotted arrows give the polarization directions at the kinematic point for $\xi = +1$ and $\xi = -1$, as measured in the coordinate system shown at the right. For this example we assume ξ to be real and independent of q^2.

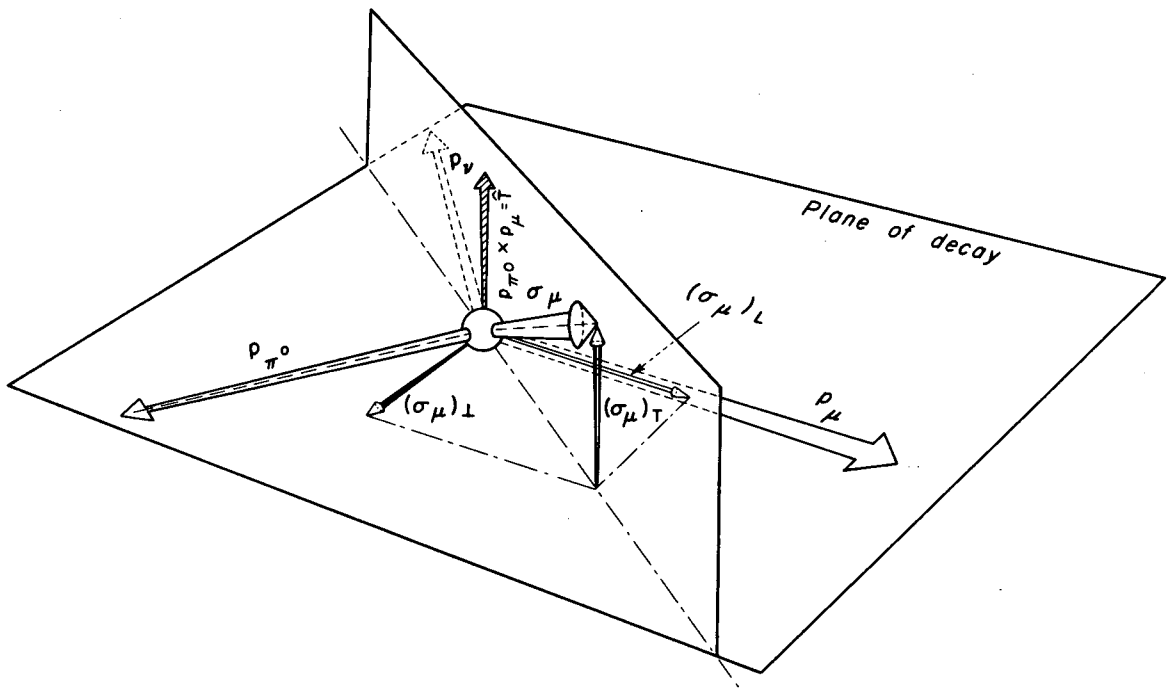

XBL6710-5337

Fig. 1. Diagram of a $K_{\mu 3}$ decay, showing the momenta $\vec{p}_\mu, \vec{p}_\pi, \vec{p}_\nu$. We have drawn an arbitrary muon polarization vector $\vec{\sigma}_\mu$, together with its components in the coordinate system $(\hat{\epsilon}_L, \hat{\epsilon}_T, \hat{\epsilon}_\perp)$.

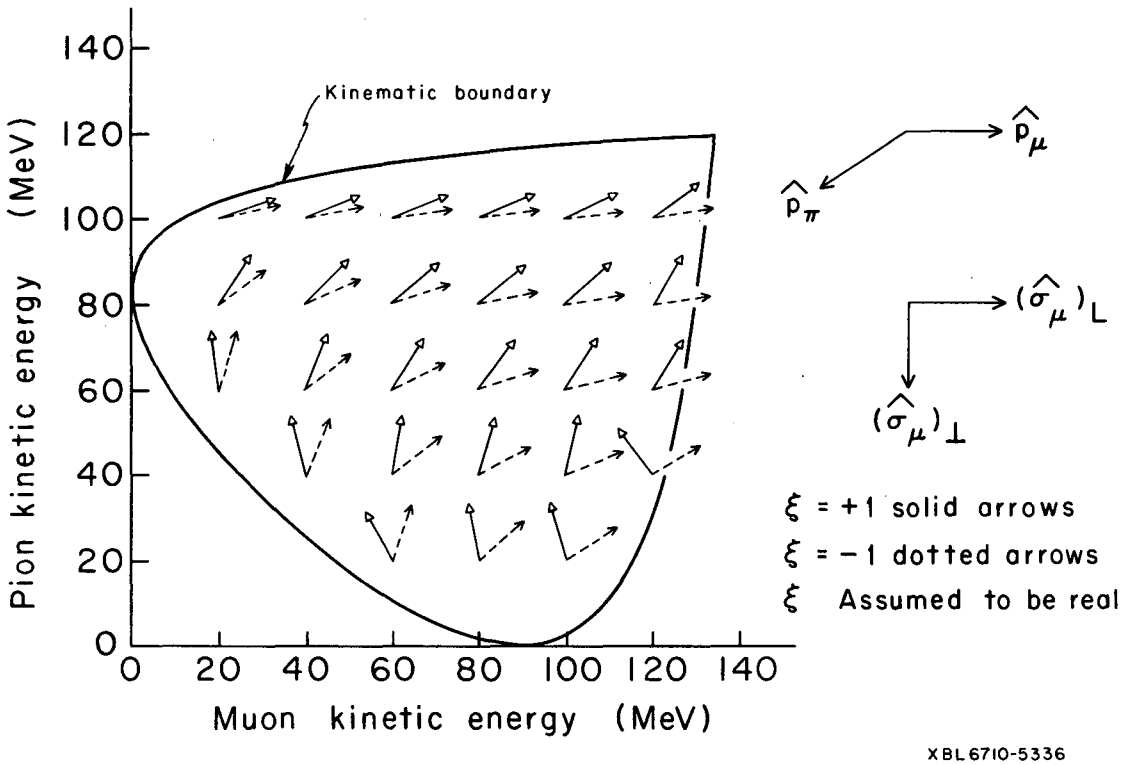

Fig. 2. Predicted direction of the muon polarization vector at various points in the $K^+_{\mu 3}$ Dalitz plot.

Figure 2 illustrates the increased sensitivity to ξ of polarization measurements for events with low π^o energy, where the polarization is largely perpendicular. As defined previously,

$$q^2 = m_K^{\ 2} + m_\pi^{\ 2} - 2m_K E_\pi,$$

so that high π^o energy corresponds to low q^2; in this region of the Dalitz plot the muon polarization is almost purely longitudinal and relatively independent of ξ.

In this experiment we measured the muon polarization vector by stopping μ^+'s from $K_{\mu 3}$ decays and observing the direction of the electron in the subsequent decays

$$\mu^+ \rightarrow e^+ + \nu_e + \bar{\nu}_\mu .$$

The differential decay spectrum for a muon with polarization $\vec{P}$ is given by[5]

$$\frac{dw}{dx d\Omega} = \frac{\lambda x^2}{\pi} \left\{ 3(1-x) + 2\rho(\tfrac{4}{3}x-1) + \xi \vec{P}\cdot\hat{p}_e [(1-x) + 2\delta(\tfrac{4}{3}x-1)] \right\} ,$$

neglecting terms proportional to the electron mass. In this equation x is the electron energy, in units of its maximum, $\hat{p}_e$ is a unit vector in the direction of the decay electron momentum, and the parameter λ is the muon decay rate. The parameters ρ, ξ, δ are determined by the specific form of the lepton current, J_λ^ℓ. (ξ used here has no relation to the form factor in $K_{\mu 3}$ decay, $\xi(q^2)$. The two component neutrino hypothesis and the V-A structure of the lepton current, as given in Eq. I-1, requires, for μ^+ decay,

$$\rho = \delta = \frac{3}{4}$$

$$\xi = +1$$

Using these experimentally verified values[6] for ρ, δ and ξ, and integrating the decay spectrum over all possible electron energies, we find

$$\frac{dw}{d(\cos\theta)} \propto \frac{1}{2}\left(1 + \frac{1}{3}\,|\vec{P}|\,\cos\theta\right) \qquad \text{(II-10)}$$

where $\cos\theta = \dfrac{\vec{P}}{|\vec{P}|} \cdot \hat{p}_e$

Equation II-10 gives the μ decay probability in terms of the direction of the decay electron, and shows that the electron vector direction preferentially lies along the direction of the muon polarization. In our experiment we inferred the muon polarization direction from the observed angular distribution of the decay electrons. As will be described later, we have verified the analyzing power of our apparatus by direct experimental measurements.

III. EXPERIMENTAL APPARATUS

A. Beam

Particles produced in a copper or uranium target placed in the Bevatron external proton beam were mass and momentum analyzed by the magnet system shown in Fig. 3. We studied the decays of K^+ mesons degraded to rest at the second focus of this secondary-particle beam. We designed the K^+ beam to achieve adequate rejection of π^+ mesons and off-momentum particles contributing to background tracks in the spark chambers and to false electronic triggers from the counter telescopes. An additional design criterion was the minimization of the total beam length and consequently, of the loss of K^+ mesons by decays-in-flight. We chose the beam momentum to be 500 MeV/c in order to maximize the yield of stopping K^+. We considered as functions of beam momentum the loss of K^+ by decay-in-flight and by nuclear interactions or multiple scattering out of the stopper, while degrading to rest.

As shown in Fig. 3, particles produced in the target at an angle of 24° to the 5.3 BeV external proton beam passed through an electrostatic spectrometer and were deflected 60° prior to being brought to an intermediate focus. Vertical and horizontal collimators at this first focus defined the mass and momentum acceptances of the beam. A second deflection of 60° provided subsequent momentum recombination at the second focus, where the K^+ mesons were degraded to rest.

The electrostatic spectrometer deflected particles vertically by distances inversely proportional to their velocities, thus separating particles of different mass in the momentum-defined beam. At the first focus the center of the π^+ and K^+ images were separated by 1/2". As

the pulses from the beam counters be greater than those from minimum-ionizing particles.

The counters forming the decay-particle telescope are shown in Fig. 5, a vertical cross section of the apparatus. In this figure the K^+ beam is directed out of the page. With the counter T5 in anti-coincidence the telescope T2-T3-T4 selected particles leaving the K^+ stopping region which came to rest in the chamber between T4 and T5. The water Cerenkov counter, C_μ, was used as a veto against fast decay particles, including μ^+ from the decay $K^+ \rightarrow \mu^+ + \nu$ and electrons from the decay $K^+ \rightarrow \pi^o + e^+ + \nu$; most of these particles were also excluded by the range requirement imposed by T5.

To be considered an acceptable K^+ event, the decay-particle signal had to come 6 to 44 nanoseconds following the signal of a stopping K^+. The minimum allowed time between a K-stop and the K-decay was chosen to insure a rejection of better than 250/1 against K^+ decays-in-flight and other prompt events. We measured the rejection factor by allowing π^+ mesons to trigger the beam telescope. For this measurement π^+ scattered through the decay-particle telescope were then a source of prompt events; we observed the number of events as a function of the time delay between beam and decay-particle signals. With the requirement that the decay signal be delayed 6 to 44 nanoseconds following the K^{STOP} signal, the logic corresponding to an acceptable K^+ decay was:

$$K^{DECAY} = (K^{STOP}) \cdot (\text{good decay})_{\text{delayed}} \qquad \text{(III-1)}$$

$$= (S1 \cdot S2 \cdot S3 \cdot S4 \cdot \overline{C_B} \cdot \overline{S5}) \cdot (T2 \cdot T3 \cdot T4 \cdot \overline{C_\mu} \cdot \overline{T5})_{\text{delayed}}$$

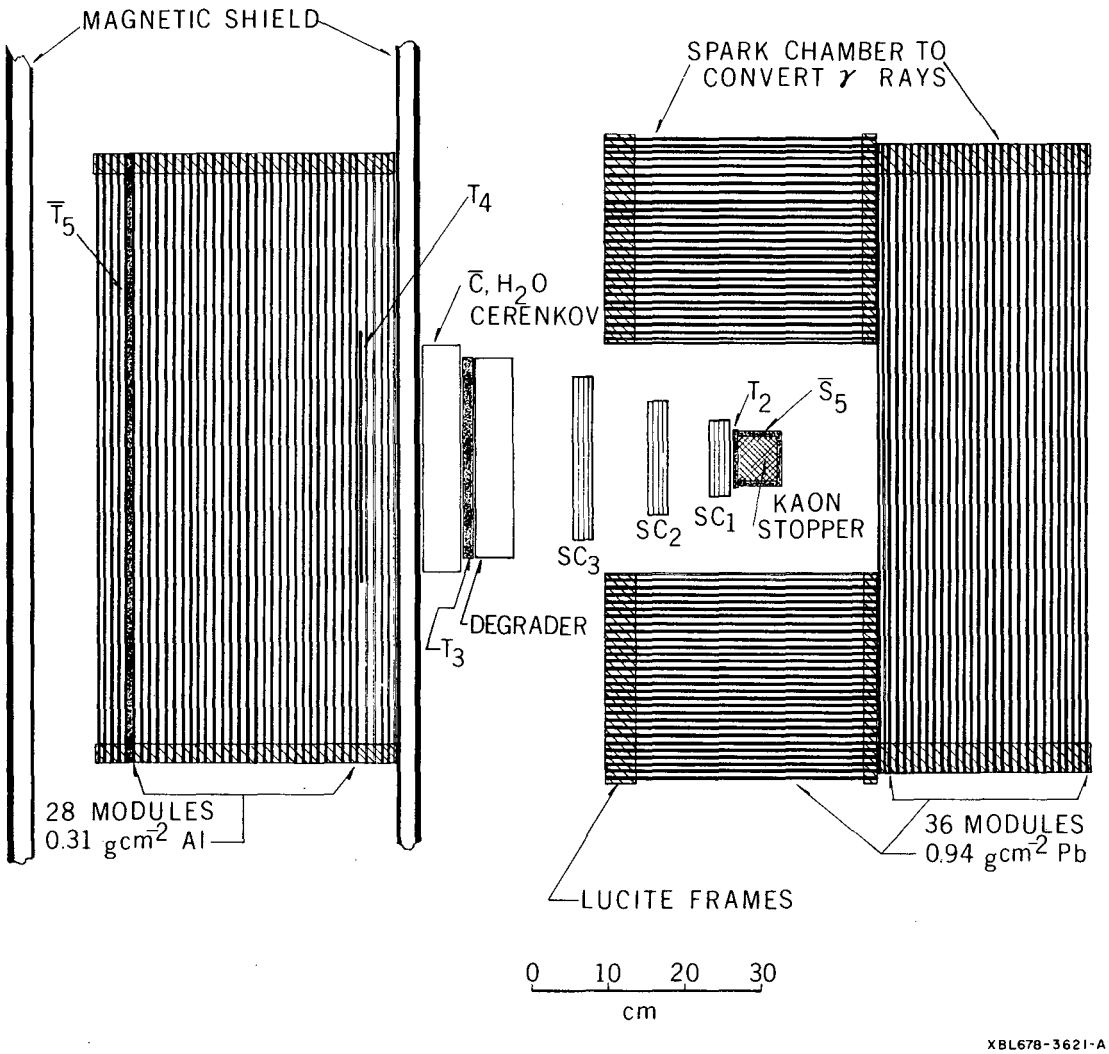

Fig. 5. Vertical cross-section of the apparatus.

This coincidence represented the criterion for an electronic trigger.

The events selected by the scintillation counters were recorded on film by photographing tracks left in spark chambers arranged as shown in Fig. 5. In order to determine completely the kinematics for each $K_{\mu 3}$ decay we observed the track of a stopping μ^+ and the tracks of electron showers from conversion of gamma rays. The π^o produced in the $K_{\mu 3}$ decay itself decayed within 10^{-16} seconds to two gamma rays:

$$\begin{array}{l} \underline{K}^+ \rightarrow \pi^o + \underline{\mu}^+ + \nu \\ \qquad\qquad\quad \hookrightarrow \underline{e}^+ + \nu + \bar{\nu} \\ \qquad\quad \hookrightarrow \underline{\gamma} + \underline{\gamma} \end{array} \qquad \text{(III-2)}$$

To measure the muon polarization, we observed the track of the positron from the subsequent μ-e decay. The five particles we detected with spark chambers are underlined in Eq. III-2. Two aluminum plate chambers, each with two gaps, were embedded in the beam telescope between counters S3 and S4. These chambers indicated the track of the K^+ before stopping, aiding in the reconstruction of the K^+ decay position within the carbon stopper. To observe the gamma-ray showers we used three 36-gap chambers surrounding the stopping region as shown in Fig. 5, a vertical cross-section. All the chambers seen in Fig. 5 were square, with the exception of the upper and lower shower chambers, whose lengths along the beam axis equalled that of the side shower chamber. The plates of the three chambers used to detect gamma rays consisted of sheets of lead each 0.8 mm thick and sandwiched between two 0.3 mm aluminum sheets. To insure rejection of charged particles entering the shower chambers, the two plates in each chamber closest

to the K^+ stopping region were thin aluminum sheets, and were used in anti-coincidence.

We used three 4-gap spark chambers, labeled SC1, SC2, SC3 in Fig. 5, to measure the direction of the charged particle from the K^+ decay. These thin plate aluminum chambers were placed directly after the counter T2 in the decay-particle telescope to reduce the effect of scattering, which would distort the measurement of the initial decay direction.

The coincidence criteria for an acceptable event required the μ^+ from a $K_{\mu 3}$ decay to stop between counters T4 and T5. As shown in Fig. 5, these counters were embedded in a 36-gap aluminum plate spark chamber. Between counters T4 and T5 was a 28-gap spark chamber module whose total thickness was 9.9 grams/cm^2 of aluminum. This 28-gap module had three sections: a section of 17 plates, each 1/16" thick, centered between two sections of 6 plates, each plate 1/32" thick. Ahead of counter T4 and beyond counter T5 were modules with 4 gaps; the 5 plates ahead of T4 were each 1/32" thick, while the 5 plate beyond T5 were each 1/16" thick. With this 36-gap spark chamber we measured the range of the muon from $K_{\mu 3}$ decay and the direction of the electron momentum in the subsequent μ-e decay. We enclosed the entire chamber in a magnetic shield to reduce precession of the muon and consequent depolarization.

C. Experimental Technique

The requirement that the charged particle from the K^+ decay stop between counters T4 and T5 imposed a restriction on its range. We placed a degrader in the decay particle counter telescope ahead of counter T3 to define this range acceptance. We changed this degrader to study K^+ decay particles with different range. Table I lists the degrader used to obtain data for various K^+ decay modes.

Table I. Degrader conditions.

Events	Degrader	Decay particle	K.E. Spectrum accepted (direct path)
$K_{\mu 3}$ (degrader a)	1" Al	μ^+	61-81 MeV
$K_{\mu 3}$ (degrader b)	3/8" Al	μ^+	52-73 MeV
$K_{\pi 2}$	2 3/4" Al	π^+	108.6 MeV
$K_{\mu 2}$	1" Al + 2 1/8" Cu	μ^+	151.7 MeV

We studied $K_{\mu 3}$ decays under two degrader conditions; 83 percent of our $K_{\mu 3}$ events were obtained with degrader a, 1" of aluminum. With this degrader the range criterion for a direct path from the K^+ decay position selected μ^+ with kinetic energy between 61 and 81 MeV. We chose this window in the μ^+ spectrum to exclude from the $K_{\mu 3}$ data much of the background from both $K_{\pi 2}$ decays ($K^+ \rightarrow \pi^+ + \pi^o$), for which $T_{\pi^+} = 108.6$ MeV, and τ' decays ($K^+ \rightarrow \pi^+ + \pi^o + \pi^o$), where the end point of the π^+ spectrum is 53.2 MeV. Additional $K_{\mu 3}$ data were taken with 3/8" aluminum degrader. To aid in our analysis of the $K_{\mu 3}$ data we studied events with the μ^+ from $K_{\mu 2}$ decays ($K^+ \rightarrow \mu^+ + \nu$) and the π^+

from $K_{\pi 2}$ decays ($K^+ \rightarrow \pi^+ + \pi^0$). The different amounts of degrader placed in the decay-particle telescope for these studies are given in Table I.

We triggered the spark chambers upon the electronic signal of an acceptable K^+ decay as defined by Eq. III-1. This coincidence signal was blocked during the time between pulses of the Bevatron; additionally we imposed a minimum delay between event triggers of 250 milliseconds to allow the apparatus to recover. For each event we recorded photographically the tracks in 9 spark chambers: 2 beam chambers, 3 shower chambers, 3 decay-particle tracking chambers, and the range chamber. With the exception of the range chamber all the spark chambers were fired promptly with the coincidence signal; the total delay from the time of a K^+-stop to the presence of voltage on the spark chamber plates was 340 nanoseconds. We delayed the trigger signal to the range chamber for 3.5 microseconds. The μ^+, stopped between counters T4 and T5, decayed with a lifetime of 2.2 microseconds; with our delay in triggering this chamber we observed the electron track in 80 percent of the μ-e decays. In order to maintain both the muon track and the track of the decay electron for as long as 3.5 microseconds we limited the DC clearing voltage on the range spark chamber to 6.6 volts. On the 8 chambers triggered promptly we applied between 30 and 40 volts to clear residual tracks. In a background study we obtained some data of $K_{\mu 3}$ events for which the range chamber was fired promptly; for these events the trigger delay time on all the chambers was 340 nanoseconds and the clearing voltage was 40 volts. All the spark chambers were filled with neon, purified through a closed-circuit recirculation

system. The view of the apparatus given by Fig. 5 corresponded to that seen by the camera. Not shown in this figure are the mirrors mounted on the apparatus to permit stereo reconstruction of tracks from two 90° views of each chamber. Mirrors viewing the upper and lower shower chambers limited the closeness of the range chamber to the K^{+} stopping region. Lucite lenses were attached to the spark chambers to allow observation of sparks regardless of their depth within the modules.

In addition to spark chamber tracks of particles, we recorded on film with each event fiducial lamps mounted on the apparatus and bright grid lines defining the position of the data. We were careful to put many reference points on the film in order to simplify its subsequent automatic computer-scanning. For each photograph we lit numeral lamps giving the event number; this number was displayed as well by a row of binary-coded lights, to be computer-scanned. A second row of binary-coded lights gave digitized information about the event: whether or not a particle was detected by counter S1 in the beam telescope within 20 nanoseconds of the K^{+} decay, and whether or not the counter S5 detected a particle within the full time interval allowed for a K^{+}- decay trigger. We digitized also for each event the time between the K-stop signal and the signal of the K decay, and displayed this information with binary-coded lights. The flashed lamps and all 18 views of the spark chambers were recorded on a 24 mm × 36 mm frame of Tri-X film, using a lens opening of f8.

Figure 6 is a typical $K_{\mu 3}$ event. The lower half of the figure is a view of the apparatus similar to that given by the vertical cross section of Fig. 5. The shower chambers are on the right of Fig. 6,

XBB 684-1740

Fig. 6. A typical $K_{\mu 3}$ event. As described in the text, the lower half of this figure corresponds to the view of the apparatus given by Fig. 5. On the left is the image of the range chamber, showing the μ^+ track as well as the e^+ track from a μ-e decay. The images of two gamma-ray showers are on the right.

while the range chamber, with stopping muon and decay-electron tracks, is on the left. The muon track in the range chamber does not appear to be colinear with its track in the chambers SC1, SC2, SC3; the images of these tracks were reflected by different mirrors. The upper half of Fig. 6 consists of images of the chambers as seen from above.

IV. ANALYSIS PROCEDURE

A. Selection of Events

We scanned a total of 80,000 pictures, candidates for $K^+_{\mu 3}$ events, with SPASS, the automatic computer-scanning system developed by Deutsch at MIT.[7] With this system we measured the position of tracks in all spark chambers except the range chamber. In the scan of the gamma-ray chambers we measured the blackening associated with each shower in addition to its conversion point. For each event we obtained as well the digitized information from the lamps. Using information from the SPASS scanning we selected 10,000 events to be hand-scanned for μ-e decays on the SCAMP machine at LRL. On SCAMP we measured the direction of the incoming μ^+ track in the range chamber, the position of the μ^+ stop, and the vector direction of the decay electron. We selected for reconstruction as $K_{\mu 3}$ events a further restricted sample, using information from both the SPASS and the SCAMP scannings. The criteria imposed based on the SPASS measurements were:

1. Two gamma-ray showers were unambiguously stereo-reconstructed, with conversion points not in the first two gaps of the chambers.
2. No pulse in coincidence with the muon was observed in the cup-shaped counter S5 which surrounded the K^+ stopping position, shielding the decay point from the shower chambers.
3. The reconstructed position of the K^+ stop must have been in the carbon stopper within the box of counters.
4. Neither of the two showers measured was at an edge of the chambers.

5. The opening angle of the two gamma rays was greater than 65°.

6. The event did not satisfy $K_{\pi 2}$ kinematics. From the initial charged particle direction and the directions of each gamma ray relative to the K-stop position we calculated the gamma-ray directions in the π^{o} center of mass, assuming the event to be a $K_{\pi 2}$ decay, and the quantity δ:

$$\delta = \hat{k}_1' \cdot \hat{k}_2' \ .$$

Here $\hat{k}_1'$, $\hat{k}_2'$ are the gamma-ray directions as transformed to the postulated π^{o} rest system. $K_{\pi 2}$ kinematics requires that $\delta = -1$; our criterion for acceptance of the event was that $\delta > -0.9$.

7. The line-of-flight of the charged decay particle as measured in the thin chambers SC1, SC2, SC3 did not have a kink. We required that $\hat{p}_1 \cdot \hat{p}_2 > 0.998$, where $\hat{p}_1$ and $\hat{p}_2$ are the particle directions calculated from tracks in SC1 and SC2, and in SC2 and SC3.

8. The distance of closest approach of the calculated K^+ line-of-flight to the decay particle line-of-flight was less than 1.0 cm. We took as the K^+ stopping position the point on the muon line-of-flight closest to the incident K^+ line-of-flight.

We used the hand scanning on SCAMP to select events with the following characteristics:

1. The scanner observed in the range chamber tracks of a muon entering and stopping and of an electron from the subsequent μ-e decay. Events without such tracks were rejected. In about 2 percent of the data (otherwise acceptable as $K_{\mu 3}$ events),

the scanner was uncertain whether or not the tracks corresponded to those of a muon and its decay electron. After a rescan by the author, we considered most of these events (51 pictures) to have acceptable range-chamber tracks. Events with both tracks extending from the μ-e vertex to the front of the range chamber were measured twice, assuming one track and then the other to be the μ^+; we selected that assignment which best matched the line-of-flight measurement on SPASS from the chambers SC1, SC2, SC3. For each event we calculated the distance at the degrader between the μ^+ line-of-flight measured from SC1, SC2, SC3 and the line-of-flight seen in the range chamber. If this distance was greater than 6 cm, the event was remeasured by the author; 1 percent of the total data (otherwise acceptable as $K_{\mu 3}$ events) were in this category, of which 4 events (0.1 percent) were rejected by the rescan.

2. The scanner agreed with SPASS that there were exactly two gamma-ray showers and that neither gamma ray converted in the first two gaps of its chamber.
3. The electron decay direction was not within a forward cone about the initial muon direction. We rejected all events unless $\hat{p}_e \cdot \hat{p}_\mu < 0.9$.
4. The μ-e vertex position was not in the counter T4. To avoid depolarization due to the μ^+ stopping in plastic scintillator, the experimenter rescanned all events whose vertex was measured to be within 1 gap of T4.

After the selection based on both the SPASS and the SCAMP measurements

the remaining 3549 events were analyzed as candidates for $K_{\mu 3}$ decays. The procedures in reconstructing the data in terms of $K_{\mu 3}$ kinematics are described in the next section. Following this analysis our final data sample consisted of 3133 completely-reconstructed $K_{\mu 3}$ events with observed μ-e decays.

B. Reconstruction of the $K_{\mu 3}$ Kinematics

For each event we had the following data:

1. Range of the charged particle originating from the K^+ decay.
2. Direction-of-motion of the charged particle originating from the K^+ decay.
3. Position of the K^+ decay.
4. Positions of the points where two gamma rays produce showers by conversion.
5. The number of sparks associated with each gamma-ray shower.

We calculated the energy of the charged particle, assuming it to be a muon, from its stopping position in the range chamber. We based this calculation on comparisons of measured range with the predicted range of particles with known energy: π^+ from $K_{\pi 2}$ and μ^+ from the $K_{\mu 2}$ decay mode. We took the K^+ decay position as that point along the line-of-flight of the track in SC1, SC2, and SC3 closest to the K^+ line-of-flight as measured by two spark chambers in the beam. From the K^+ decay position and the gamma-ray conversion points we determined the unit vectors $\hat{\epsilon}_{\gamma 1}$, $\hat{\epsilon}_{\gamma 2}$ pointing in the direction of each gamma ray.

With the measured quantities E_μ, $\vec{p}_\mu$, $\hat{\epsilon}_{\gamma 1}$, $\hat{\epsilon}_{\gamma 2}$, the kinematics of the decay was not uniquely determined. In general there were two solutions compatible with the data, corresponding to different momenta of the π^0. The ambiguity was removed by measuring the energy of the two gamma rays. The two kinematical solutions had different gamma-ray energies; with a rough measurement of the gamma-ray energies we were able to choose between the solutions.

In Appendix A we derive the formula used to determine the

kinematically predicted gamma-ray energies. About 18.7 percent of the events fell outside the boundary of the Dalitz plot and did not have a kinematic solution for the gamma-ray energies. For each of these events we calculated the change in the measured gamma-ray opening angle necessary to put the event onto the nearest edge of the Dalitz plot. If this change was less than 3°, it was made and the gamma-ray energies found; otherwise the event was rejected. With this selection 5 percent of the data were eliminated.

In order to measure the gamma-ray energy and its expected error from the spark count, we used a relation derived from a study of showers of known energy in $K_{\pi 2}$ data. For $K_{\pi 2}$ events we knew the π^{o} energy and direction-of-motion; we could calculate each gamma-ray energy from the position in the apparatus where a shower was produced by conversion. For the $K_{\pi 2}$ events we compared each calculated gamma-ray energy with the measured number of sparks associated with its shower. For this data we made a least-square fit to find the dependence of the observed gamma-ray energy, E^{obs}, upon the measured spark count. We made a similar fit to find the expected uncertainty, δE^{obs}, in the gamma-ray energy as a function of the measured spark count.

In the reconstruction of $K_{\mu 3}$ events we compared each of the two kinematically predicted pairs of gamma-ray energies with the energies determined from the spark counts. For each kinematically predicted pair of energies we calculated the chi-square:

$$\chi_j^2 = \left(\frac{E_1^{obs} - E_{1,j}^{kin}}{\delta E_1^{obs}}\right)^2 + \left(\frac{E_2^{obs} - E_{2,j}^{kin}}{\delta E_2^{obs}}\right)^2 . \qquad \text{(IV-1)}$$

Here E^{obs}, δE^{obs} are the experimentally derived gamma energy and its uncertainty, and E_j^{kin} is the energy predicted by kinematics. The index $j(j = 1,2)$ references the two choices for the gamma energies. We selected that pair of gamma energies with the lower chi-square.

A study of $K_{\pi 2}$ data was used to set an upper limit for the chi-square. The energy of each gamma ray in a $K_{\pi 2}$ decay is uniquely predicted from the observed kinematics. Using the known energies E_1^{kin} and E_2^{kin}, we calculated for the $K_{\pi 2}$ events the chi-square given by Eq. IV-1. We noted that value of the chi-square above which were the chi-square of 10 percent of the $K_{\pi 2}$ data. $K_{\mu 3}$ events whose smaller chi-square was greater than this value were rejected. This selection reduced the data by 8.4 percent.

By finding the gamma-ray energies we arrived at a complete solution of the $K_{\mu 3}$ kinematics. To completely specify the position in the Dalitz plot of the K^+ decay-at-rest we need to know two variables, say T_μ and T_{π^o}. The muon kinetic energy we knew from its range; the pion kinetic energy we determined by finding the gamma-ray energies:

$$T_{\pi^o} = E_{\gamma 1} + E_{\gamma 2} - m_{\pi^o}.$$

In order to analyze the muon polarization it was necessary to define for each event a coordinate system with axes corresponding to the orientation of the K-decay configuration rather than to directions in the lab. Knowing the muon and pion momenta, $\vec{p}_\mu$ and $\vec{p}_\pi$, we constructed three orthogonal axes: a longitudinal axis, along the muon momentum, a transverse axis out of the decay plane (in the sense $\vec{p}_\pi \times \vec{p}_\mu$), and a perpendicular axis -- in the decay plane towards the pion momentum. For each $K^+_{\mu 3}$ event we constructed this coordinate system, defined

by Eq. II-5, and shown in Fig. 1. From the measurement of the laboratory direction of the electron in the μ-e decay we calculated the electron direction relative to the K-decay corrdinate system (Eq. II-5). The solution of the $K_{\mu 3}$ kinematics and the calculation of the electron decay direction in this coordinate system completed the reconstruction of the event.

C. Muon Polarization Analysis

1. Measurement of Polarization Components in K^+ Rest Frame

We measure the muon polarization by studying the angular distribution of the electron direction in the μ-e decays. In μ^+ decay the vector direction $\hat{p}_e$ of the electron momentum is preferentially directed along the polarization direction of the muon. The angular distribution has the form:

$$dw = \frac{1}{2}(1 + \frac{P_n}{3} x)dx \qquad \text{(IV-2)}$$

where P_n is the component of the muon polarization along an axis $\hat{n}$, and $x = \hat{p}_e \cdot \hat{n}$. The decay probability, dw, is normalized to 1. Since the form of the probability function is known, we analyze the data with the maximum likelihood method to determine the muon polarization components. This likelihood has the form[8]

$$L(P_n) = \prod_{i=1}^{N} f(P_n, x_i) \qquad \text{(IV-3)}$$

The likelihood L, a function of the assumed muon polarization component P_n, is defined as the product over the N total $K_{\mu 3}$ events of the normalized probability distribution, f, defined in each event:

$$f(P_n, x_i) = \frac{1}{c(P_n)} (1 + \frac{P_n}{3} x_i). \qquad \text{(IV-4)}$$

Equation IV-4 is equivalent to Eq. IV-2 with the addition of the normalization factor c. This parameter corrects for a dependence of the experimental detection efficiency of μ-e decays upon the vector direction of the decay electron. $x_i = (\hat{p}_e \cdot \hat{n})_i$ is the cosine of the electron direction along the $\hat{n}$ axis for the ith event. The most probable value of the polarization P_n is that which maximizes the

likelihood function $L(P_n)$. For a sufficiently large sample of events the shape of $L(P_n)$ is Gaussian; the customary estimate of the error is that applicable to a Gaussian distribution. Specifically, using the maximum likelihood method we find from the data the result:

P_n^o where $L(P_n)$ maximized

$\pm\Delta P_n$ (1 standard deviation) where $L(P_n^o \pm \Delta P_n) = e^{-1/2}\, L(P_n^o)$.

For each event we have measured the electron decay direction in the coordinate system of longitudinal, transverse, and perpendicular axes given by Eq. II-5. The apparatus was an equally efficient detector for μ-e decays for all electron directions except vector directions continuing along the muon track. Because of this effect no events were accepted in which the electron decay direction was within a small cone about the longitudinal axis. As shown in Appendix B, the normalization factor c needed to correct the likelihood for this cut is:

$$c(P_L) = (1 + \cos\theta_o)\left[1 - \frac{P_L}{6}(1 - \cos\theta_o)\right]$$
$$c(P_T) = c(P_\perp) = 1 + \cos\theta_o \,. \qquad \text{(IV-5)}$$

Here θ_o is the half angle of the cone about the longitudinal axis ($\cos\theta_o = 0.9$). P_L, P_T, $P_\perp$ refer to assumed longitudinal, transverse, and perpendicular polarization components. The likelihood functions for these components then take the form

$$L(P_L) = \prod_{i=1}^{N} \left\{ \left[1.9\left(1 - \frac{0.1}{6}P_L\right)\right]^{-1} \left[1 + \frac{P_L}{3}(\hat{p}_e \cdot \epsilon_L)_i\right] \right\} \qquad \text{(IV-6)}$$

$$L(P_T) = \prod_{i=1}^{N} \left\{ (1.9)^{-1} \left[1 + \frac{P_T}{3}(\hat{p}_e \cdot \epsilon_T)_i\right] \right\} \qquad \text{(IV-7)}$$

$$L(P_\perp) = \prod_{i=1}^{N} \left\{ (1.9)^{-1} \left[1 + \frac{P_\perp}{3} (\hat{p}_e \cdot \hat{\epsilon}_\perp)_i \right] \right\} \qquad \text{(IV-8)}$$

The axes $\hat{\epsilon}_L$, $\hat{\epsilon}_T$, $\hat{\epsilon}_\perp$ refer to the coordinate system (Eq. II-5) defined for each event.

As discussed in a later section, we calibrated directly the analyzing power of our apparatus by measuring the longitudinal polarization of muon rom the decay $K^+ \rightarrow \mu^+ + \nu$. The measured polarization agreed with the expected value of -1. In Section V-A we discuss this calibration as well as possible sources of depolarization in the $K_{\mu 3}$ data.

2. Determination of ξ

We determined the parameter ξ directly from the observed electron angular distributions in the μ-e decays. We assumed that the muon in each $K_{\mu 3}$ event was fully polarized in a direction given by Eq. II-6. With the kinematics completely reconstructed, we defined a normalized probability distribution as in Eq. IV-2, taking the axis $\hat{n}$ to be the predicted direction of the muon polarization, $\hat{\sigma}_\mu$. This direction, for each event, is a function of the specific kinematics as well as the value of the parameter ξ. The magnitude of the polarization, P_n, along this direction we took to be 1. We constructed the likelihood function, depending only on ξ, as the product over all the events of the separate probability distributions:

$$L(\xi) = \prod_{i=1}^{N} \frac{1}{c_i(\xi)} \left[1 + \frac{1}{3}[\hat{p}_e \cdot \hat{\sigma}_\mu(\xi)]_i\right] \qquad \text{(IV-9)}$$

The muon polarization direction is given by Eq. II-6 as a vector in the coordinate system $(\hat{\epsilon}_L, \hat{\epsilon}_T, \hat{\epsilon}_\perp)$ defined by the K-decay; $\hat{p}_e$ is the observed direction of the decay electron in this system, and $\hat{\sigma}_\mu$ is a unit vector along the predicted direction of polarization, $\vec{P}$. Both the electron and the polarization directions are specific to each event as reconstructed. As shown in Appendix B, the normalization factor $c(\xi)$ for the ith event has the form

$$c_i(\xi) = (1 + \cos\theta_o)\left[1 - \frac{1}{6}(1 - \cos\theta_o)[\hat{p}_e \cdot \hat{\sigma}_\mu(\xi)]_i\right]$$

As in Eq. IV-5, $\cos\theta_o$ is the maximum acceptable value of $\hat{p}_e \cdot \hat{\epsilon}_L$ in the data; we have taken $\cos\theta_o = 0.9$. Our result for ξ is that value which maximizes the likelihood function, Eq. IV-9. The uncertainty

in this determination we found by noting the values of ξ for which the likelihood function was reduced from its maximum by a specified factor. We made the likelihood analysis for various assumptions about ξ: ξ real and constant, ξ complex and constant, or ξ real but energy-dependent. Consequently the likelihood $L(\xi)$ was a function of 1 or 2 parameters. Table II gives the value of the likelihood, with respect to its maximum, used to determine the uncertainty in the measurement of ξ. It should be emphasized that the appropriate limits of uncertainty for a two parameter likelihood are markedly greater than those appropriate for a one parameter likelihood.[8]

Table II. Calculation of uncertainty limits in a likelihood analysis.

Number of likelihood parameters	Value of L/L^{max} at limit of: 1 std. deviation	2 std. deviations
1	$e^{-0.5}$	e^{-2}
2	$e^{-1.14}$	$e^{-3.10}$

Having determined the parameter ξ from the polarization data, we re-analyzed the $K_{\mu 3}$ events to measure the magnitude of the muon polarization along the predicted direction, σ_μ. We constructed a one-parameter likelihood function similar to that used to find ξ. (Eq. IV-9) This likelihood is

$$L(P) = \prod_{i=1}^{N} \frac{1}{c_i(\xi,P)} \left[1 + \frac{P}{3} \left[\hat{p}_e \cdot \hat{\sigma}_\mu(\xi)\right]_i \right] \qquad \text{(IV-10)}$$

with

$$c_i(\xi,P) = (1 + \cos\theta_o)\left[1 - \frac{P}{6}(1 - \cos\ _o)[\hat{p}_e\cdot\hat{\sigma}_\mu(\xi)]_i\right].$$

The likelihood is a function of the magnitude P of the muon polarization; given ξ, we maximized the likelihood to determine P. The uncertainty in the measurement of P was found by calculating values of $L(P)/L^{max}$ as in Table II.

V. KNOWN SOURCES OF ERROR

A. Uncertainties in Analysis of $K_{\mu 3}$ Events

Each event of our final $K_{\mu 3}$ data sample provides a separate measurement of $\xi(q^2)$. For each event with specified kinematics we determine the parameter $\xi(q^2)$ by correlating the vector direction of the electron momentum in μ-e decay with the predicted muon polarization direction. The likelihood analysis gives as our result for ξ that value most compatible with the individual measurements of ξ from each event. With this method of determining ξ it is not necessary to know the dependence of the detection efficiency upon the position of the event in the $K_{\mu 3}$ Dalitz plot. Since the measurement of ξ is made for each event, the result for all the data is independent of their Dalitz plot distribution.

Using a Monte Carlo analysis, we studied the effect of the measurement uncertainties on reconstruction of $K_{\mu 3}$ events. We generated by computer a large artifical sample of $K_{\mu 3}$ events with μ-e decays as predicted for a given value of the parameter ξ, and selected those events which would have been detected by the apparatus. For each artificial event we changed randomly the kinematical quantities by small amounts to simulate the effect of the measurement errors on the actual $K_{\mu 3}$ events. We reconstructed and analyzed these Monte Carlo events in a manner identical to that used for the $K_{\mu 3}$ data. We found that the result for ξ was insensitive to the presence of our known measurement uncertainties. In particular, both the 30 to 50% uncertainty in the gamma-ray energy measurements and the ±3 MeV error in the μ^+ energy had little effect on the kinematic reconstruction

and negligible effect on the determination of ξ.

In one of many Monte Carlo studies, we generated 12,000 artificial $K_{\mu 3}$ events with kinematical quantities as expected for $\xi = -0.95$ (real and constant). We chose this value of ξ as it is the result of the analysis of the 3133 actual $K_{\mu 3}$ events. The analysis of this artificial data sample gave $\xi = -0.95 \pm 0.17$. We then generated another sample of 12,000 artificial events with the same input value of ξ. For each event we changed randomly the muon energy and the gamma-ray energies to simulate the effect of the measurement uncertainties on the actual data. The analysis of this sample gave $\xi = -0.91 \pm 0.17$. The artificial data in these two Monte Carlo studies are statistically independent of each other. These studies show that the presence of measurement uncertainties has no significant effect on the determination of ξ, as there is an expected statistical uncertainty of $\pm$ 0.17 in the result for ξ from each data sample. This conclusion is valid as well for the actual $K_{\mu 3}$ data, where the expected statistical uncertainty in ξ is $\pm$ 0.3.

The reconstruction of the π^0 vector momentum was the most difficult step in establishing the kinematics of each $K_{\mu 3}$ event. We used the gamma-ray energies, estimated from the shower spark counts, to choose between two predicted values of the π^0 momentum. As discussed above, we found by Monte Carlo studies that the presence of our measurement uncertainties in the gamma-ray energies had no significant effect on the determination of ξ. Additionally, we studied the actual $K_{\mu 3}$ data to see whether or not events with incorrectly chosen π^0 momentum were present in an amount which significantly biased our result for ξ.

Faulty π^o reconstruction leads to two systematic effects, dependent on the direction-of-motion and on the energy of the π^o. If the wrong π^o solution is chosen, a faulty K-decay coordinate system (Eq. II-5) will be constructed. The incorrect π^o energy will lead to a further error in the prediction of the muon polarization direction as a function of ξ. We separated the actual $K_{\mu 3}$ data into batches with the two possible π^o vector directions close to each other, or not close, and with the two possible π^o energies nearly identical or different. We determined from each of these samples values for ξ statistically consistent with each other and with the result for ξ from all the data. There was no evidence for the presence of a systematic error due to incorrect solutions of the π^o reconstruction.

We estimated the frequency and distribution of background tracks in the shower chambers from pictures taken of $K_{\mu 2}$ decays. There were no gamma rays associated with $K_{\mu 2}$ decays, but random tracks in the shower chambers were occasionally interpreted as being conversion showers of gamma rays. We assumed these random tracks to be present in the $K_{\mu 3}$ data with the same frequency and distribution in the chambers as found in the $K_{\mu 2}$ data. The selection criteria for $K_{\mu 3}$ events required that 2 and only 2 showers be observed. Because of the limited geometrical acceptance of the shower chambers, we detected only one of the gamma rays for many $K_{\mu 3}$ decays. With a random track present in a shower chamber, $K_{\mu 3}$ decays with only one of the π^o gamma rays detected could be falsely reconstructed as complete $K_{\mu 3}$ events. Using the Monte Carlo analysis, we determined that the presence of these background tracks did not significantly affect the result for ξ. We

generated two samples of artificial $K_{\mu 3}$ events, assuming a value -0.95 for the parameter ξ (real and constant). These samples were much larger than the sample of actual $K_{\mu 3}$ events. To one of the samples we added data to simulate the presence of background tracks in the shower chambers. The analysis of 12,000 artificial $K_{\mu 3}$ events with simulated background tracks gave $\xi = -0.88 \pm 0.17$. The analysis of a statistically independent sample of 12,000 events without background tracks gave $\xi = -0.95 \pm 0.17$.

We studied the effect on the result for ξ of variations in the criteria used to select $K_{\mu 3}$ events. Since the muon polarization vector and ξ were related for each kinematical configuration, each event provided a separate determination of ξ. For this reason the use of arbitrarily rigid kinematical selection criteria did not bias the measurement of ξ. We analyzed our $K_{\mu 3}$ data repeatedly, using various selection criteria. We found the determination of ξ insensitive to changes in the selection criteria.

The determination of ξ involved a correlation for each $K_{\mu 3}$ event between the $K_{\mu 3}$ kinematics and the direction of the muon polarization vector, as found from the μ-e decay. As described in the following sections, we measured the muon polarization for samples of $K_{\mu 2}$ and of $K_{\pi 2}$ events, with μ-e decays in the range chamber. The scanning, the selection criteria, and the calculation of the muon polarization were identical for the μ-e calibration events as for the $K_{\mu 3}$ events. The μ^+ in the $K_{\mu 2}$ decay has a helicity of -1; our measurement, $P_L = -1.0 \pm 0.1$, is evidence of our ability to observe polarizations with the apparatus.

Using the Monte Carlo method described above, we found that a 10% depolarization of the muon has no observable effect on the measurement of ξ. We generated by computer 12,000 artificial $K_{\mu 3}$ events, assuming ξ real and constant, and equal to -0.95. For these events we generated μ-e decays with the muon only 90% polarized along the direction predicted by ξ. The analysis of this artificial data gave $\xi = -0.93 \pm 0.17$. We found $\xi = -0.95 \pm 0.17$ from a statistically independent sample of 12,000 artificial events, generated with the muon fully polarized in the direction predicted by the input value of ξ.

After determining ξ from the $K_{\mu 3}$ data, we measured the magnitude of the muon polarization along the direction predicted for each event by our value of ξ. The result, discussed in a later section, was consistent with the absence of depolarization.

Among sources of systematic error in the polarization measurement was the use of pulses from counters C_μ and T5 in anticoincidence. We lost events if the μ^+ decayed promptly and the decay electron passed through either C_μ or T5 within the sensitive time of the anticoincidence. By adding delays to the anti-counters, we found this sensitive time to be 16 nanoseconds, about 0.7% of the μ^+ mean life. Using the observed angular distribution to calculate the number of electrons passing through each counter, we estimated a total loss of less than 0.5% of all μ-e decays. The effect of this loss was negligible. A more serious source of error was our inability to observe μ-e decays in cases where the e^+ track was in the same direction as the track of the μ^+ before stopping. As previously described, we eliminated all events having μ-e decays within a forward cone about the muon direction;

we incorporated this selection into the polarization analysis by modifying the likelihood normalization. We chose the angle of the forward cone to more than cover decay directions for which the scanning efficiency was poor; as with our other selection criteria, the result is insensitive to variations in this cut-off. Except for this forward decay loss we considered our detection of μ-e decays to be independent of the e^+ direction and energy. Because the e^+ decay directions are broadly distributed about the μ^+ polarization vector, the determination of the polarization direction is insensitive to measurement errors of individual e^+ tracks. We calculated that our $\pm 10^\circ$ uncertainty in the e^+ decay direction introduced an effective depolarization of less than 1%. Another source of depolarization was the presence of a magnetic field in the range chamber, causing the μ^+ polarization vector to precess in the interval before the μ-e decay. To reduce this effect, we enclosed the range chamber within an iron shield; as shown in Appendix D the measured field of less than 200 milligauss did not cause significant depolarization.

1. Study of $K_{\mu 2}$ Events

As a calibration for the polarization analysis, we measured the muon polarization in the decay $K^+ \rightarrow \mu + \nu$ ($K_{\mu 2}$). We placed degrader in the decay-particle telescope sufficient to stop within the range chamber muons from the $K_{\mu 2}$ decay mode. This degrader eliminated by range all other K^+ decays except $K^+ \rightarrow \pi^0 + e^+ + \nu$ (K_{e3}) and $K^+ \rightarrow e^+ + \nu$ (K_{e2}). The water Cherenkov counter in front of the range chamber provided a rejection factor of 100/1 against electrons and insured a pure sample of $K_{\mu 2}$ events.

With the exception of the degrader in front of the range chamber, the apparatus for the $K_{\mu 2}$ studies was unchanged from that used to obtain the $K_{\mu 3}$ data. We scanned for μ-e decays a total of 4107 pictures on SCAMP. We ignored tracks in the shower chambers, but otherwise we used procedures identical to those used in scanning the $K_{\mu 3}$ film. We found 3104 events with visable μ-e decays in the range chamber. As with the $K_{\mu 3}$ data, we referred the measurements of the electron decay directions to coordinate systems defined for each event. Since a $K_{\mu 2}$ decay had no defined decay plane but only the single direction along the muon momentum, $\vec{p}_\mu$, we constructed for each event orthogonal axes using a direction fixed in the apparatus. We defined the coordinate system $(\epsilon_L, \epsilon_a, \epsilon_b)$:

$$\hat{\epsilon}_L = \frac{\vec{p}_\mu}{|\vec{p}_\mu|}$$

$$\hat{\epsilon}_a = \frac{\hat{y} \times \vec{p}_\mu}{|\hat{y} \times \vec{p}_\mu|} \qquad \text{(V-1)}$$

$$\hat{\epsilon}_b = \frac{\vec{p}_\mu}{|\vec{p}_\mu|} \times \frac{\hat{y} \times \vec{p}_\mu}{|\hat{y} \times \vec{p}_\mu|} ,$$

with $\hat{y}$ the unit vector vertical in the laboratory frame. We rejected events in which the decay electron direction was close to the longitudinal axis; as in the selection of $K_{\mu 3}$ events we required:

$$\hat{p}_e \cdot \hat{\epsilon}_L < 0.9 . \qquad \text{(V-2)}$$

After this cut our data consisted of 3021 $K_{\mu 2}$ events with μ-e decays.

Figure 7 shows the observed angular distribution of the electron decay direction for the $K_{\mu 2}$ events as given in the coordinate system $(\hat{\epsilon}_L, \hat{\epsilon}_a, \hat{\epsilon}_b)$. In the decay $K^+ \rightarrow \mu^+ + \nu$ $(K_{\mu 2})$ the neutrino has helicity -1. Since the K has zero spin and the muon and neutrino are emitted in opposite directions, angular momentum conservation requires that the muon spin direction also be opposite to its momentum. The lines drawn in Fig. 7 show the expected distributions of the electron decay direction, as given by Eq. II-10, for muons with helicity -1. The normalization of the expected distributions is based on the 3021 $K_{\mu 2}$ events satisfying Eq. V-2. For purposes of illustration we present in Fig. 7 the data before this cut. In the polarization analysis we eliminated the events in the bin of $\hat{p}_e \cdot \hat{\epsilon}_L$ furthest to the right.

We determine the muon polarization components from the $K_{\mu 2}$ data with the maximum likelihood method described previously. The likelihood function for the longitudinal polarization has the form given by Eq. IV-6; while for the polarization components along the axis $\hat{\epsilon}_a, \hat{\epsilon}_b$,

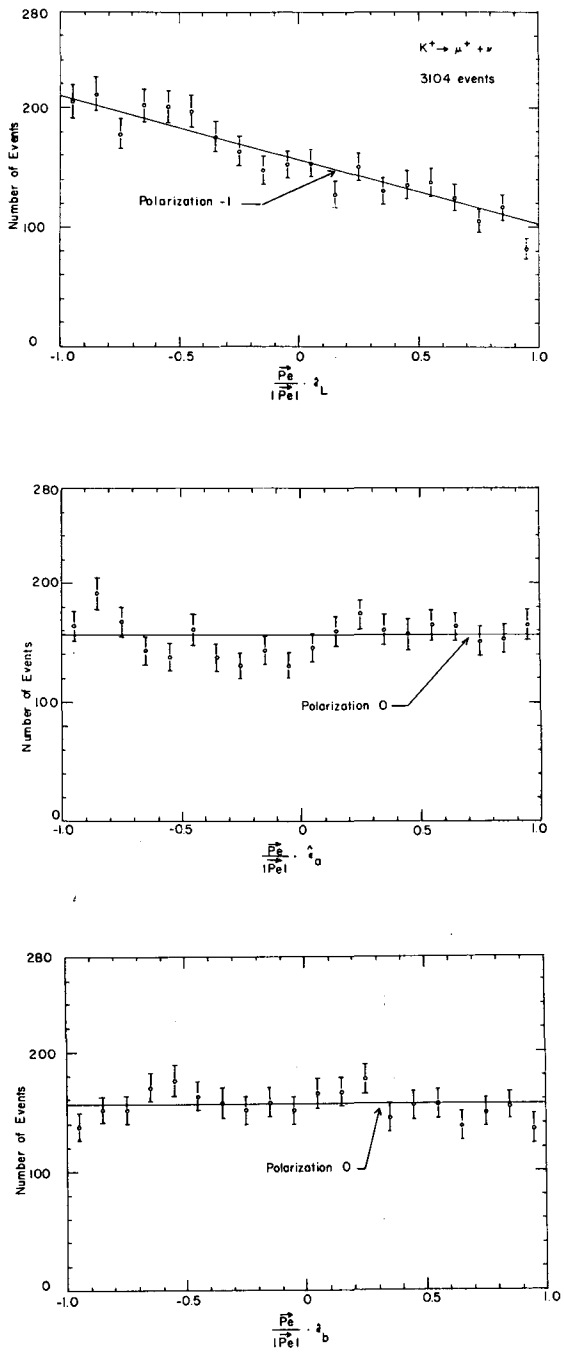

XBL 686-1051

Fig. 7. Angular distribution of the electron momentum vector in μ-e decays, from 3104 $K^+_{\mu 2}$ events, referred to the axes $\hat{\epsilon}_L$, $\hat{\epsilon}_a$, $\hat{\epsilon}_b$.

the likelihood function takes the form of Eq. IV-7. This method of polarization analysis is identical to that used to determine the muon polarization components in the $K_{\mu 3}$ decays. The likelihood functions for the $K_{\mu 2}$ data are shown in Fig. 8; the results for the muon polarization components along the axes $(\hat{\epsilon}_L, \hat{\epsilon}_a, \hat{\epsilon}_b)$ are:

$$P_L = -1.0 \pm 0.1$$

$$P_a = 0.0 \pm 0.1$$

$$P_b = -0.1 \pm 0.1 \quad .$$

The measurement of the muon longitudinal polarization component is in agreement with the expected value of -1 for $K_{\mu 2}$ decays. This result is consistent with the assumption that there was no effective depolarization of the muon by the apparatus or the analysis techniques. The measurement of the muon polarization components along axes $\hat{\epsilon}_a$, $\hat{\epsilon}_b$ investigates possible dependence of the detection efficiency upon the orientation of the μ-e decay plane in the apparatus; the results for these components is consistent with the absence of such dependence.

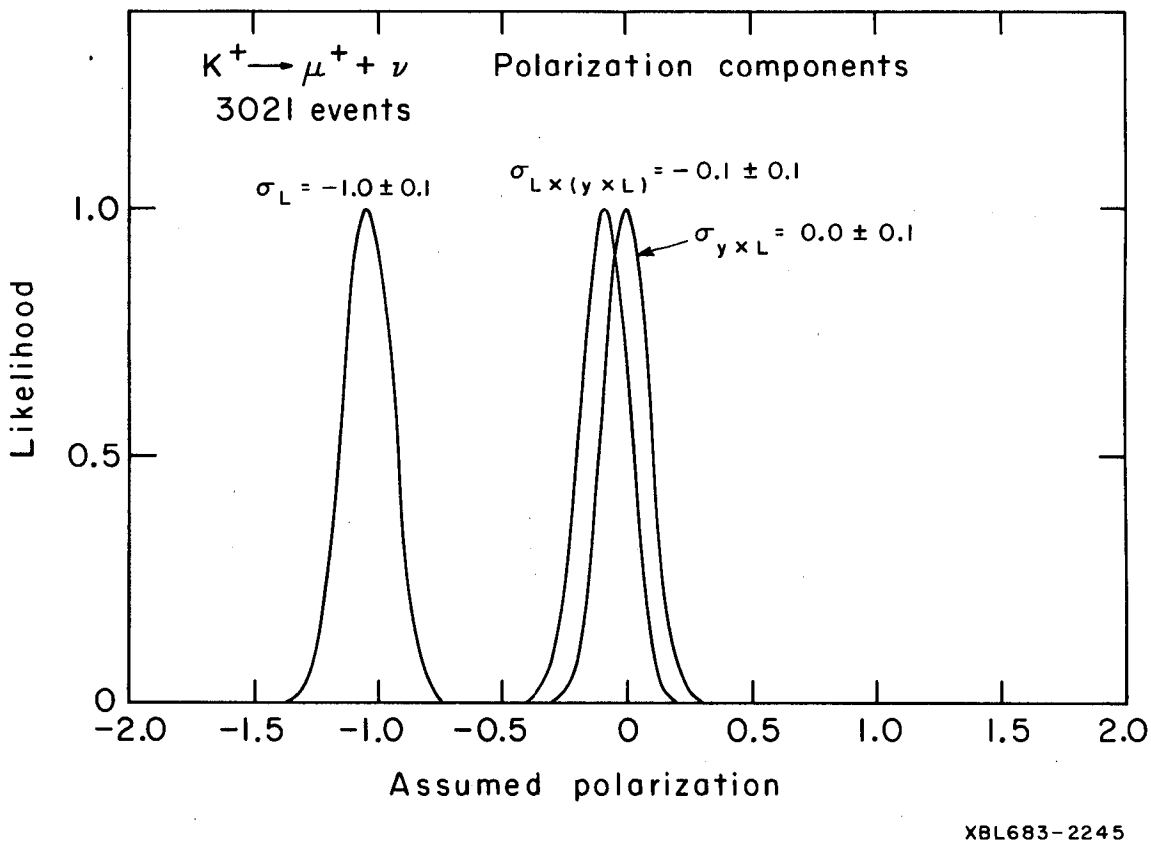

Fig. 8. Likelihood functions for muon polarization components in $K^+_{\mu 2}$ decay.

2. Study of $K_{\pi 2}$ Events

We investigated further the technique of polarization measurement with events from the decay mode $K^+ \rightarrow \pi^+ + \pi^0$ ($K_{\pi 2}$). We increased the thickness of the degrader placed in the decay-particle telescope so that π^+ mesons from $K_{\pi 2}$ decays stopped in the range chamber. As estimated in a later section, these $K_{\pi 2}$ events included a background of approximately 2% from $K_{\mu 3}$ decays, statistically insignificant for the polarization analysis. Except for the additional degrader the apparatus was identical to that used to obtain the $K_{\mu 3}$ data. We did not apply the test used to eliminate $K_{\pi 2}$ decays, because now we wanted to study $K_{\pi 2}$ events. The selection criteria were otherwise the same as those used for the $K_{\mu 3}$ data. We scanned the data for decay electrons in the range chamber and reconstructed events as if they were $K_{\mu 3}$ decays. We assumed the charged particle was a muon, and calculated its energy from the observed range through the increased degrader. By assuming the event to be a $K_{\mu 3}$ decay, we calculated as previously described the π^0 vector momentum from the gamma-ray energies and the shower positions. We measured the polarization components with respect to the coordinate system $(\hat{\epsilon}_L, \hat{\epsilon}_T, \hat{\epsilon}_\perp)$ described previously, determined for each event from the kinematics of the hypothesized $K_{\mu 3}$ decay.

For the $K_{\pi 2}$ events we observed the angular distribution of electrons from the decay chain:

$$
\begin{array}{l}
K^+ \rightarrow \pi^+ + \pi^0 \\
\quad\quad\;\; \big|\!\rightarrow \mu^+ + \nu \\
\quad\quad\quad\quad \big|\!\rightarrow e^+ + \nu + \bar{\nu} \quad .
\end{array}
$$

We did not detect the track of the muon, emitted with only 4 MeV in the π^+ decay. Since the π^+ decay was isotropic in direction, the expected electron distribution was isotropic. The $K_{\pi 2}$ events, reconstructed and analyzed as $K_{\mu 3}$ decays, were therefore predicted to show zero muon polarization.

The distributions of the electron decay directions in the coordinate system $(\epsilon_L, \epsilon_T, \epsilon_\perp)$ are given in Fig. 9. We have plotted only the 567 $K_{\pi 2}$ events with

$$\hat{p}_e \cdot \hat{\epsilon}_L < 0.9 \ ,$$

the standard selection criterion used for all the polarization studies. This cut eliminated 17 events from the bin in $\hat{p}_e \cdot \hat{\epsilon}_L$ furthest to the right. The lines drawn in Fig. 9 correspond to an isotropic μ-e decay distribution, and are normalized to the 567 events.

Using the maximum likelihood method described previously, we find the muon polarization components:

$$P_L = -0.3 \pm 0.2$$

$$P_T = -0.1 \pm 0.2$$

$$P_\perp = +0.2 \pm 0.2 \ .$$

These results are consistent with the prediction that the electron angular distributions correspond to decays of unpolarized muons. They give no evidence for systematic effects in the analysis procedures which would cause false polarization measurements.

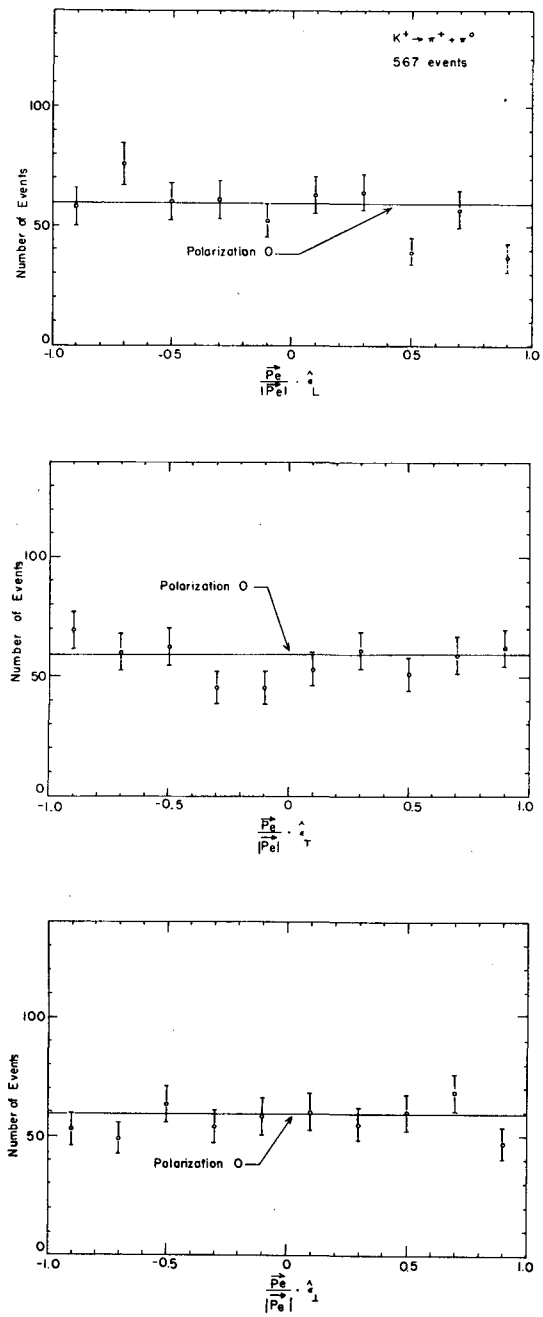

XBL 686-1052

Fig. 9. Angular distribution of the electron momentum vector in π-μ-e decays, from 567 $K^+_{\pi 2}$ events, referred to the axes $\hat{\epsilon}_L, \hat{\epsilon}_T, \hat{\epsilon}_\perp$. Because of the elimination of events with $\hat{p}_e \cdot \hat{\epsilon}_L > 0.9$, the data points are not expected to fit the solid lines.

B. Presence of Background Events in the $K_{\mu 3}$ Data

1. Summary of Background Contributions

We considered events other than $K_{\mu 3}$ decays which could be present as background in the data. Such events must pass the selection criteria described previously. They must have two apparent showers in the gamma-ray chambers, and a track in the range chamber with an apparent μ-e decay vertex. They must be kinematically reconstructable as $K_{\mu 3}$ events but fail the kinematic test for a $K_{\pi 2}$ decay. As will be described in the following section, we determined experimentally the actual contamination of our data by events whose frequency of apparent μ-e decays did not follow the μ^+ lifetime. We calculated the expected contribution from all sources of background; the details of these calculations will be presented in subsequent sections.

The backgrounds considered are those due to the following K^+ decay modes:

$$K^+ \rightarrow \pi^+ + \pi^o \qquad (K_{\pi 2})$$

$$K^+ \rightarrow \pi^+ + \pi^o + \pi^o \qquad (\tau')$$

$$K^+ \rightarrow \pi^+ + \pi^o + \gamma \qquad (K_{\pi\pi\gamma})$$

$$K^+ \rightarrow \pi^o + e^+ + \nu \qquad (K_{e3}) \ .$$

The $K_{\pi 2}$ decay was the most serious source of background events in the $K_{\mu 3}$ data. For the $K_{\pi 2}$ mode we estimated two sources of background: $K_{\pi 2}$ decays with a π^+ nuclear interaction in the range chamber, and $K_{\pi 2}$ decays with a π^+ decay-in-flight ($\pi^+ \rightarrow \mu^+ + \nu$). In Table III we list the results of the background calculations. Two sources, K_{e3} decays

Table III. Results of background calculations.

Source of background	Est. fraction Bkg./$K_{\mu 3}$ events	Does frequency of "decays" follow μ^+ lifetime?
$K^+ \to \pi^+ + \pi^o$ ($K_{\pi 2}$)		
with π^+ decay-in-flight	2.9×10^{-2}	yes
with π^+ nuclear interaction	$< 5.3 \times 10^{-2}$	no
$K^+ \to \pi^+ + \pi^o + \pi^o(\tau')$	5.0×10^{-4}	yes
$K^+ \to \pi^+ + \pi^o + \gamma$ ($K_{\pi\pi\gamma}$)	1.4×10^{-2}	yes
$K^+ \to \pi^o + e^+ + \nu$ (K_{e3})	0.8×10^{-2}	no

and $K_{\pi 2}$ decays with a π^+ interaction in the range chamber, have "μ-e decays" whose frequency is independent of the time delay on the range chamber trigger. As discussed in the following section, the analysis of the prompt data shows that the total contribution of all such backgrounds is (3 ± 2) percent of the $K_{\mu 3}$ data. The estimated contribution of other possible backgrounds is less than 5 percent.

We have studied the effect of these backgrounds on our determination of ξ by adding these events to $K_{\mu 3}$ events generated in a Monte Carlo analysis. From this simulated data our analysis determined a value of ξ statistically unchanged from the value used to generate the $K_{\mu 3}$ events. The primary effect of the presence of these backgrounds was to enlarge slightly the error limits assigned to ξ by the likelihood analysis.

A detailed account to justify the numbers given in Table III is contained in Section VB-3. A reader uninterested in these experimental details should skip to Section VI (Results).

2. Study of $K_{\mu 3}$ Events with Prompt μ-e Decay

In order to determine experimentally the amount of background events with charged particles other than muons, we collected a sample of events with a reduced delay on the range chamber trigger. For the data used in the polarization analysis we delayed firing the range chamber for about 1.5 muon lifetimes after the time of the K^+ decay. We chose this delay long enough to observe a large fraction of the μ-e decays, yet not so long that random tracks in the chamber constituted a background. The fraction of stopping muons with an observed decay in the range chamber was greatly reduced by firing the chamber promptly. As the apparatus was otherwise unchanged, a comparison of the fraction of decays observed for prompt and for delayed trigger measured the amount of contamination of our data by background events, whose detection was independent of the trigger delay time. Events from the $K_{\pi 2}$ or K_{e3} decay modes for which an interaction in the range chamber was interpreted as a μ-e decay should have occurred in equal frequency in the two samples of data. The analysis of the prompt-trigger events allowed a direct calculation of the amount of such backgrounds.

Table IV shows the comparison between the data with a normal delay and with a prompt trigger on the range spark-chambers. The delay time listed is the time from the passage of the muon through the chamber to the time after which the decay electron would not produce a track. Events were selected as being $K_{\mu 3}$ decays using the normal selection criteria. The numbers of $K_{\mu 3}$ events shown in Table IV reflect all but the final reconstruction test -- that of the chi-square fit of the

Table IV. Comparison of prompt and delayed $K_{\mu 3}$ data.

Data	Length of delay	No. of accepted $K_{\mu 3}$ events	No. $K_{\mu 3}$ events with μ-e decay	Without μ-e decay	Fraction of $K_{\mu 3}$ events with μ-e decay
prompt	0.34±0.03 μsec	1107	165	942	0.149
delayed	3.5 ±0.1 μsec	4895	3533	1362	0.722

shower energies to $K_{\mu 3}$ kinematics. For much of the data scanned on SCAMP we did not measure the muon stopping position in the range chamber if the event had no apparent μ-e decay. The final reconstruction of an event, which reduces the data by about 10 percent, requires the knowledge of the muon energy. We have made this reconstruction for all the $K_{\mu 3}$ events in Table IV assuming the unmeasured muon tracks have a range midway through the chamber, and then applied the chi-square test. This final selection reduced equally the four samples of $K_{\mu 3}$ events given in Table IV, and the comparison of the prompt with the delayed data was unchanged with these new numbers.

From the delay times and the muon lifetime we calculated the expected value of the ratio R:

$$R = \frac{\text{fraction of prompt } K_{\mu 3} \text{ events with } \mu\text{-e decays}}{\text{fraction of delayed } K_{\mu 3} \text{ events with } \mu\text{-e decays}} .$$

As described in Appendix C, we find this theoretical value R_T to be 0.19 ± 0.02, the error coming from the delay length uncertainties. With the numbers of $K_{\mu 3}$ events in Table IV the experimental value R_E is 0.21 ± 0.02.

The $K_{\mu 3}$ events listed in Table IV have been subjected to all the selection criteria except the final reconstruction fit. We considered

the correction to R_E needed because of the elimination of forward μ-e decays. Assuming a muon longitudinal polarization of $+0.8 \pm 0.1$ as indicated by the analysis, we observed with this cut (93.7 ± 0.2) percent of the μ-e decays. Recalculation of the ratio R_E with a correction to the number of decays observed gave a ratio statistically unchanged from 0.21. This ratio remained unchanged when we assumed various amounts of the decays lost in the forward cone were interpreted by the scanner as $K_{\mu 3}$ events without μ-e decays.

By comparing R_E with R_T, we measured the presence of a background whose frequency is independent of the trigger delay time. We assume this background to occur with equal frequency in the data with delayed and with prompt triggers on the range chamber. As shown in Appendix C, the fraction f_B of the observed decays due to such a background is:

$$f_B = \frac{R_E - R_T}{1 - R_E} .$$

From the value of R_E and R_T we find

$$f_B = 0.03 \pm 0.02.$$

Sources of these background events include K_{e3} decays and $K_{\pi 2}$ decays, with a π^+ interaction in the range chamber. We determine experimentally that the total contamination of the $K_{\mu 3}$ data from all such backgrounds is (3 ± 2) percent.

3. Calculation of Background Contributions

$K_{\pi 2}$ events

The decay $K^+ \rightarrow \pi^+ + \pi^0$ ($K_{\pi 2}$) is the major source of background in the $K_{\mu 3}$ data. The $K_{\pi 2}$ decay mode occurs 12 times more frequently than the 20% of the $K_{\mu 3}$ mode accepted by the range chamber. The upper limit on the π^+ kinetic energy, imposed by the anti-coincidence counter at the end of the range chamber, is 89 MeV, or 20 MeV lower than the π^+ energy in $K_{\pi 2}$. Pions which decay in flight ($\pi^+ \rightarrow \mu^+ + \nu$), or which suffer nuclear interactions in the range chamber, can satisfy the range criterion; and the initial $K_{\pi 2}$ decay could be a background event in the $K_{\mu 3}$ data. It is entirely possible for $K_{\pi 2}$ events to simulate the $K_{\mu 3}$ decay configuration and to be kinematically reconstructable as $K_{\mu 3}$ events. Both the $K_{\pi 2}$ and the $K_{\mu 3}$ decay modes produce a π^0; our apparatus has a greater detection efficiency for the π^0 gamma rays from $K_{\pi 2}$ decays than for those from the actual $K_{\mu 3}$ events in our data. The apparatus is most efficient for events with the π^0 direction-of-motion opposite to that of the charged decay particle; this optimal configuration for detection occurs for all the $K_{\pi 2}$ decays but for only a portion of the $K_{\mu 3}$ decays. For all these reasons we consider the $K_{\pi 2}$ mode to be, potentially, a serious source of background.

We designed the apparatus to reduce the actual contamination of the $K_{\mu 3}$ data from $K_{\pi 2}$ decays. As shown in Fig. 5, we placed three thin-plate aluminum spark chambers next to the K^+ stopping region. These chambers enabled us to measure the direction of the charged decay particle before significant scattering took place. With the measurement of the gamma-ray conversion points and of the initial charged particle direction we could test kinematically to determine if the event was a

$K_{\pi 2}$. In this way we eliminated most of the $K_{\pi 2}$ background before the scanning for a μ-e decay in the range chamber. For each event we assumed the charged particle was a π^+ from a $K_{\pi 2}$ decay and transformed the vector directions of each gamma ray into the accompanying π° center-of-mass system. We defined the quantity

$$\delta = \hat{k}_1' \cdot \hat{k}_2' \quad , \tag{V-3}$$

where $\hat{k}_1'$, $\hat{k}_2'$ are the calculated unit vectors in the directions of the gamma rays in the π^0 rest frame, assuming the event to be a $K_{\pi 2}$. In Fig. 10 the distribution in δ is plotted for a sample of raw $K_{\mu 3}$ data as well as for $K_{\pi 2}$ data. In all graphs the actual $K_{\pi 2}$ events are sharply peaked at $\delta = -1$; the events away from the peak are $K_{\mu 3}$ decays as well as $K_{\pi 2}$ decays with faulty measurements of the π^+ direction or of the γ shower origins. It should be noted that the obvious $K_{\pi 2}$ peak in the $K_{\mu 3}$ data is due to events which satisfied the $K_{\mu 3}$ range requirement--that is events which have π^+ decay-in-flight or π^+ interactions in the range chamber. As will be demonstrated, our selection criterion for the $K_{\mu 3}$ events that $\delta > -0.9$ was 95% efficient in eliminating $K_{\pi 2}$ background events.

a) $K_{\pi 2}$ events with π^+ decay-in-flight

We calculated by Monte Carlo techniques the amount of background in our data from the $K_{\pi 2}$ decay mode, with associated π^+ decay-in-flight. The proportion of these background events to the $K_{\mu 3}$ events is given by

$$F_{DIF} = \frac{N(K_{\pi 2}^{DIF})}{N(K_{\mu 3})} = f_\delta f_\epsilon \cdot p_{DIF} \cdot \frac{\Gamma_{\pi 2}}{\Gamma_{\mu 3}} \cdot \frac{f_s^{\pi 2}}{\sum\limits_{\text{allowed } E_\mu} f_s^{\mu 3} \dfrac{\Delta\Gamma_{\mu 3}}{\Gamma_{\mu 3}\, \Delta E_{\mu 3}} \Delta E_{\mu 3}} \tag{V-4}$$

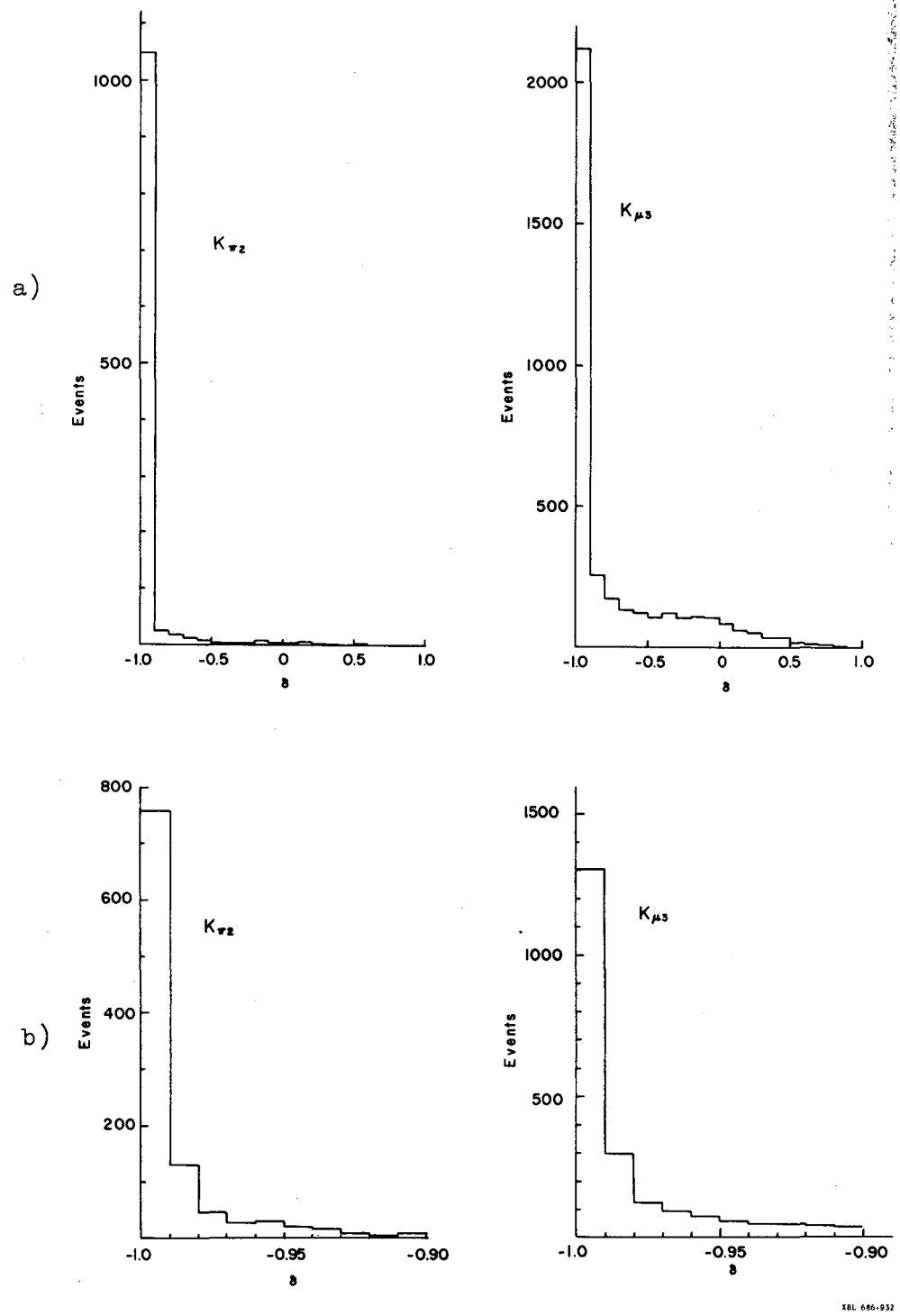

Fig. 10. Distribution in the parameter δ for initial samples of $K_{\pi 2}$ and $K_{\mu 3}$ data. a) all events. δ is a cosine and can have values -1 to +1. We accepted $K_{\mu 3}$ events if $\delta > -0.9$; events in the $K_{\mu 3}$ data with $\delta < -0.9$ were considered probable $K_{\pi 2}$ decays, and were rejected. b) events with $\delta < -0.9$. To show the sharp peaking in δ, we expand the first bin ($-1.0 \leq \delta < -0.9$) of the curves above.

where p_{DIF} is the π^+ decay-in-flight probability, $\Gamma_{\pi 2}/\Gamma_{\mu 3}$ the ratio of the decay rate for $K_{\pi 2}$ to the rate for $K_{\mu 3}$, and $f_s^{\pi 2}$ the fraction of $K_{\pi 2}$ decays with two gamma-ray showers detected. For $K_{\mu 3}$ events we computed the π° detection efficiency $f_s^{\mu 3}$ as a function of the muon energy, and summed in 1 MeV bins over E_μ (allowed by the range criteria) the product of $f_s^{\mu 3}$ with the relative differential muon spectrum, $\Delta\Gamma_{\mu 3}/\Gamma_{\mu 3}\Delta E_{\mu 3}$.

In Eq. V-4 f_δ is the fraction of $K_{\pi 2}$ events with acceptable $\delta(>-0.9)$, and f_ϵ is the fraction with $\epsilon > 0.998$. The parameter ϵ measures the straightness of the track through the spark chambers SC1 SC2, SC3

$$\epsilon = \hat{p}_{12} \cdot \hat{p}_{23} \quad .$$

Here $\hat{p}_{12}$, $\hat{p}_{23}$ are unit vectors in the directions of the decay particle determined from the track positions in SC1, SC2 and in SC2, SC3. A π^+ decay-in-flight in these chambers would be eliminated from the data if $\epsilon < 0.998$.

We calculated the π^o detection efficiencies f_s by Monte Carlo techniques. We generated in the computer a large samples of events, each with two gamma rays as from a π^o decay, and noted the fraction of events which survived selection criteria reflecting the overall acceptance of the apparatus. For the Monte Carlo calculation we estimated the geometrical acceptance and energy-dependent efficiency of the lead-plate spark chambers for detecting gamma rays. We used the gamma-ray reconstruction efficiency determined from $K_{\pi 2}$ data--where each gamma ray has a known energy-angle relation. For each artificial event with two acceptable gamma rays we reconstructed the π^o and attempted to fit the event to $K_{\mu 3}$ kinematics, as in the analysis of the actual data. We found the randomly generated $K_{\pi 2}$ events fit $K_{\mu 3}$ kinematics when the

charged particle was interpreted as a muon with a kinetic energy between 55 and 90 MeV, the acceptance of the range chamber. The calculation of the $K_{\mu 3}$ efficiencies $f_s^{\mu 3}$ for various muon energies includes the selection of events with δ, defined by Eq. V-3, greater than -0.9, as required for the actual $K_{\mu 3}$ data. In generating the $K_{\mu 3}$ events and in calculating the muon differential spectrum we assumed the form factor ratio, ξ, to be real, energy-independent, and of magnitude -1. The shape of the muon spectrum[9] and the results of the $K_{\mu 3}$ Monte Carlo analysis were not sensitive to changes in the value of ξ. The results for $f_s^{\mu 3}$ as a function of muon energy are plotted in Fig. 11; the upper curve is the fraction of events generated with reconstructable π^o, and the lower curve is this fraction with the additional requirement that $\delta > -0.9$. This lower curve was used in the evaluation of Eq. V-4.

Our result for the $K_{\pi 2}$ events was $f_s^{\pi 2} = 0.55$. We estimated f_δ, the fraction of $K_{\pi 2}$ events with $\delta > -0.9$, from the observed distribution in δ of $K_{\pi 2}$ data shown in Fig. 10. After using curve b of Fig. 11 to estimate the number of $K_{\mu 3}$ events expected in the $K_{\pi 2}$ data, we determined

$$f_\delta = 0.055 \quad .$$

The direction of a muon from a π^+ decay-in-flight before the third tracking chamber practically coincides in the lab with the initial π^+ direction, because of the low muon energy in the decay center-of-mass. For this reason the factor f_δ is applicable to early π^+ decays as well as to decays-in-flight beyond the tracking chambers.

In our calculation of the π^+ decay-in-flight probability we followed the path of the π^+ from the K^+ decay point to the anti-counter at the end of the range chamber. For every position of degrader along this path we calculated the minimum and maximum muon energies acceptable by the

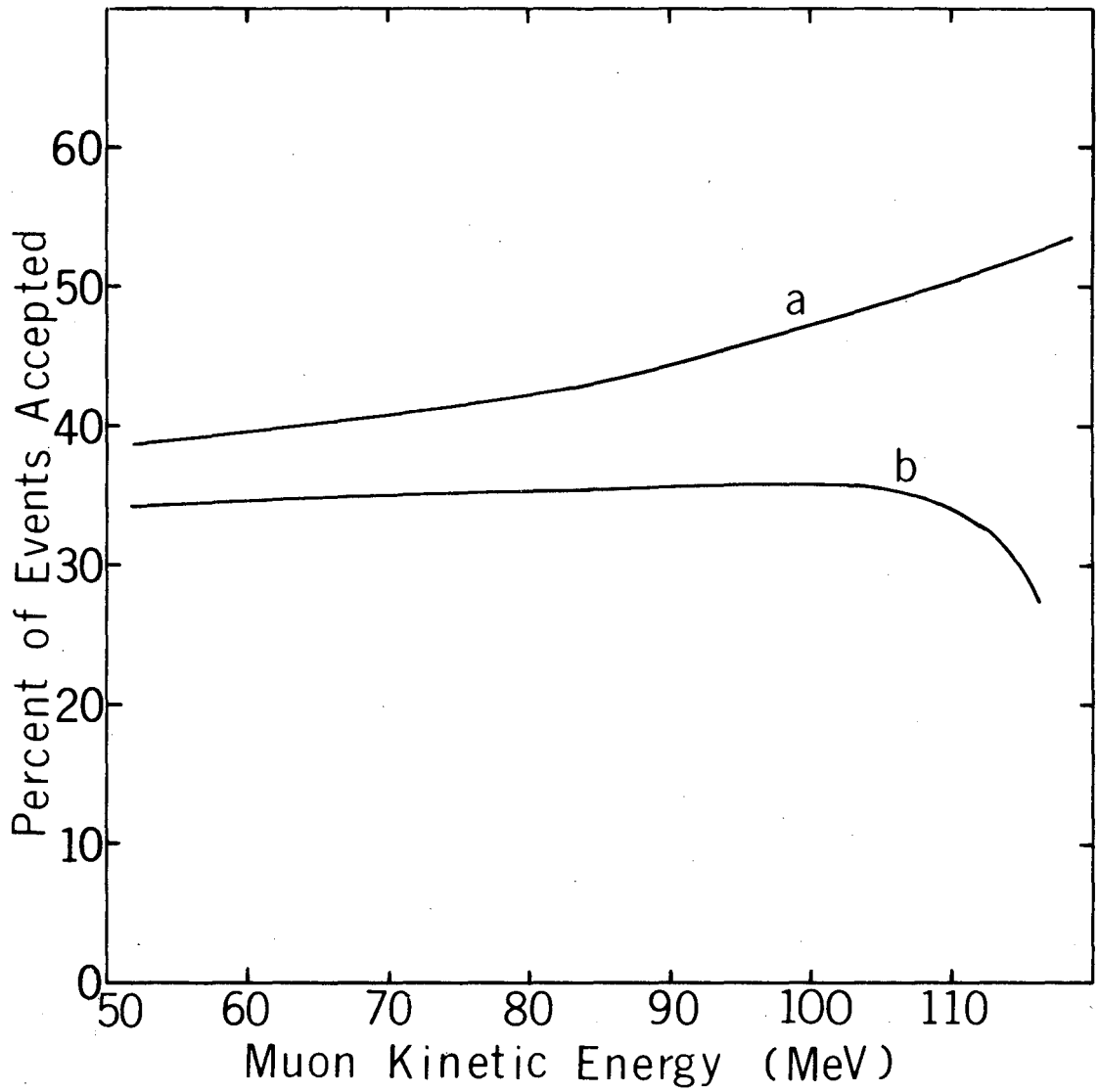

XBL 685-882

Fig. 11. Calculated acceptance for $K_{\mu 3}$ events, as a function of μ^+ energy; a) events with π^o detected, b) events with π^o detected and satisfying $\delta > -0.9$.

range chamber. Knowing the π^+ energy at each position we calculated the muon energy spectrum in the lab from a decay-in-flight. From the acceptable muon-energy limits we determined the corresponding limits on the decay angles in the π^+ rest frame, and consequently the fraction of decays-in-flight yielding a muon stopping in the range chamber; this factor times the decay-in-flight probability over the distance from the previous degrader position gave the probability p_{DIF} of an acceptable π^+ decay-in-flight. In Table V we list our results for p_{DIF} for different regions of the π^+ path. We have combined individual subsections in listing the values of p_{DIF} for region 4 (from the 3rd tracking chamber to the range chamber) and for region 5 (the range chamber). Since we took $K_{\mu 3}$ data under two separate degrader conditions we have calculated p_{DIF} separately for each situation. Data taken under condition b (5/8" less aluminum) comprised 17% of the events.

Table V also shows the value of f_ϵ in each region, the fraction of the decay-in-flight events with $\epsilon > 0.998$. For regions 2 and 3 we calculated the acceptable decay-in-flight angles in the lab; and, assuming the decays uniformly distributed along the π^+ path, we found the expected distribution in ϵ. Over half the decays in these regions should have been rejected because of a detectable kink in the observed track.

Evaluating Eq. V-4, with the $K_{\pi 2}$ and $K_{\mu 3}$ branching ratios 20.9 and 3.4%,[10] and combining $f_\delta \cdot f_\epsilon \cdot p_{DIF}$ calculated for each region we find the proportion of π^+ decay-in-flight events to $K_{\mu 3}$ events to be:

$$F_{DIF} = 3.1 \times 10^{-2} \text{ , degrader a (1" aluminum)}$$
$$= 2.2 \times 10^{-2} \text{ , degrader b (3/8" aluminum)}$$

Our result for all the $K_{\mu 3}$ data is

$$F_{DIF} = 2.9 \times 10^{-2} \quad .$$

Table V. Calculation of decay-in-flight probability

region	f_ϵ	f_δ	p_{DIF} degrader a	p_{DIF} degrader b
1. K^+ decay point to SC1	1.0	5.5×10^{-2}	0.55×10^{-3}	0.58×10^{-3}
2. SC1 to SC2	0.46	5.5×10^{-2}	1.79×10^{-3}	1.88×10^{-3}
3. SC2 to SC3	0.40	5.5×10^{-2}	2.10×10^{-3}	2.22×10^{-3}
4. SC3 to T4	1.0	5.5×10^{-2}	7.34×10^{-3}	5.93×10^{-3}
5. T4 to T5	1.0	5.5×10^{-2}	3.32×10^{-3}	1.27×10^{-3}

We calculated the average muon polarization of these background events by noting the π^+ center-of-mass decay angles corresponding to the minimum and maximum muon energies acceptable by the range chamber. Since the range of a particle stopping in the chamber must be less than that of the π^+, the range requirement selected those π^+ decays with the muon emitted in center-of-mass directions largely opposite to the π^+ direction-of-motion. Muons are emitted isotropically in the π^+ center-of-mass, and have a helicity of -1 in this decay frame. Because of the range chamber acceptance, in the lab system the average muon polarization components are zero except for the component along the π^+ direction-of-motion. Only muons in a backward cone about this direction satisfy the range requirement, so in the lab this polarization component will be large and positive. For each region along the π^+ path, as given in Table V, we calculated the limits of acceptable center-of-mass decay angles, and from these limits found the corresponding muon polarization.

Using the decay-in-flight probabilities, p_{DIF}, calculated for each region, we then found the average muon longitudinal polarization for all these background events; our result was $P_L = +0.7$.

b) $K_{\pi 2}$ events with π-nuclear interaction

Nuclear interaction of the π^+ in the range chamber provides an additional source of background events from the $K_{\pi 2}$ decay mode. If the π^+ interacts in the range chamber, with no secondary continuing through the anti-counter, T5, the $K_{\pi 2}$ decay will satisfy the trigger requirements for the $K_{\mu 3}$ data. This decay will be a background event present in the $K_{\mu 3}$ data after analysis if it is not eliminated by the kinematic test for $K_{\pi 2}$: the requirement that $\delta > -0.9$. The fraction of such $K_{\pi 2}$ events with respect to actual $K_{\mu 3}$ events is given by:

$$F_{NI} = \frac{N(K_{\pi 2}^{NI})}{N(K_{\mu 3})} = p_{NI} \cdot f_\delta \cdot R \qquad \text{(V-5)}$$

where

$$R = \frac{\Gamma_{\pi 2}}{\Gamma_{\mu 3}} \cdot \frac{f_s^{\pi 2}}{\sum\limits_{\text{allowed } E_\mu} f_s^{\mu 3} \cdot \frac{\Delta\Gamma_{\mu 3}}{\Gamma_{\mu 3}\Delta E_{\mu 3}} \cdot \Delta E_{\mu 3}} \qquad \text{(V-6)}$$

In Eq. V-5, p_{NI} is the probability of a π^+ interacting in the 9.9 gr/cm^2 aluminum equivalent of the range chamber. The factor f_δ is the fraction of $K_{\pi 2}$ decays that escape the cut, $\delta > 0.9$ as shown in the previous section, $f_\delta = 5.5 \times 10^{-2}$. The quantity R is the ratio of the probability of a $K_{\pi 2}$ decay with a detectable π^o to the corresponding probability of $K_{\mu 3}$ decays with detectable π^o and μ^+. As defined in Eq. V-6, R was used in the estimate of the background from π^+ decay-in-flight; in the

previous section we found:

$$R = 43.1 \text{ (degrader a)}$$
$$= 41.9 \text{ (degrader b)}$$

The kinetic energies of the π^+ reaching the counters defining the range acceptance are as follows:

	degrader ($K_{\mu 3}$) a	b
T_π at T4	70 MeV	80 MeV
T_π at T5	46 MeV	57 MeV

To calculate the interaction probability p_{NI} we need to know the π^+ aluminum inelastic cross-section at π kinetic energies from 50 to 80 MeV. $K_{\pi 2}$ decays with subsequent elastic π^+-nucleus interactions in the range chamber (or in degrader before the chamber) will not contribute to the $K_{\pi 2}$ background, as the π^+ generally will undergo little energy loss or change of direction, and so will be vetoed by the anticounter. Using the available measurement[11] of the π^+ <u>total</u> cross section on carbon, from 40 to 70 MeV,

$$\sigma_{TOT} \cong 98 \text{ mb}$$

we find for the upper limit

$$p_{NI} \leq 2.2 \times 10^{-2} \quad .$$

From Eq. V-5, we determine the fractional background to be

$$F_{NI} \leq 5.3 \times 10^{-2} \quad .$$

This estimate of the nuclear interaction background from $K_{\pi 2}$ decays is an upper limit, as it includes those interactions which were actually vetoed by the anti-counter. Additionally, in the background estimate

we did not account for the selection of events by the requirement that the particle stopping in the range chamber have an apparent μ-e decay. A study of events normally eliminated from the $K_{\mu 3}$ data, because of $\delta \sim -1$, showed that the $K_{\pi 2}$ background events had a percentage of "μ-e decays" half that of the events considered $K_{\mu 3}$. Since the decay-in-flight events are expected to be a significant source of $K_{\pi 2}$ background, we infer that the hand scanning of the range chamber results in a further reduction of the π-nuclear interaction background. The decay-in-flight events have genuine μ-e vertices in the range chamber, and are indistinguishable from $K_{\mu 3}$ events on the scanning table, while inelastic π-nucleus events may be rejected because of a multi-track vertex, or simply interpreted as having no visible decay.

τ' Background Calculation

The τ and τ' decays, $K^+ \rightarrow \pi^+ + \pi^+ + \pi^-$ and $K^+ \rightarrow \pi^+ + \pi^o + \pi^o$, occur with branching ratios[10] 5.5% and 1.7%, respectively. Although three times as frequent, the τ decay contributes less than the τ' mode toward background events in the $K_{\mu 3}$ mode. Both τ and τ' decays must satisfy the range requirement; additionally, a τ decay must charge exchange to produce a π^o and must have no charged particle penetrating the cup counter which shields the shower chambers. We shall estimate the background contributed by the τ' mode and show this contamination, and hence that from the τ mode, to be negligible.

The maximum π^+ kinetic energy in the τ' mode is 53.2 MeV, 5 MeV below the minimum of 58 MeV required for a π^+ to reach T4. The lower limits in the π^+ energy, imposed by the range criterion, for each degrader condition are:

degrader	min. T_{π^+}	% of $K_{\mu 3}$ data taken
a	68	82.8
b	58	17.2

We calculated the contribution to the $K_{\mu 3}$ data of τ' decays with the π^+ satisfying the range requirment by straggling or slight uncertainties in the range estimate--such as that due to the uncertainty in the K^+ stopping position. The observed range of π^+ events in a study of the $K_{\pi 2}$ decay mode fits a Gaussian distribution with a standard deviation $\sigma = 3$ MeV. Using this value of σ (an over estimate for data taken with a $K_{\mu 3}$ degrader) we smeared the theoretical π^+ energy spectrum in τ' decay:

$$w'(E_\pi) = \int_0^{E_0} dE'\ w(E')\ \frac{1}{\sqrt{2\pi}\cdot\sigma}\ e^{-(E'-E)^2/2\sigma^2}\ . \qquad \text{(V-7)}$$

Here E_0 is the maximum π^+ energy (192.8 MeV), and $w(E')$ is the theoretical π^+ spectrum, assumed pure phase space:

$$w(E') = \frac{8\pi^2 p'_\pi \sqrt{E_0 - E'_\pi}}{\sqrt{E_0 - E'} + \frac{2m_{\pi^0}^2}{m_K^2}}\ . \qquad \text{(V-8)}$$

As noted by Rossi[12], the distribution in range of a particle of given energy is Gaussian, to an accuracy of a few percent; this approximation is sufficiently precise for our calculation.

Recent experiments[13] have shown that the π^+ spectrum is not given by phase space, but more accurately by a linear matrix element of the form

$$M(T_\pi) \sim 1 + a\left[\frac{2T_\pi}{T_\pi^{max}} - 1\right]$$

with T_π the π^+ kinetic energy, and T_π^{max} its maximum. Since the constant a has been found to be negative,[13] our calculations, involving the upper end of the π^+ spectrum, give an overestimate of the τ' background.

From Eq. V-7 we calculated the tail of the experimental π^+ spectrum extending into the range chamber. We found the contribution of this direct τ' decay to $K_{\mu 3}$ data to be very small:

$$F_{\tau',\text{direct}} = \frac{N(\text{direct } \tau')}{N(K_{\mu 3})} < 10^{-4}\ .$$

a)

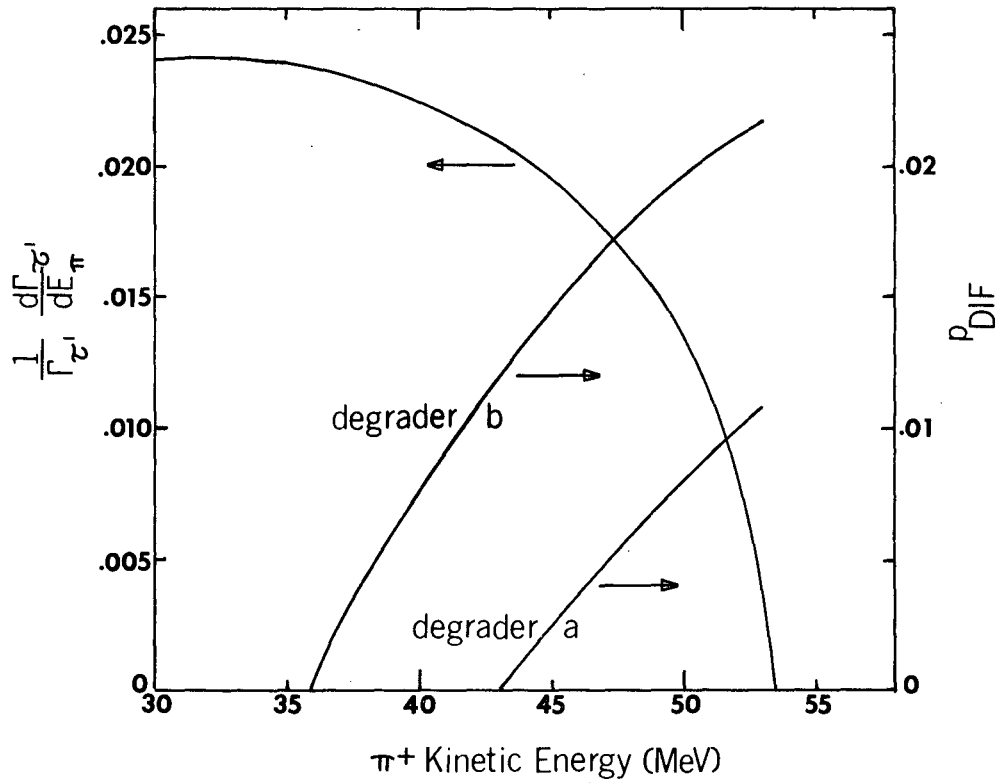

b)

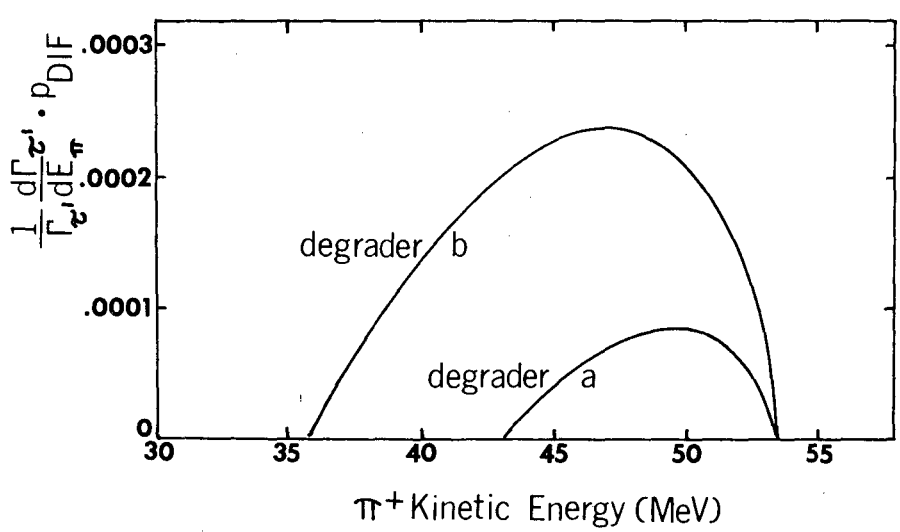

XBL 686-931

Fig. 12. Study of τ' mode: a) π^+ differential energy spectrum, on the left, and the factor p_{DIF} for the two degrader conditions, shown on the right; p_{DIF} is the calculated probability of an acceptable π^+ decay-in-flight. b) Product of π^+ energy spectrum and the decay-in-flight factor p_{DIF}, for the two degrader conditions.

A more serious source of background comes from τ' decays in which the π^+ decays-in-flight. The position of these events to actual $K_{\mu 3}$ events is given by

$$F_{\tau' DIF} = \frac{N(\tau' DIF)}{N(K_{\mu 3})} = \frac{\Gamma_{\tau'}}{\Gamma_{\mu 3}} \cdot \frac{\sum_{\text{allowed } E_\pi} f_s^{\tau'} \cdot p_{DIF}^{\tau'} \cdot \frac{\Delta\Gamma_{\tau'}}{\Gamma_{\tau'}\Delta E_\pi} \cdot \Delta E_\pi}{\sum_{\text{allowed } E_\mu} f_s^{\mu 3} \cdot \frac{\Delta\Gamma_{\mu 3}}{\Gamma_{\mu 3}\Delta E_\mu} \cdot \Delta E_\mu} \quad . \qquad \text{(V-9)}$$

In Eq. V-9 $\Gamma_\tau'/\Gamma_{\mu 3}$ is the ratio of the τ' and $\mu 3$ rates, p_{DIF} is the probability of a π^+ decay-in-flight with the μ^+ accepted by the range chamber, and $f_s^{\tau'}$ is the π^o reconstruction efficiency for τ' decays. In the denominator of Eq. V-9 we sum over muon energies allowed by the range chamber the product of the calculated π^o reconstruction efficiency for $K_{\mu 3}$ events, $f_s^{\mu 3}$, times the $K_{\mu 3}$ differential μ^+ spectrum. In Eq. V-6 we gave this same term in calculating the $K_{\pi 2}$ background.

We calculated the decay-in-flight probability, p_{DIF}, for π^+ from τ' decays as previously described for π^+ from the $K_{\pi 2}$ mode. By combining the individual probabilities for decay-in-flight, with muon of proper range, at each successive degrader along the π^+ path, we found the overall probability p_{DIF} for an acceptable decay-in-flight. We determined this factor as a function of the initial π^+ energy, rather than at a single point as for $K_{\pi 2}$; the results are plotted for the two degrader conditions in Fig. 12. Also shown in this figure is the π^+ energy spectrum, calculated from Eq. V-8, and the product of the spectrum with the decay-in-flight probability, p_{DIF}.

Using Monte Carlo techniques we determined the π^o reconstruction efficiency for τ' decays, $f_s^{\tau'}$. For a given π^+ energy we generated τ' decays and noted the fraction of events that passed a series of reconstruction stages. We repeated the calculations for various values T_μ, between 55 and 85 MeV, of the assumed muon kinetic energy, observed in the range chamber. We found no significant dependence of the reconstruction probability upon T_μ. In Fig. 13 we show the results for the efficiency, at successive stages of reconstruction, as a function of the π^+ kinetic energy. The top line represents the probability of 2 (and only 2) showers being detected; this calculation used the same criteria as described previously in the discussion of the $K_{\pi 2}$ background. The second line from the top reflects the requirement that the π^o be reconstructable so as to allow the event to lie on the $K_{\mu 3}$ Dalitz plot, while the third line shows the effect of the additional requirement that $\delta > -.09$ (the test for $K_{\pi 2}$ kinematics). The final efficiency $f_s^{\tau'}$ is given by the bottom line, reflecting the requirement that the shower energies correspond to those predicted by one of the possible $K_{\mu 3}$ kinematical configurations. This test was made in the same manner on the actual $K_{\mu 3}$ data, and is given by Eq. IV-1. The stages of reconstruction reflected in Fig. 13 are the same as used in the calculation of $f_{\mu 3}^s$, and shown in Fig. 11; for the $K_{\mu 3}$ events the second and fourth step have no effect on the efficiency.

From the results shown in Figs. 11 and 13, and from the previously mentioned calculation of the $K_{\mu 3}$ acceptance, we found, with Eq. V-9,

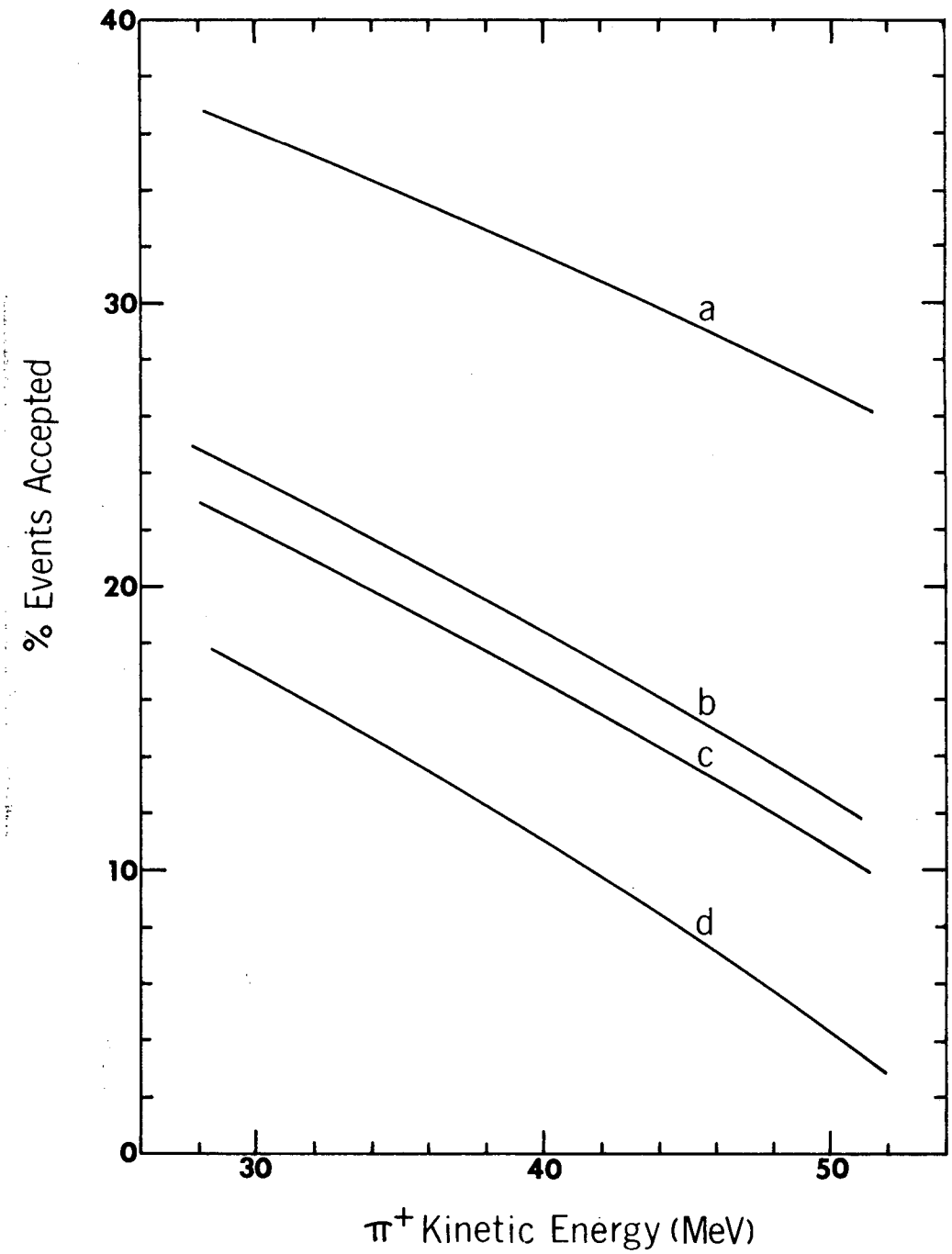

XBL 685-894

Fig. 13. Calculated acceptance for τ' events: a) events with two γ's detected, b) events with reconstructable π^o, fitting $K_{\mu 3}$ kinematics, c) events with $\delta > -0.9$, d) events whose shower energies match those predicted by $K_{\mu 3}$ kinematics.

$$F_{\tau'_{DIF}} = 2.38 \times 10^{-4} \text{ , degrader a}$$

$$1.61 \times 10^{-3} \text{ , degrader b}$$

and for all the data,

$$F_{\tau'_{DIF}} = \frac{N(\tau'_{DIF})}{N(K_{\mu 3})} \cong 5 \times 10^{-4} .$$

$K_{\pi\pi\gamma}$ Background

We calculated the contribution of the decay $K^+ \rightarrow \pi^+ + \pi^o + \gamma$ to the background in $K_{\mu 3}$ events. The fraction of $K_{\pi\pi\gamma}$ background events to actual $K_{\mu 3}$ events in our data is given by:

$$F_{\pi\pi\gamma} = \frac{\Gamma_{\pi\pi\gamma}}{\Gamma_{\mu 3}} \cdot \frac{A(\pi\pi\gamma)}{A(\mu 3)} \qquad \text{(V-10)}$$

with

$$A(\pi\pi\gamma) = \sum_{\text{allowed } E_\pi} f^s_{\pi\pi\gamma} \cdot \frac{\Delta\Gamma_{\pi\pi\gamma}}{\Gamma_{\pi\pi\gamma}\Delta E_\pi} \cdot \Delta E_\pi \qquad \text{(V-11)}$$

$$A(\mu 3) = \sum_{\text{allowed } E_\mu} f^s_{\mu 3} \cdot \frac{\Delta f_{\mu 3}}{\Gamma_{\mu 3}\Delta E_{\mu 3}} \cdot \Delta E_\mu \, . \qquad \text{(V-12)}$$

The factors given by Eq. V-11 and V-12 are the integrated products of the charged particle differential rate times the reconstruction efficiency at the given energy; the sums are over the charged particle energies allowed by the range chamber. The factor $A(\mu 3)$ was used in the $K_{\pi 2}$ and τ' background estimates, where we found:

$$\begin{aligned} A(\mu 3) &= 7.8 \times 10^{-2} \text{ , degrader a} \\ &= 8.1 \times 10^{-2} \text{ , degrader b .} \end{aligned} \qquad \text{(V-13)}$$

To determine the acceptance $A(\pi\pi\gamma)$ we assumed the $K_{\pi\pi\gamma}$ decay proceeded purely by inner bremsstrahlung with the matrix element given by[14]

$$M \sim \left(\frac{p_K}{p_K \cdot p_\gamma} - \frac{p_+}{p_+ \cdot p_\gamma} \right) \cdot \varepsilon \qquad \text{(V-14)}$$

where p_K, p_+, p_γ are the K^+, π^+, and γ four-momenta, respectively, and ε is the photon polarization vector. Fig. 14 shows the π^+ energy spectrum derived from this matrix element. We used a Monte Carlo analysis to determine $f^s_{\pi\pi\gamma}$, the π^o reconstruction efficiency. For different values of the π^+ energy we generated large samples of events using the decay distribution which follows from Eq. V-14. These events were subjected to the same reconstruction criteria used in calculating the corresponding efficiency for $K_{\mu 3}$, $f^s_{\mu 3}$. The result for the factor $f^s_{\pi\pi\gamma}$ as a function of the π^+ energy is shown in Fig. 15. The upper curve gives the fraction of $K_{\pi\pi\gamma}$ events with two detectable gamma-ray showers; this curve approaches 55% at high E_π, the value found for the kinematically similar $K_{\pi 2}$ decay. We found that all the $K_{\pi\pi\gamma}$ events with observable showers were reconstructable as $K_{\mu 3}$ events, as were the $K_{\pi 2}$ events. In this calculation we took as the muon energy for each event that energy corresponding to the "observed" π^+ range. Curve b in Fig. 15 reflects the additional requirment on the $K_{\pi\pi\gamma}$ events that $\delta > -0.9$; this selection eliminates events by increasing amounts as the decay configuration approaches that of $K_{\pi 2}$. The final requirement, that of goodness-of-fit to $K_{\mu 3}$ kinematics is met by all the $K_{\pi\pi\gamma}$ events.

With the results for $d\Gamma_{\pi\pi\gamma}/dE_\pi$ and $f^s_{\pi\pi\gamma}$ we estimated from Eq. V-10 the $K_{\pi\pi\gamma}$ background for the two degrader conditions:

$$F_{\pi\pi\gamma} = 1.48 \times 10^{-2} \text{ , degrader a}$$

$$= 1.33 \times 10^{-3} \text{ , degrader b}$$

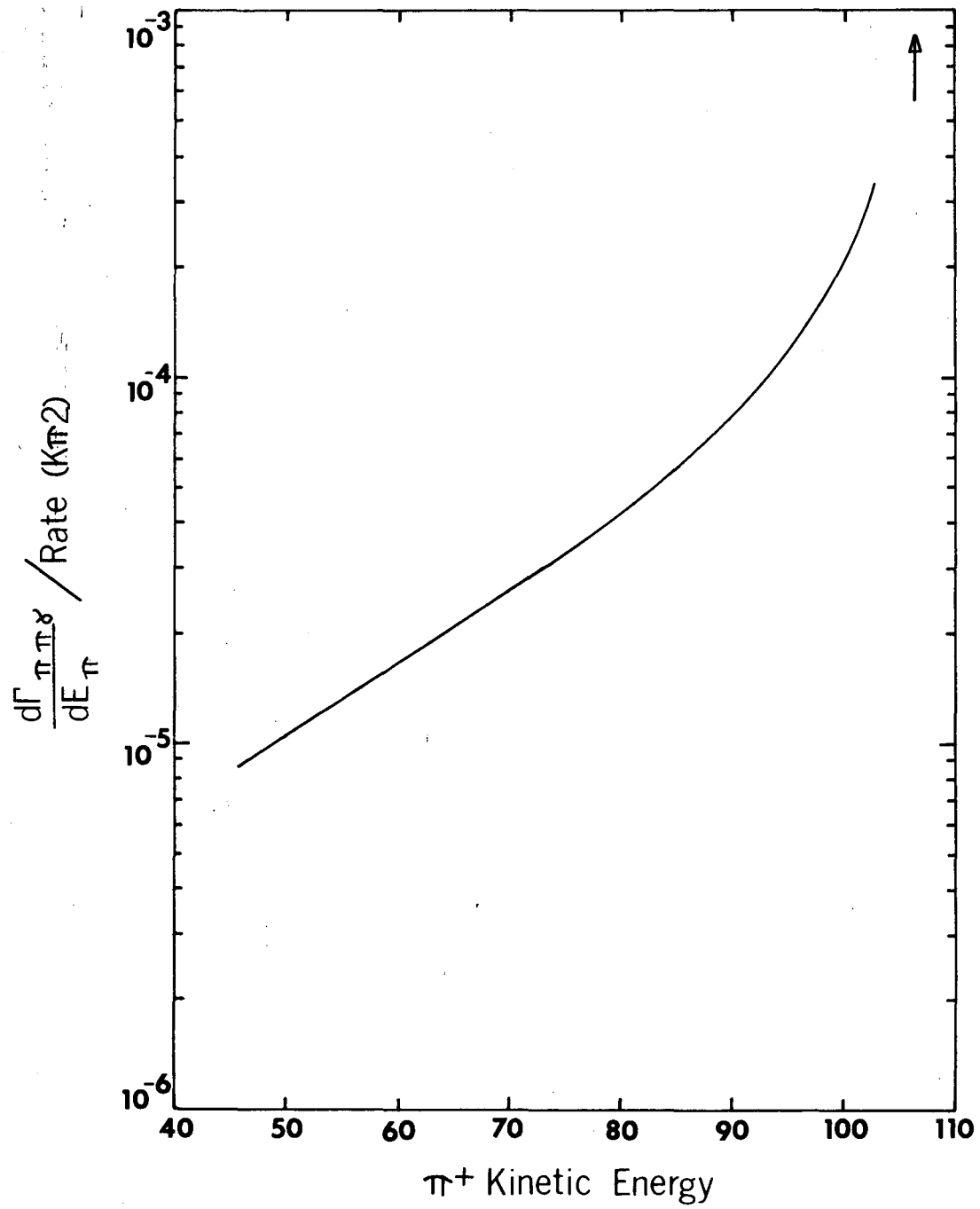

XBL 685-893

Fig. 14. Calculated π^+ differential energy spectrum in $K^+ \rightarrow \pi^+ + \pi^0 + \gamma$ (inner bremstrahlung only).

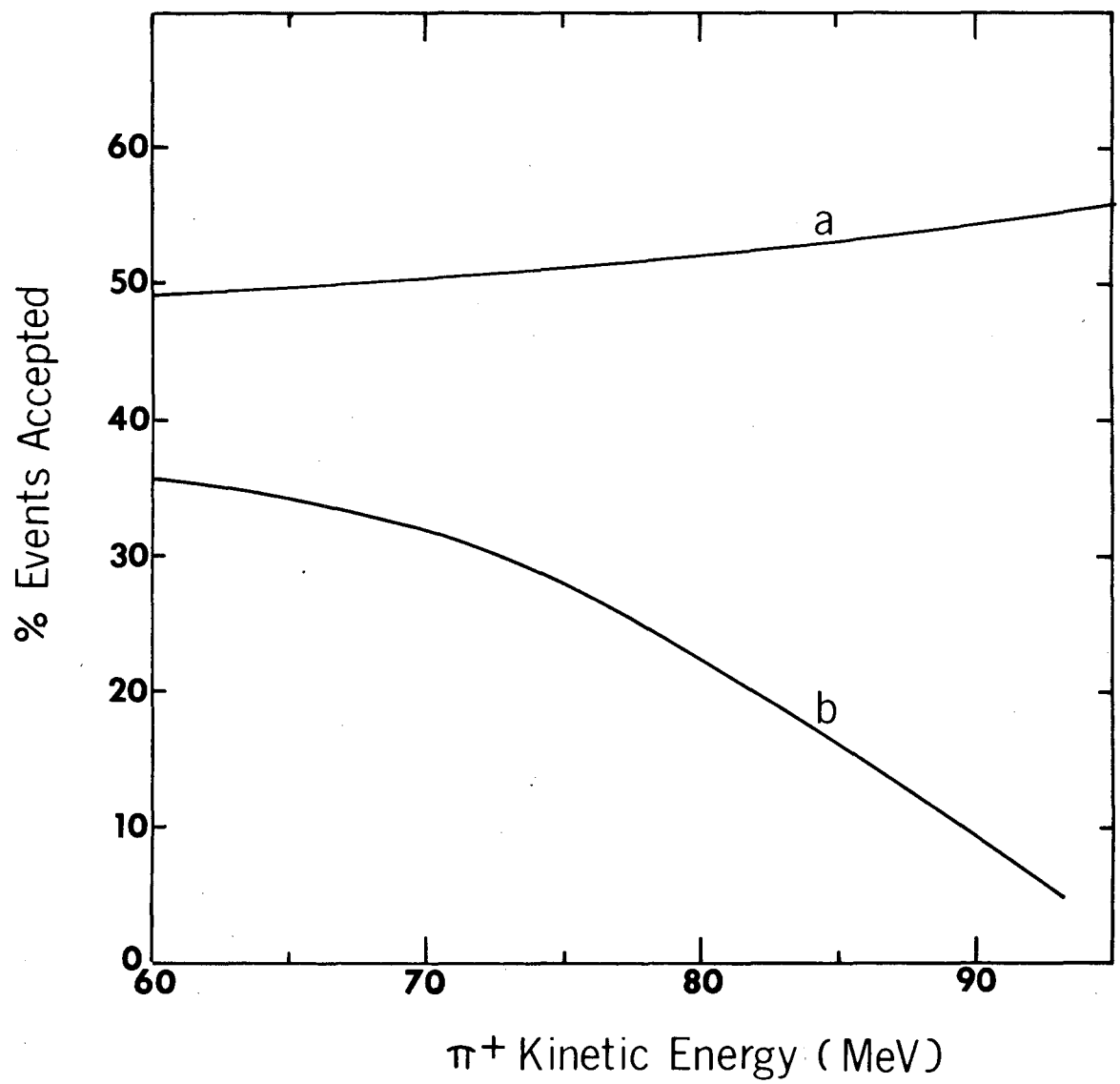

XBL 685-892

Fig. 15. Calculated acceptance for $K_{\pi\pi\gamma}$ events: a) events with π^0 detected, b) events with $\delta > -0.9$.

or, for all the $K_{\mu 3}$ data:

$$F_{\pi\pi\gamma} \cong 1.4 \times 10^{-2} .$$

This estimate is an upper limit, as it does not include the reduction in $K_{\pi\gamma\gamma}$ background events by π^+ nuclear interactions between the K^+ decay position and the range chamber.

From these background events we expect to observe μ-e decays with the decay electron direction uniformly distributed. Each muon is fully polarized; but, because of the low muon energy, we do not observe its momentum direction. Since the decay muon is emitted isotropically, the decay electrons will also be isotropic, and we measure zero polarization.

K_{e3} Background

We estimated the amount of background contributed by the K_{e3} decay mode, $K^+ \rightarrow \pi^o + e^+ + \nu$. The fraction of such events relative to the number of $K_{\mu 3}$ events is

$$F_{e3} = \frac{N(K_{e3})}{N(K_{\mu 3})} = f_{C\mu} \cdot f_r \cdot \frac{\Gamma_{e3}}{\Gamma_{\mu 3}} \cdot \frac{A(e3)}{A(\mu 3)} \qquad \text{(V-15)}$$

with

$$A(e3) = \sum_{\text{allowed } E_e} f_s^{e3} \cdot \frac{\Delta\Gamma_{e3}}{\Gamma_{e3}\Delta E_e} \cdot \Delta E_e \, . \qquad \text{(V-16)}$$

The acceptance factor for K_{e3} events, $A(e3)$, is the product of the π^o reconstruction efficiency with the e^+ differential spectrum, summed over the electron energies accepted by the range chamber. The factor $A(\mu 3)$ is similarly defined, and is given by Eq. V-13. The K_{e3} decay must give a pulse in T4, the counter at the front of the range chamber, without being vetoed either by the water Cherenkov counter C_μ, or by the counter T5, at the end of the range chamber. We determined by measurement with the cosmic-ray muons that the efficiency of the Cherenkov counter was 99.8 percent for particles with $\beta \sim 1$. To allow for the processes in which an e^+ annihilates in front of the Cherenkov counter, with a subsequent pair production before T4, we take the fraction f_{C_μ} of K_{e3} events surviving the C_μ veto to be 0.01. We estimate the fraction f_r of events reaching T4 which are not vetoed by T5 to be 25 percent.

In Fig. 16 we show the results of a Monte Carlo calculation of the reconstruction factor f_s for K_{e3} events. We calculated this

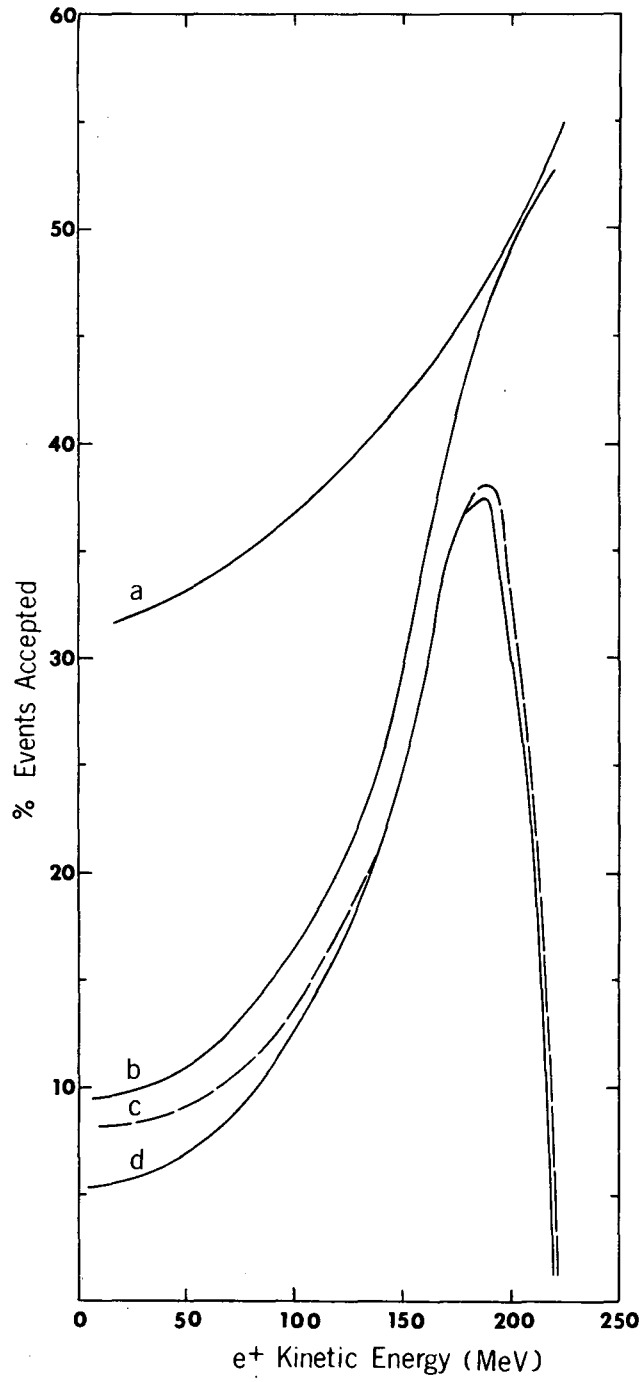

XBL 685-895

Fig. 16. Calculated acceptance for K_{e3} events: a) events with two γ's detected, b) events with reconstructable π^o, fitting $K_{\mu 3}$ kinematics, c) events with $\delta > -0.9$, d) events whose shower energies match those predicted by $K_{\mu 3}$ kinematics.

efficiency as a function of the electron energy as well as the energy assumed for the "muon" in the attempt to reconstruct the event as a $K_{\mu 3}$. The dependence of f_s^{e3} upon the assumed "muon" energy, varied within the limits imposed by the range criteria, was not significant. As shown in Fig. 16, K_{e3} events at the low energy end of the electron spectrum are generally not reconstructable as $K_{\mu 3}$ events, with the "muon" assumed to have ~ 70 MeV kinetic energy. The gamma-ray showers generated for K_{e3} events with high electron energies are easily reconstructable into a π^o consistent with $K_{\mu 3}$ kinematics. Many of these latter events are eliminated by the criterion that $\delta > -0.9$, the elimination of events with $K_{\pi 2}$ kinematics.

Using the differential electron spectrum for vector interaction[9] we calculated the acceptance defined by Eq. V-16, summing over all electron energies fromthe minimum required by T4 to the end of the electron spectrum, 228 MeV. The results for both degrader conditions are:

degrader	E_e^{Min}	A(e3)
a	88 MeV	0.17
b	59 MeV	0.18

With $\Gamma_{e3}/\Gamma_{\mu 3}$ given[10] by 1.41, we estimated the proportion of K_{e3} background events to $K_{\mu 3}$ events, using Eq. V-15, to be

$$F_{e3} = 7.7 \times 10^{-3} \text{ , degrader a}$$

$$= 7.9 \times 10^{-3} \text{ , degrader b}$$

or, for all $K_{\mu 3}$ data,

$$F_{e3} \sim 0.8 \times 10^{-2} .$$

As with the background $K_{\pi 2}$ events (with π-nuclear interaction) we expect that many K_{e3} events are eliminated in the scanning for μ-e decays. Both sources of backgrounds do not have associated μ-e decays in the range chamber, and the frequency of these background "decays" is independent of the time delay of the range chamber trigger. Our study of the percentage of events with μ-e decays for different time delays on the range chamber trigger is a direct experimental measurement of the amount of such backgrounds.

VI. RESULTS

A. Study of $K^+_{\mu 3}$ Decay

We obtained 3133 completely reconstructed $K_{\mu 3}$ events with observed μ-e decays. The Dalitz plot of these events is shown in Fig. 17, where for clarity we have grouped the events in bins of 20 and 10 MeV in π^o and μ^+ kinetic energy, respectively. Our apparatus accepted $K_{\mu 3}$ decays with the μ^+ kinetic energy, T_μ, equal to 70 ± 20 MeV, but with the full spectrum of T_π. For given T_μ the data are strongly peaked toward high values of T_π, reflecting the basic interaction structure, given by Eq. I-3, as well as the increased efficiency of the apparatus in detecting a π^o of high energy and direction opposite to the μ^+.

Figure 18 gives the angular distributions of the electron momentum vector for the μ-e decays associated with the 3133 $K_{\mu 3}$ events which satisfy all the selection criteria. These distributions refer to the coordinate system $\hat{\epsilon}_L$, $\hat{\epsilon}_T$, $\hat{\epsilon}_\perp$ defined by Eq. II-5. For illustration the data are grouped in bins of 0.1 in the cosines. The lines drawn show the distributions expected for decays of muons with average polarization components as found by the likelihood analysis. These lines are normalized to the total of 3133 events with

$$\hat{p}_e \cdot \hat{\epsilon}_L < 0.9.$$

The events eliminated by this cut would have appeared in the bin furthest to the right in the top graph. These events have also been excluded from the lower two graphs. The effect of this selection is evident in Fig. 18; the loss of events with the electron momentum vector along $\hat{\epsilon}_L$ is reflected by the depletion of events with small cosines with respect to the axes $\hat{\epsilon}_T$ and $\hat{\epsilon}_\perp$.

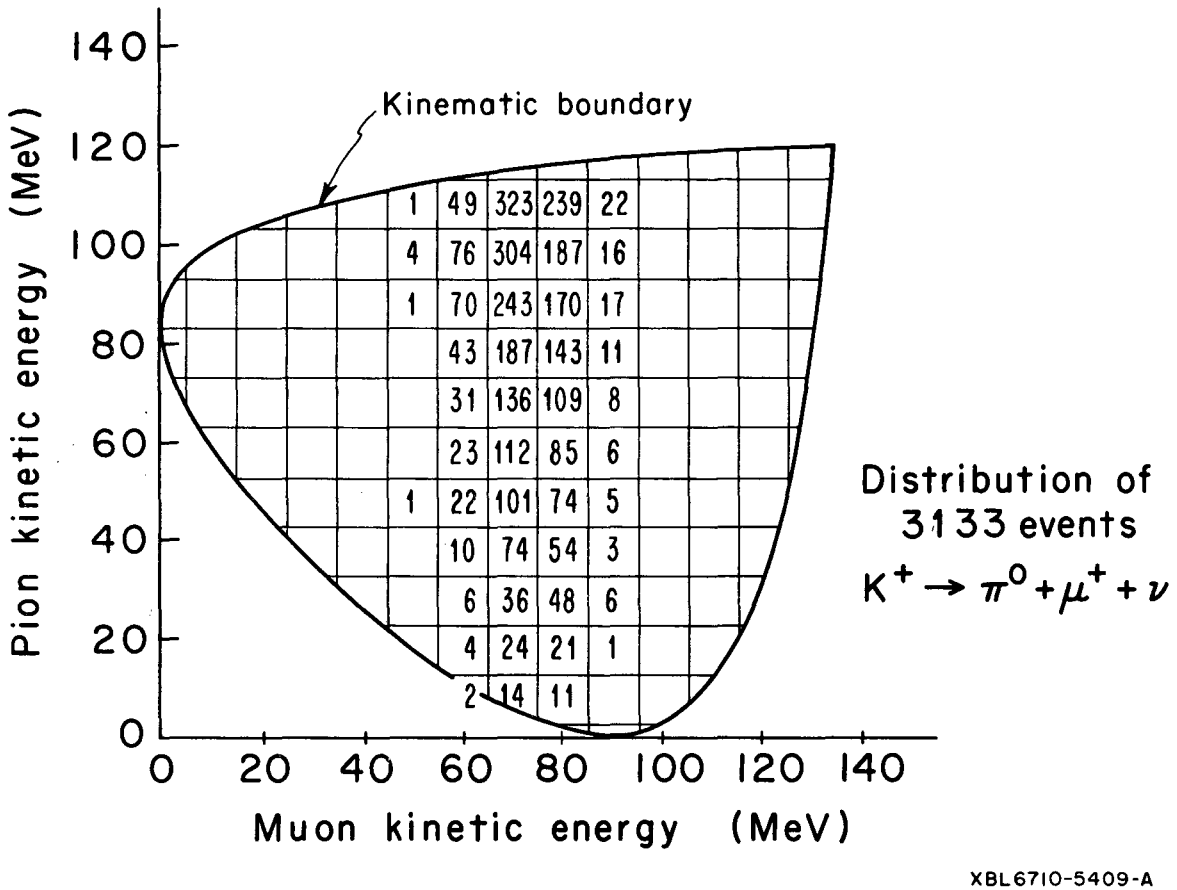

Fig. 17. Dalitz plot of 3133 $K^+_{\mu 3}$ events.

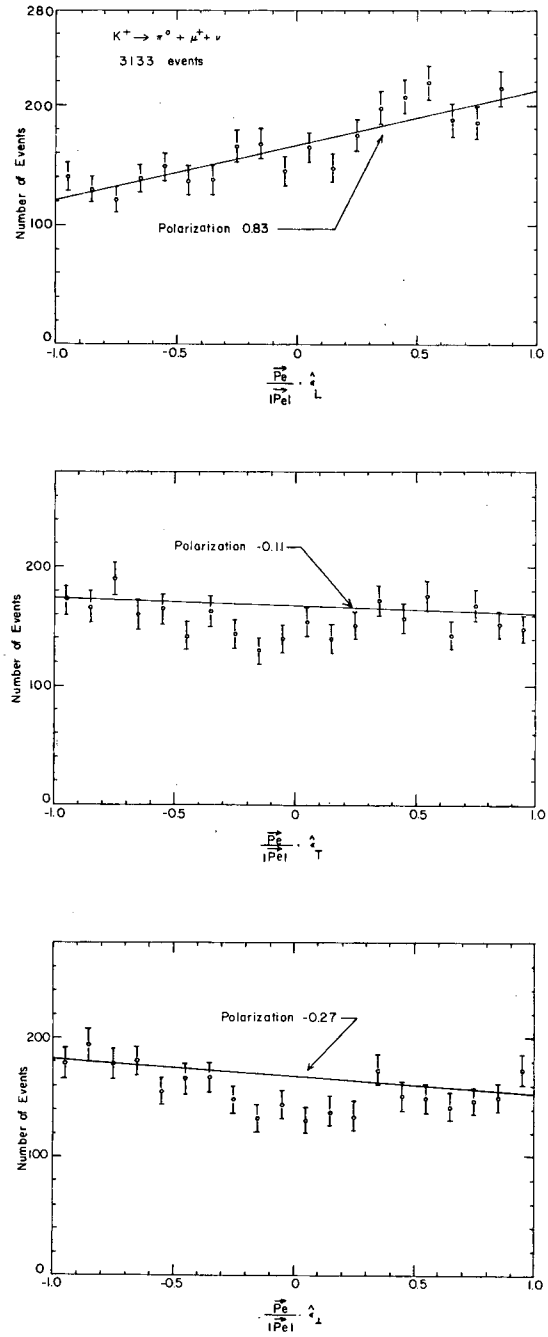

XBL 686-1053

Fig. 18. Angular distribution of the electron momentum vector in μ-e decays, from 3133 $K^+_{\mu 3}$ events, referred to the axes $\hat{\epsilon}_L, \hat{\epsilon}_T, \epsilon_\perp$. The lines drawn are normalized to the 3133 events with $\hat{p}_e \cdot \hat{\epsilon}_L < 0.9$. The dip in the lower two graphs for cosines near zero reflects the loss of events with $\hat{p}_e \cdot \hat{\epsilon}_L > 0.9$. Because of this cut, the data points are not expected to fit the solid lines.

The likelihood functions for the muon polarization components for all the $K_{\mu 3}$ events are shown in Fig. 19. These components are along the longitudinal, transverse, and perpendicular axes $(\hat{\epsilon}_L, \hat{\epsilon}_T, \hat{\epsilon}_\perp)$ defined for each K^+ decay, and given by Eq. II-5. As seen in Fig. 2, muons from events with high π^o energy are expected to be strongly polarized in the longitudinal direction. This prediction agrees with the result of Fig. 19, an average over the Dalitz plot and hence heavily weighted toward high T_{π^o}. The component of polarization out of the decay plane is -0.1 ± 0.1, consistent with zero and time reversal invariance, while the perpendicular component is small and negative as predicted in Fig. 2. Since these components are averages over the Dalitz plot, they are not expected to form a unit vector; it is for a particular event, with specified kinematics, that the muon should be fully polarized in some direction. In Table VI we tabulate the results for the μ^+ polarization components for all the events and in separate bins in the π^o kinetic energy.

Table VI. Muon polarization components, $K^+_{\mu 3}$ events.

T_{π^o} (MeV)	q^2_{ave} $(MeV)^2$	Events	P_L	P_T	$P_\perp$	ΔP
> 76.5	3.70×10^4	2258	+0.9	-0.1	-0.2	each ± 0.1
46.5-67.5	7.18×10^4	488	+0.8	-0.2	-0.1	each ± 0.2
28.5-46.5	9.09×10^4	265	+0.8	-0.2	-0.8	each ± 0.3
0.0-28.5	11.0×10^4	122	-0.1	+0.5	-1.1	each ± 0.5
all events	4.95×10^4	3133	+0.8	-0.1	-0.3	each ± 0.1

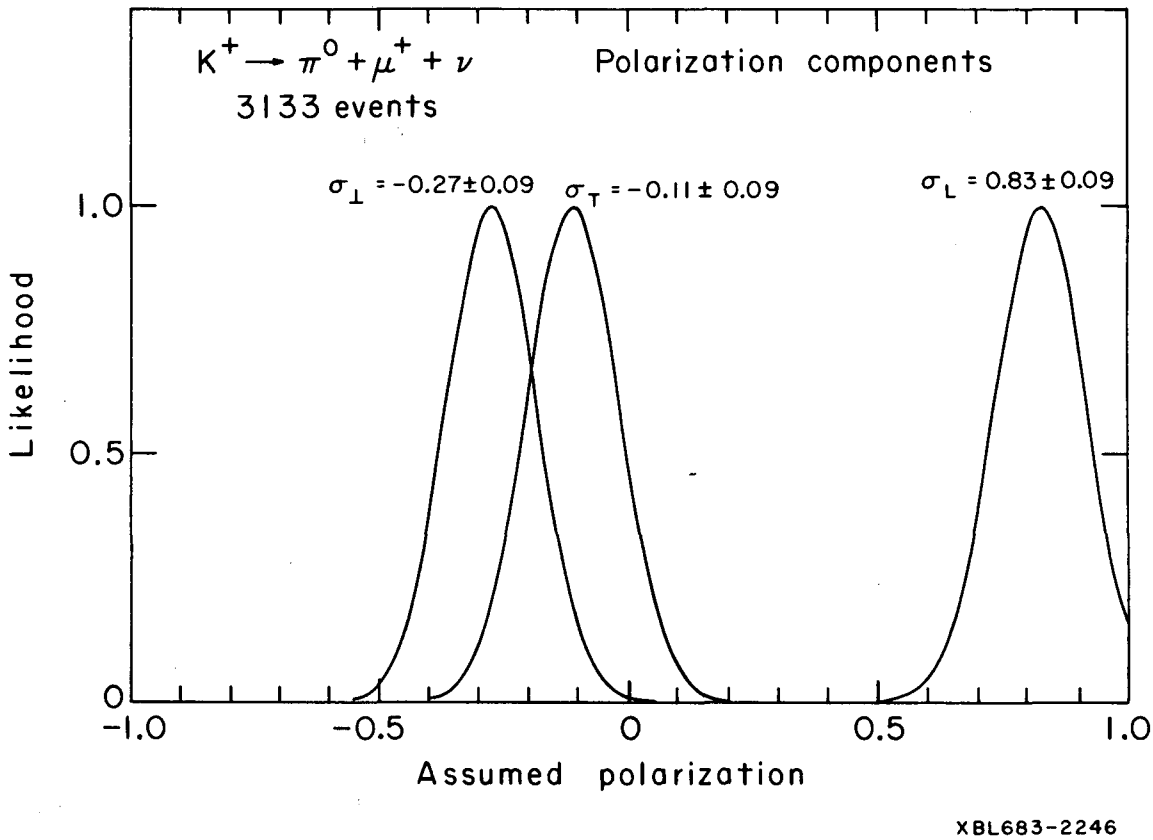

Fig. 19. Likelihood functions for average muon polarization components in 3133 $K^+_{\mu 3}$ events.

For each bin we list the average value of q^2, the square of the momentum transfer to the leptons; in the K^+ rest frame:

$$q^2 = m_K^2 + m_{K^o}^2 - 2m_{\pi^o}E_{\pi^o}.$$

Most of our data are in the low q^2 (high π^o energy) region of the Dalitz plot. The bins were chosen to give equal accuracy in the measurement of ξ; they are of unequal size, due to the varying sensitivity of the polarization method over the Dalitz plot. As noted in Table VI for high q^2 (low T_{π^o}) events, we found the μ^+ strongly polarized along the perpendicular axis with a small longitudinal component. For progressively lower bins in q^2 this perpendicular component decreases and the μ^+ becomes almost fully longitudinally polarized. This general variation of the polarization components over the Dalitz plot compares favorably with that predicted by Eq. II-6 and illustrated in Fig. 2.

We analyzed our data by the maximum likelihood method previously described to determine the value of the parameter ξ. For a given value of ξ the muon polarization direction is predicted for each completely reconstructed $K_{\mu 3}$ event. The solution for ξ is that value for which the electron decay directions in all the data best fit the expected angular distributions about the polarization axes. As discussed in the Introduction, ξ may be complex as well as energy-dependent. Figure 20 shows the result of the likelihood analysis of all the $K_{\mu 3}$ events for ξ assumed complex but constant. The three contours enclose 40%, 67%, and 96% of the volume under the two-dimensional likelihood function; the solution given in Table VII uses the middle contour as the limit of 1 standard deviation. We list in Table VII additionally the results

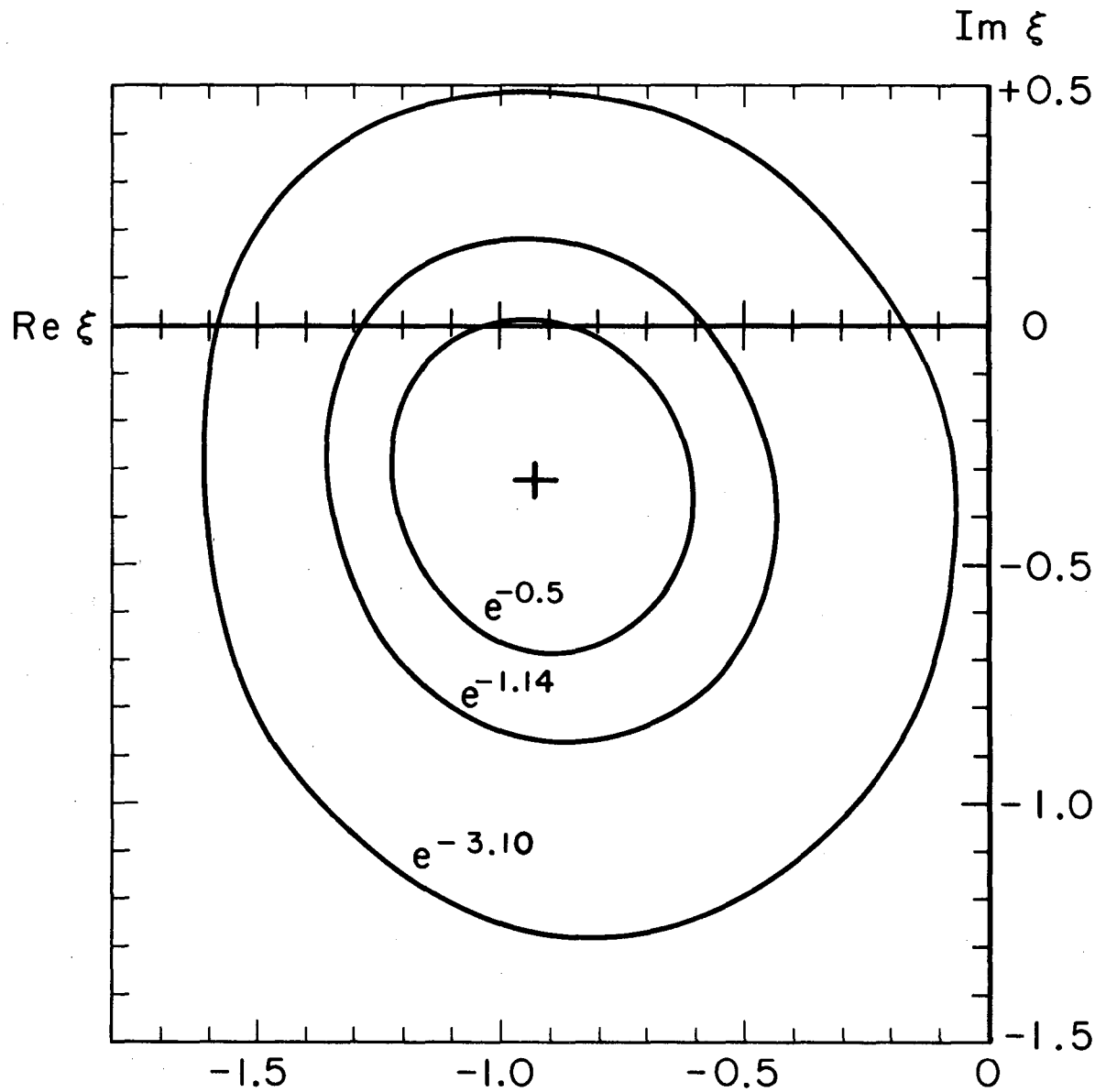

XBL682-1973

Fig. 20. Likelihood functions for ξ, assumed complex and constant, from 3133 $K^+_{\mu 3}$ events. The $e^{-1.14}$ contour corresponds to the limit of 1 standard deviation about the most probable value, Re ξ = -0.9, Im ξ = -0.3.

Table VII. Results for complex ξ.

q^2_{ave} $(MeV)^2$	Events	Re ξ	Im ξ
3.70×10^4	2258	$-1.0^{+1.0}_{-0.9}$	-0.8 ± 0.9
7.18×10^4	488	$-2.0^{+0.9}_{-0.8}$	$-0.7^{+0.9}_{-1.0}$
9.09×10^4	265	$-0.7^{+1.2}_{-0.9}$	$-0.3^{+0.9}_{-1.0}$
11.0×10^4	122	$-0.4^{+2.2}_{-1.4}$	$+0.8^{+1.8}_{-1.2}$
all events	3133	$-0.9^{+0.5}_{-0.4}$	-0.3 ± 0.5

for complex ξ from data binned in q^2. For each bin ξ is assumed constant; the errors again correspond to the middle ($e^{-1.14}$) contour. Time reversal invariance requires ξ be real; our measurement from all the data is consistent with Im $\xi = 0$, as can be seen in Fig. 20. This conclusion is unchanged by measuring Im ξ in separate bins in q^2. In terms of a phase angle φ defined by

$$\xi = |\xi| \, e^{i\varphi}$$

we find

$$|\xi| = 1.0 \pm 0.5$$

$$\varphi = (200 \pm 30)^\circ$$

with the error assigned from the $e^{-1.14}$ contour. This result is consistent with the requirement of time reversal invariance that φ be 0° or 180°.

Assuming ξ to be real and constant we obtain the results given

in Table VIII. The errors quoted are those appropriate to a 1 dimensional likelihood.

Table VIII. Results for ξ, assumed real.

q^2_{ave} $(MeV)^2$	Events	Re ξ (Im $\xi \equiv 0$)	P_{TOTAL}
3.70×10^4	2258	-0.9 ± 0.6	0.9 ± 0.1
7.18×10^4	488	-1.9 ± 0.55	0.8 ± 0.2
9.09×10^4	265	$-0.7 {}^{+0.7}_{-0.6}$	1.1 ± 0.3
11.0×10^4	122	$-0.2 {}^{+0.6}_{-0.7}$	1.2 ± 0.4
all events	3133	-0.95 ± 0.3	0.9 ± 0.1

The values for Re ξ from different bins in q^2 are consistent with each other and with the result for all the data:

$$\text{Re } \xi = -0.95 \pm 0.3 \quad (\text{Im } \xi = 0).$$

In Fig. 21 we have plotted our measurements of Re ξ as a function of q^2; they do not show any significant dependence of Re ξ upon q^2. Table VII shows that this conclusion is valid for complex ξ as well. To make this conclusion more quantitative, we express the energy dependence of ξ

$$\xi(q^2) = \xi_o(1 + \lambda\, q^2/m^2_{\pi^o}) \qquad \text{(VI-1)}$$

we can analyze the data in a two parameter likelihood to obtain the constants ξ_o and λ, assuming ξ real. Our result is

$$\xi_o = -1.2$$

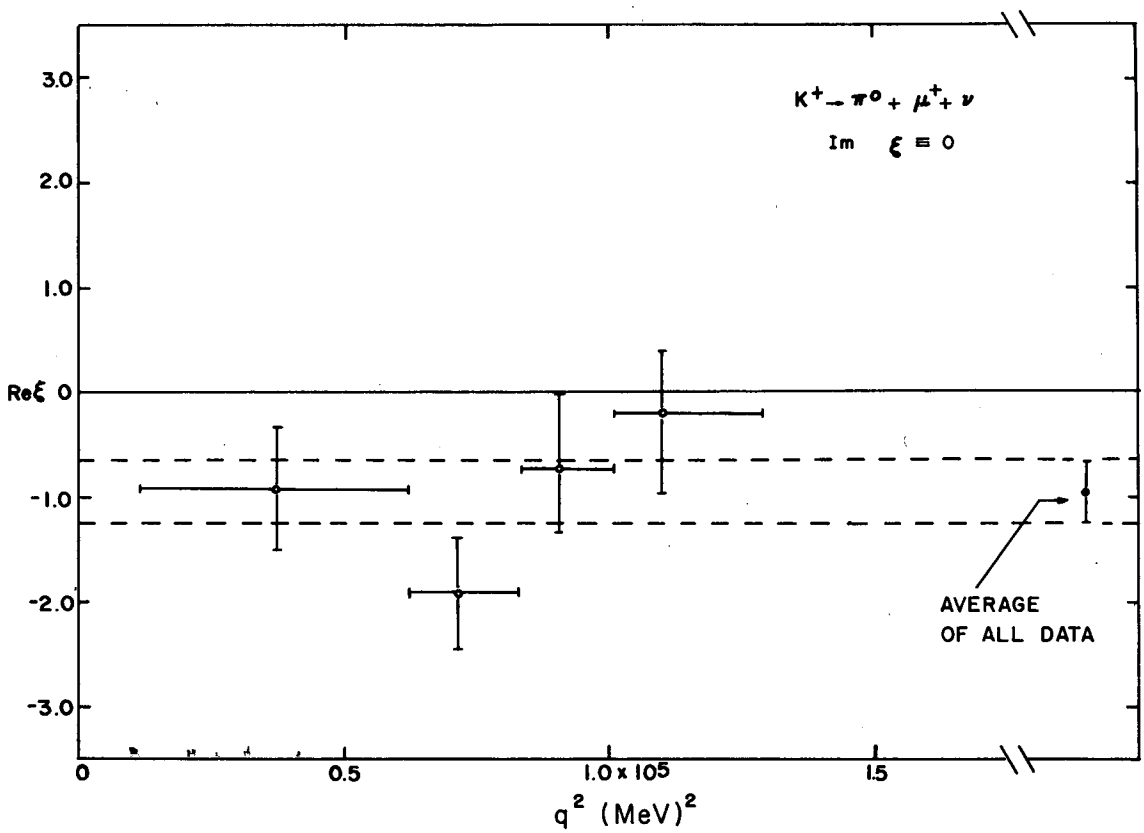

XBL 683-4806

Fig. 21. Results of likelihood analyses for ξ, assumed real and constant, from data in four bins of q^2. The result for all the data is also shown: $\xi = -0.95 \pm 0.3$.

$$\lambda = -0.04$$

with the contours giving the limits of 1 and 2 standard deviations as shown in Fig. 22. For any value of λ less than 0.3 in magnitude, ξ must be negative to be compatible with the data. The form of Eq. IV-1 is motivated by the expressions relating the form factors f_+ and f_- to masses of possible intermediate states:

$$f_\pm(q^2) = f_\pm(0)\cdot\frac{m_\pm^2}{m_\pm^2 - q^2} \qquad \text{(VI-2)}$$

where, if $m_\pm^2 \gg q^2$,

$$f_\pm(q^2) \cong f_\pm(0)\left(1 + \frac{q^2}{m_\pm^2}\right) \qquad \text{(VI-3)}$$

$$\cong f_\pm(0)\left(1 + \lambda_\pm \frac{q^2}{m_{\pi^o}^2}\right)$$

here

$$\lambda_\pm = m_{\pi^o}^2/m_\pm^2$$

so that the expansion VI-3 is good only for

$$\lambda_\pm \ll m_{\pi^o}^2/q^2$$

but since the range in q^2 is from m_μ^2 to $(m_K - m_{\pi^o})^2$ we have

$$\lambda_\pm < 0.2.$$

Accepting the value of $\lambda_+ \approx 0$, as measured,[15] we can write

$$\xi(q^2) = \frac{f_-(q^2)}{f_+(q^2)} = \xi(0)\left(1 + \lambda_- \frac{q^2}{m_{\pi^o}^2}\right)$$

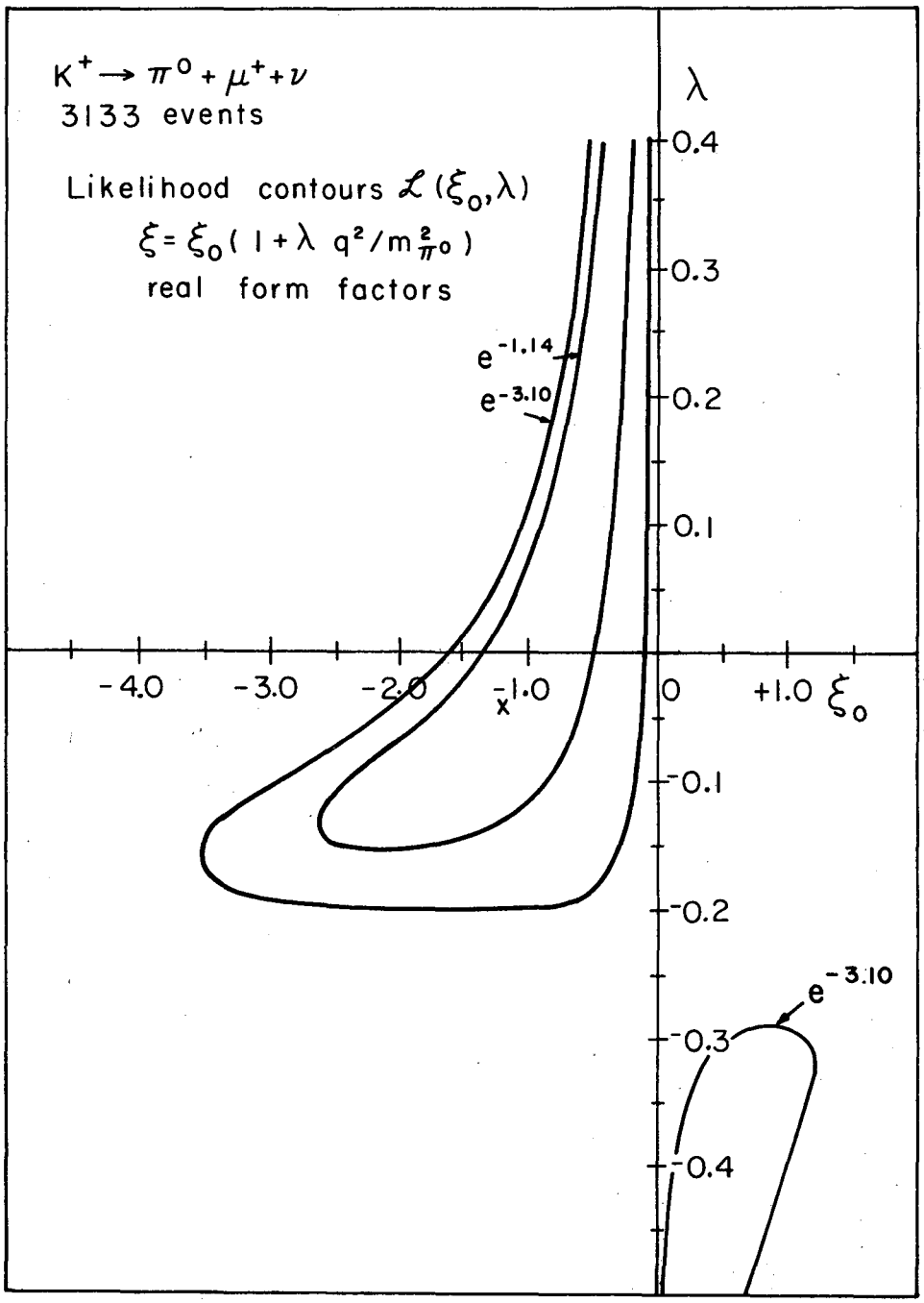

XBL683-2414

Fig. 22. Likelihood function for ξ, real and energy-dependent, from 3133 $K_{\mu 3}$ events. The $e^{-1.14}$ and $e^{-3.10}$ contours give the limits of 1 and 2 standard deviations.

which is Eq. VI-1, with $\lambda = \lambda_-$. Thus we can interpret Fig. 22 as suggesting there is no large linear q^2 dependence in the f_- form factor. If the λ parameter is due to a pole term dependence, the results in Fig. 22 are invalid for $\lambda > 0.2$. An analysis of our data for q^2 dependence of the form

$$\xi(q^2) = \xi_o \cdot \frac{m^2}{m^2 + q^2}$$

gives the result that any values of m greater than 500 MeV are equally good; the corresponding values of ξ_o are all ~ -1.0. We find the lower limit for acceptable m to be ~ 250 MeV.

Given the values of ξ listed in Table VIII we analyzed the data to determine the magnitude of μ^+ polarization, P_{TOTAL} along the direction predicted for each event. For all the data we found this component to be + 0.9 ± 0.1, in agreement with the expected value of +1.0. The results for P_{TOTAL} from data in separate bins of q^2 are listed in Table VIII; they are consistent with each other and with the predicted value. We obtain essentially the same values if, instead of assuming ξ to be real, we calculate P_{TOTAL} using the results for complex ξ given in Table VII.

The discussion of this section can be summarized as follows: with $\xi = |\xi| e^{i\varphi}$, we find $|\xi| = 1.0 \pm 0.5$, $\varphi = (200 \pm 30)^o$; for $\xi(q^2) = \xi(0)(1 + 2 q^2/m_{\pi o}^2)$, we have $\xi(0) = -1.0$, $\lambda = -0.04$, the errors given by the contours of Fig. 22; and for ξ real and constant, our result is $\xi = -0.95 \pm 0.3$.

B. Measurement of K^+ Mean Life

We determined the K^+ mean life for each of the decay modes, $K_{\mu 3}$, $K_{\mu 2}$, and $K_{\pi 2}$. For each event the observed time between the K^+ stop and the subsequent decay signal was displayed by a row of binary-coded lights and recorded on film with the spark chamber tracks. We used a delay-time to pulse-height converter with an analog-to-digital converter to digitize the observed K-decay time. The time distribution of the 3133 $K_{\mu 3}$ events is shown in Fig. 23. Zero time is at the right of the figure. Also shown are the $K_{\pi 2}$ data and half the $K_{\mu 2}$ data. During some of the $K_{\mu 2}$ runs the display control for the binary lights failed to store certain bit configurations; these data are not included in the analysis.

We calibrated the time digitizer by delaying the K-decay signal and allowing the system to be triggered by pions in the beam which scatter towards the range chamber. We found the calibration to be

$$1 \text{ channel} = (2.2 \pm 0.2) \text{ nsec.}$$

To keep our measurement of the mean life free from the resolving-time effect of the apparatus we limited the data to events from channel 20 through channel 8, as shown in Fig. 23.

We calculated the lifetimes and their uncertainties from the data in Fig. 21 using the method of Peierls.[16] In this analysis the mean life τ is the solution to the equation

$$\frac{s}{\tau} + \frac{T/\tau}{(e^{T/\tau} - 1)} - 1 = 0$$

where T is the time during which data are taken and s is the observed mean life

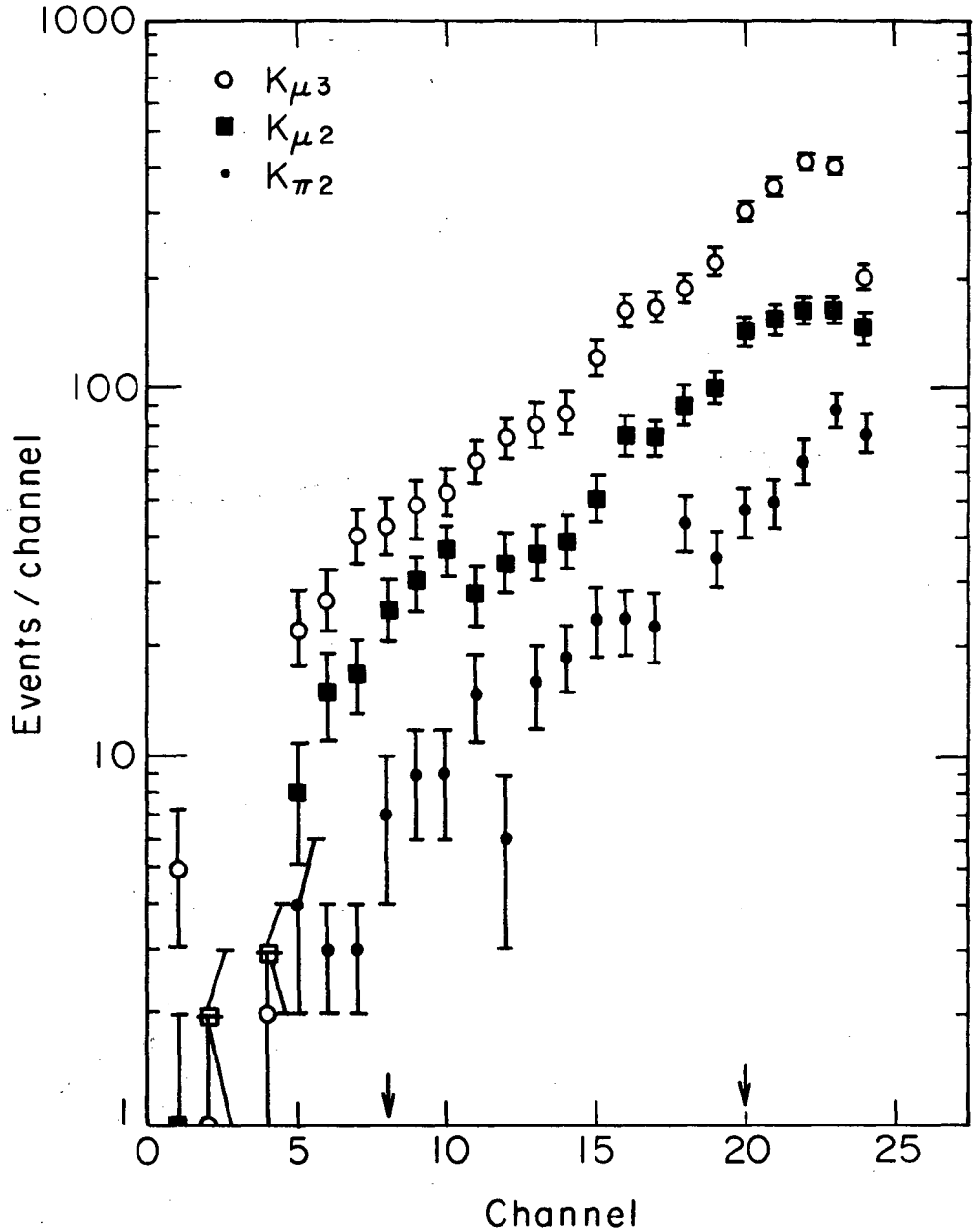

XBL685-2789

Fig. 23. Observed time distribution of K^+ decays. (1 channel = $(2.2 \pm 0.2) \times 10^{-9}$ sec)

$$s = \frac{\sum_{\text{all decays}} t_i}{\text{no. of decays}} \quad ; \qquad t_i = \text{time of } i^{th} \text{ decay.}$$

Following the procedure of Peierls[16] we have found the uncertainty in the mean life, $\Delta\tau$, to be given by

$$\Delta\tau = \frac{1}{\sqrt{N}} \left[\frac{\tau^3(1-e^{-T/\tau})^2}{a(1-e^{-T/\tau})-b[1-e^{-T/\tau}(1+\frac{T}{\tau})]} \right]^{1/2}$$

with

$$a = s(\frac{s}{\tau} - 2)+e^{-T/\tau}(2s - \frac{s^2}{\tau} + \frac{T^2}{\tau})$$

$$b = 2[s - \tau + e^{-T/\tau}(T + \tau - s)].$$

Table IX gives our results for the $K_{\mu 3}$, $K_{\mu 2}$, and $K_{\pi 2}$ lifetimes. Each

Table IX. Results of measurements of K^+ mean life.

Decay Mode	Events	Mean life (channels)	(nsec)
$K_{\mu 3}$	1635	6.0 ± 0.5	13.2 ± 1.6
$K_{\mu 2}$	773	6.6 ± 0.7	14.5 ± 2.0
$K_{\pi 2}$	278	6.3 + 1.2	13.9 ± 2.9
combined result		6.2 ± 0.4	13.5 ± 1.5

of these measurements is consistent with each other, as expected for the lifetimes of different decay modes of the same particle. If we lump together the three measurements of the K^+ mean life, we have $\tau = (13.5 \pm 1.5)$ nsec, in reasonable agreement with the accepted[10] value, $\tau = (12.34 \pm 0.05)$ nsec

We investigated the possibility of a dependence of the parameter

ξ on the proper time of the $K^+_{\mu 3}$ decay. We divided the $K_{\mu 3}$ data into two samples according to the observed decay time of each event and analyzed each sample to determine ξ, assumed real and constant. We found $\xi = -0.8 \pm 0.4$ from $K_{\mu 3}$ decays occurring promptly (in channels 25 through 20) and $\xi = -1.0 \pm 0.4$ from $K_{\mu 3}$ at longer times (channels 19 through 1). These results are consistent with the assumption that ξ is independent of the decay time.

VII. DISCUSSION

In a study of the muon polarization direction for completely reconstructed $K^+_{\mu 3}$ decays we measure the form factor $\xi(q^2)$. Assuming ξ to be real and independent of q^2, we find

$$\xi = -0.95 \pm 0.3.$$

Since the direction of the μ^+ polarization vector is predicted as a function of $\xi(q^2)$ for each event of specified kinematics, the experiment allows a determination of the q^2 dependence. Our measurement of the muon polarization is directly sensitive also to the presence of an imaginary part of ξ, corresponding to the violation of time-reversal invariance, as we determine the polarization component out of the decay plane. The results indicate that the form factor $\xi(q^2)$ is real and constant, within limits given in the previous section.

We find the magnitude of the μ^+ polarization along the direction predicted by our result for ξ to be 0.9 ± 0.1. This value confirms the prediction of the two-component neutrino theory that the muon be fully polarized along some direction, and is in good agreement with the description of $K_{\mu 3}$ decay given by Eq. I-3. Background events in the $K_{\mu 3}$ data or systematic errors in the reconstruction of events reduce the apparent magnitude of the muon polarization; our measurement suggests that these effects are small.

Previous measurements of $\xi(q^2)$ in K^+ and K^o decay are summarized in the review article of Lee and Wu.[15] We list these results for ξ in Table X, which is copied from the review article. Recently published experiments to determine ξ which are not included in this review are listed in Table XI. Two measurements of a single component

Table X. SUMMARY OF MEASUREMENTS OF ξ

Source	Experiment	ξ Values
Callahan et al. (17)	μ^+ spectrum	Re ξ = $0.0^{+1.1}_{-0.9}$
		$\lvert$Im $\xi\rvert$ = 0.0 ± 1.0
	Muon longitudinal polarization	Re ξ = $-0.7^{+0.9}_{-3.3}$
		$\lvert$Im $\xi\rvert$ = $0.5^{+1.4}_{-0.5}$
	$K_{\mu 3}^+/K_{e3}^+$ branching ratio	For Im ξ = 0 Re ξ = $+0.40 \pm 0.40$ or = -6.98 ± 0.40
	π^0 spectrum and $\pi\mu$ angular correlation	For Im ξ = 0 Re ξ = $+0.72 \pm 0.37$
	Muon total polarization $\langle s_\perp(\mu)\rangle = 0.04 \pm 0.35$	Re ξ = -1.4 ± 1.8 Im ξ = $+1.6 \pm 1.3$
	Combined results from above experiments	Re ξ = $+0.34 \pm 0.24$ Im ξ = $0.09^{+0.57}_{-0.87}$

Table X - (continued)

Source	Experiment	ξ Values
Bisi et al. (18)	μ^+ spectrum	Im ξ = 0 Re ξ > -3.3
	$K_{\mu 3}$ branching ratio	Im ξ = 0 Re ξ = 0.6 ± 0.5 or -7.3 ± 0.5
	or	Im ξ = 3.5 ± 0.50 Re ξ = -0.75 ± 0.5
Jensen et al. (19)	μ^+ and π^0 spectra and angular correlations	Re ξ = -1.2 ± 1.0 $0 \leq \lvert$Im $\xi\rvert \leq 2.4$ at 90% confidence level
Giacomelli et al. (20)	μ^+ spectrum	For Im ξ = 0 Re ξ = $+0.7 \pm 0.5$
Brown et al. (21)	μ^+ and π^0 spectra and angular correlations	For Im ξ = 0 Re ξ = $+1.8 \pm 1.6$
Cutts et al. (22)	μ^+ spectrum and $P_{\mu\parallel}$	For Re ξ = 0 $0.8 <$ Im $\xi < 2.6$ For Im ξ = 0 $0.2 <$ Re $\xi < 1.4$
Smirnitski & Weissenberg (23)	$P_{\mu\parallel}$ (longitudinal polarization)	For Im ξ = 0 Re ξ = $+2$
Groves et al. (24)	μ^- spectrum	For Im ξ = 0 Re ξ = 0
Borreani et al. (25)	$P_{\mu\parallel}$ (longitudinal polarization)	For Im ξ = 0 Re ξ = $1.2^{+2.4}_{-1.8}$
Bartlett et al. (26) For K^0 decay	$\langle s_\perp(\mu)\rangle = +0.02 \pm 0.07$	Im ξ = $+0.1 \pm 0.35$, assuming Re $\xi = 0$

Table XI. Recent measurements of ξ in K^+ and K^o decay.

Source	Decay	Experiment	Result for ξ, assumed constant
Eisler et al.[27]	$K^+_{\mu 3}$	Dalitz plot distributions	Re ξ = -0.5 ± 0.9, Imξ 2.3
Carpenter et al.[28]	$K^o_{\mu 3}$	Dalitz plot distributions	Re ξ = 1.2 ± 0.8, Imξ ≡ 0
Auerbach et al.[29]	$K^o_{\mu 3}$	μ^+ perpendicular polarization	Re ξ = -1.2 ± 0.5, Imξ ≡ 0
Young et al.[30]	$K^o_{\mu 3}$	μ^+ transverse polarization	Im ξ = -0.01 ± 0.07, Reξ ≡ 0
Bettels et al.[31]	$K^+_{\mu 3}$	μ^+ total polarization	Re ξ = -1.0 ± 0.3, Imξ ≡ 0
This experiment[32]	$K^+_{\mu 3}$	μ^+ total polarization	Re ξ = -0.95 ± 0.3, Imξ ≡ 0
			or:
			Re $\xi = -0.9 \begin{smallmatrix} +0.5 \\ -0.4 \end{smallmatrix}$
			Im ξ = -0.3 ± 0.5

of μ^+ polarization in $K^o_{\mu 3}$ decay have recently been reported.[29,30] These results for ξ from K^o experiments, as given in Table XI, are consistent with the results of this experiment, in agreement with the requirement of the $\Delta I = 1/2$ rule that ξ be the same in K^+ and K^o decay. Previous determinations of $\xi(q^2)$ in $K^+_{\mu 3}$ decay are primarily from studies of the Dalitz plot distributions or from measurements of the ratio of the rates $K^+_{\mu 3}/K^+_{e3}$:

$$R = \frac{\Gamma(K^+ \to \pi^o + \mu^+ + \nu)}{\Gamma(K^+ \to \pi^o + e^+ + \nu)} . \qquad \text{(VII-1)}$$

These experiments are insensitive to the presence of Im ξ, and their determination of the real part of ξ is strongly affected by possible q^2-dependences. In practice it is necessary in these experiments to assume ξ to be real and constant. The measurement of ξ from the ratio R, Eq. VII-1, requires the further assumption of μ-e universality, under which principle the form factors in K_{e3} and $K_{\mu 3}$ decay are identical at identical values of q^2. The determination of $\xi(q^2)$ from the measurement of the direction of the muon polarization vector for events of specified kinematics is independent of these assumptions. This experiment has the further advantage that $\xi(q^2)$ is found independently from each completely-reconstructed $K_{\mu 3}$ event. For this reason our results are not sensitive to systematic effects in selecting the event; we were able to apply strong criteria to assure a pure sample of data.

In Table X the measurement of ξ with the smallest quoted uncertainty is that reported by Callahan et al.;[17] their result of $\xi = +0.34 \pm 0.24$ is in disagreement with our measurement. The value for ξ given by

Callahan et al.[17] is a combined result for separate experiments from the same data sample. As seen in Table X, the number quoted for ξ is derived primarily from a measurement of the $K_{\mu 3}$ Dalitz plot distribution (π^0 spectrum and π-μ angular correlations) and a measurement of the parameter R (Eq. VII-1) from the observed $K_{\mu 3}$ and K_{e3} decay rates. Both these methods of determining ξ have experimental difficulties not encountered in the muon polarization method. The methods of Callahan et al.[17] require an accurate knowledge of the experimental detection efficiency as a function of the $K_{\mu 3}$ kinematics. By contrast, in the polarization experiment ξ is determined from each event rather than from the data, collectively, and so is independent of the $K_{\mu 3}$ detection efficiency. One does need to know the detection efficiency for μ-e decays -- the analyzing power of the apparatus -- but one can calibrate the apparatus directly with $K_{\mu 2}$ events.

The measurements of Callahan et al.[17] and similar experiments require far more serious corrections to the data than those needed in polarization experiments. To give an example, the $K_{\pi 2}$ decay mode ($K^+ \rightarrow \pi^+ + \pi^0$) with a π^+ decay-in-flight is a serious source of background in all $K_{\mu 3}$ experiments; with the μ^+ continuing along the π^+ direction-of-motion, the event is kinematically indistinguishable from a $K_{\mu 3}$ decay. In our analysis we simply eliminate from the $K_{\mu 3}$ data all events with kinematics resembling that of a $K_{\pi 2}$ decay. Certainly we lose some $K_{\mu 3}$ events in this way, but we do not bias our result for ξ. The $K_{\mu 3}$ branching ratio and Dalitz plot measurements require a correction for data lost in such a manner as well as an accurate

calculation of the remaining background contamination. To calculate background contributions accurately one again needs to know detection efficiencies with precision.

In Table XI we give the result of a recent experiment by Bettels et al.,[31] in which the polarization method is used to determine ξ. This result, $\xi = -1.0 \pm 0.3$, is in good agreement with our measurement. The apparatus used by Bettels et.al.[31] was completely different from our spark chamber apparatus. In their experiment $K^+_{\mu 3}$ decays were observed in a heavy liquid bubble chamber. Due to the presence of a strong magnetic field in the chamber, only that component of polarization parallel to the field could be measured. For each $K_{\mu 3}$ event with subsequent μ-e decay they observed the direction of the decay electron momentum with respect to the magnetic field direction. The data sample of Bettels et al.[31] consists of 6000 $K_{\mu 3}$ events, compared to the 3133 events in our experiment. With a magnetic field they lose polarization information; consequently the uncertainty quoted in the result for ξ is the same in both experiments.

Stiening[33] has suggested an explanation of the discrepancy between the values of ξ determined from muon polarization experiments and from the $K_{\mu 3}/K_{e3}$ branching ratio measurements. We have remarked that the determination of ξ from Eq. VII-1 requires the assumption of μ-e universality -- the assumption that the form factors in $K_{\mu 3}$ and K_{e3} decay are identical. Stiening[33] notes that if one allows universality to be violated, the measurement of ξ from the two methods can be made compatible. The amount of violation of universality required is not ruled out by present tests of universality in strange-

particle decays. Even with universality violation, however, there remains the disagreement between the polarization experiments and the experiments measuring the $K_{\mu 3}$ Dalitz plot distributions.

ACKNOWLEDGMENTS

I acknowledge with pleasure my indebtedness to Professor Emilio Segre for his counsel and warm support throughout my graduate career. I am grateful also to Professor William Chinowsky who introduced me to high-energy physics and who has followed my progress with interest and encouragement. I am deeply indebted to Dr. Rae Stiening for his close supervision and participation in this research project. My thanks go also to Dr. Clyde Wiegand and Professor Martin Deutsch for their central roles in the design, execution, and analysis of this experiment.

I wish to express my gratitude to Peter Kijewski and Min Chen for many hours of hard work during the experiment as well as for valuable advice and assistance in the analysis of the data. I owe much to Elaine McLeisch for her conscientious efforts at the scanning table and to Charlotte Dehay for her aid in processing the data. I am grateful to Mrs. Rosemary Fowell for her assistance with this manuscript. To Gordon and Christina Cutts go especial thanks for their hospitality during the completion of this work.

APPENDICES

A. Solution of $K_{\mu 3}$ Kinematics

We calculate the possible solutions of the kinematics to the decay $K^+ \rightarrow \pi^o + \mu^+ + \nu$ with the subsequent decay-in-flight $\pi^o \rightarrow \gamma + \gamma$. We observe the K decay at rest at a known position and measure the direction and range of the charged decay particle, as well as the positions of the gamma ray conversion points. As shown in Fig. 24, we define the quantities:

$\hat{p}_\mu$ = unit vector in the direction of the charged particle,

$\hat{k}_1, \hat{k}_2$ = unit vector in the directions of the gamma rays,

$\psi = \cos^{-1}(\hat{k}_1 \cdot \hat{k}_2)$ = opening angle of the gamma rays (defined $< 180^o$),

$\theta_1 = \cos^{-1}(\hat{k}_1 \cdot \hat{p}_\mu)$,

$\theta_2 = \cos^{-1}(\hat{k}_2 \cdot \hat{p}_\mu)$,

$E_\mu, \vec{p}_\mu$ = total energy and momentum of the charged decay particle.

All these quantities are experimentally determined.

Applying conservation of momentum to $K_{\mu 3}$ decay gives the following equations

$$p_K = p_\pi + p_\mu + p_\nu \tag{A-1}$$

and

$$p_\pi = k_1 + k_2 \ . \tag{A-2}$$

Here p_K, p_π, p_μ, p_ν are the four-momenta of the K^+, π^o, μ^+ and ν; and k_1, k_2 are the four-momenta of the gamma rays. From Eq. (A-2) we obtain

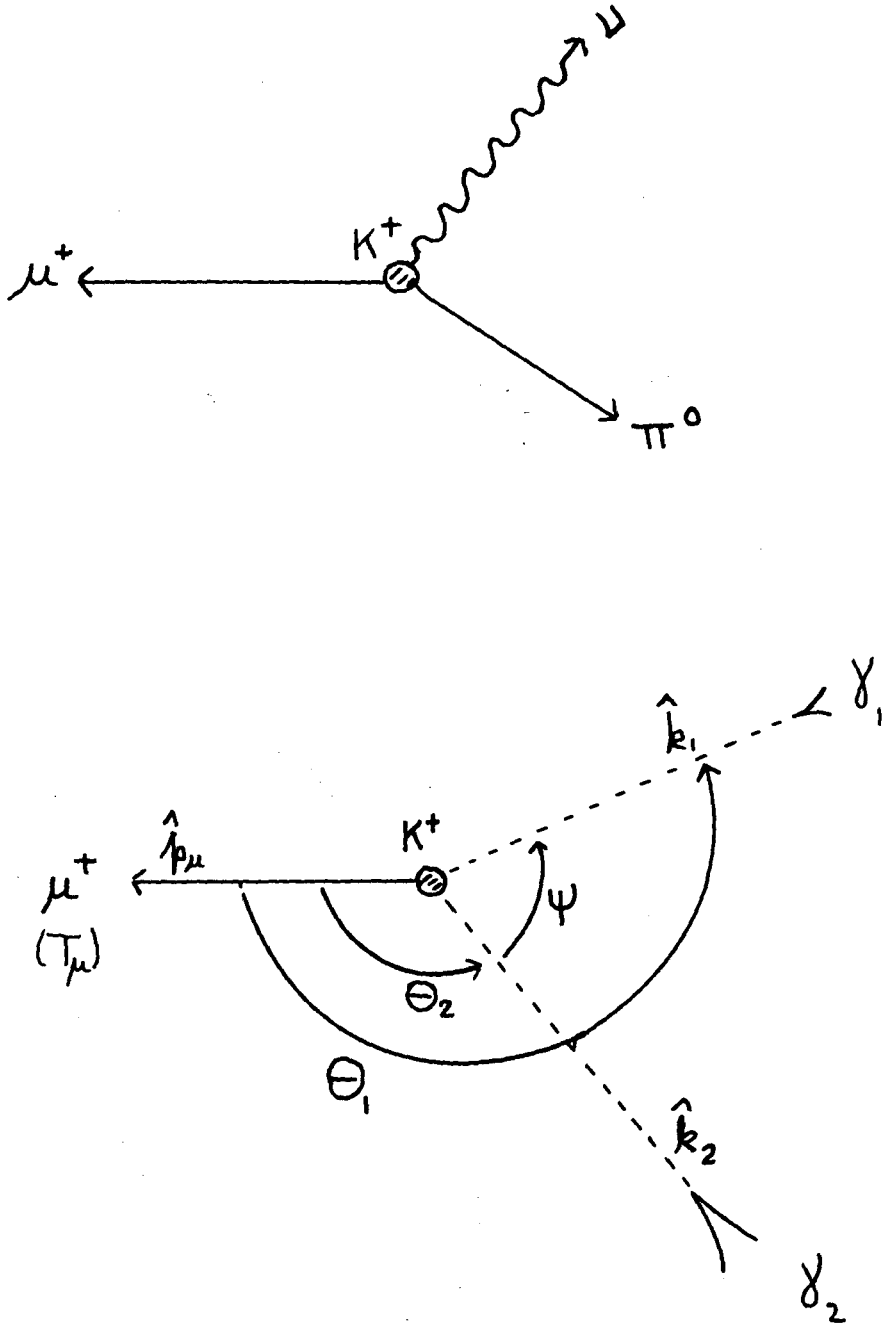

XBL 686-1050

Fig. 24. a) Diagram of a $K_{\mu 3}^{+}$ decay; b) the decay with measured parameters indicated.

$$E_1 E_2 = \frac{m_\pi^2}{2(1-\cos\psi)} \tag{A-3}$$

where $E_{1,2} = |\vec{k}_{1,2}|$, while from Eq. (A-1), evaluating p_K in the K^+ rest frame,

$$m_k(E_\mu + E_1 + E_2) = W + E_\mu(E_1 + E_2) - |\vec{p}_\mu|(E_1 \cos\Theta_1 + E_2 \cos\Theta_2) \ , \tag{A-4}$$

$$W = \frac{1}{2}(m_k^2 + m_\pi^2 + m_\mu^2) \ .$$

Combining equations (A-3) and (A-4), we find:

$$E_1 = \frac{(W - m_k E_\mu) \pm \left[(W - m_k E_\mu)^2 - 2m_\pi^2 \dfrac{(m_k - E_\mu + |\vec{p}_\mu|\cos\Theta_1)(m_k - E_\mu + |\vec{p}_\mu|\cos\Theta_2)}{(1-\cos\psi)}\right]^{\frac{1}{2}}}{2(m_k - E_\mu + |\vec{p}_\mu|\cos\Theta_1)} \tag{A-5}$$

$$E_2 = \frac{m_\pi^2}{2E_1(1-\cos\psi)}$$

Equation (A-5) gives the two possible pairs of gamma-ray energies consistent with $K_{\mu 3}$ kinematics, corresponding to the two possible signs in the numerator of the expression for E_1. All the variables are defined in Eq. (A-5) and are experimentally measured. For each pair of gamma energies the corresponding complete solution to the $K_{\mu 3}$ kinematics follows directly as, $E_\pi = E_1 + E_2$ and $\vec{p}_\pi = \vec{k}_1 + \vec{k}_2$.

B. Calculation of Likelihood Normalizations

The likelihood function used in determining the parameter ξ has the form:

$$L(\xi) = \prod_{i=1}^{N} f(\xi, x_i)$$

where the product is taken over N events of the normalized μ-e decay distribution function

$$f(\xi, x_i) = \frac{1}{c_i}\left(1 + \frac{P}{3} x_i\right) .$$

Here $x_i = [\hat{p}_e \cdot \hat{\sigma}_\mu(\xi)]_i$, and P is the magnitude of the muon polarization along its predicted direction $\hat{\sigma}_\mu$. The normalization constant c_i is obtained from the condition

$$\int_{-1}^{+1} f(\xi, x) E(x) dx = 1$$

The function $E(x)$ represents the experimental efficiency of the apparatus in detecting μ-e decays. We had difficulty in observing the decay if the electron direction $\hat{p}_e$ continued along the direction of the incident muon, $\hat{p}_\mu$. Because of this inefficiency we imposed a cut in the data, eliminating all events with the electron decay within a forward cone about $\hat{p}_\mu$. Outside this cone we took the efficiency $E(x)$ to be unity. The normalization integral then becomes

$$\int_{\substack{\text{all } x \text{ outside} \\ \text{cone about } \hat{p}_\mu}} f(\xi,x)dx = \frac{1}{2\pi} \cdot \int_{\substack{\text{all } \Theta,\varphi \text{ outside} \\ \text{cone about } \hat{p}_\mu}} f(\xi,\cos\Theta)\sin\Theta d\Theta d\varphi = 1$$

Figure 25 shows the space over which the normalization integral is to be made. The $\hat{z}$ axis is the polarization direction, $\hat{\sigma}_\mu$, and the $\hat{x}$ and $\hat{y}$ axes are chosen such that the muon direction $\hat{p}_\mu$ lies in the yz plane. We define

$$\Theta_2 = \cos^{-1}(\hat{p}_\mu \cdot \hat{z})$$

$$\Theta_o = \text{half angle of cone about } \hat{p}_\mu$$

Events with $\hat{p}_e \cdot \hat{p}_\mu > \cos\Theta_o$ were excluded from the data. We integrate the probability distribution over all decay distributions outside this cone. This distribution function is:

$$f(\xi, \cos\Theta) = \frac{1}{c}(1 + \frac{P}{3}\cos\Theta)$$

which, in a coordinate system about $\hat{p}_\mu$:

$$\hat{z}' = \hat{p}_\mu$$

$$x' = \hat{x}$$

becomes

$$f = \frac{1}{c}[1 + \frac{P}{3}(\cos\Theta_2 \cos\Theta' - \sin\Theta_2 \sin\Theta' \sin\varphi')],$$

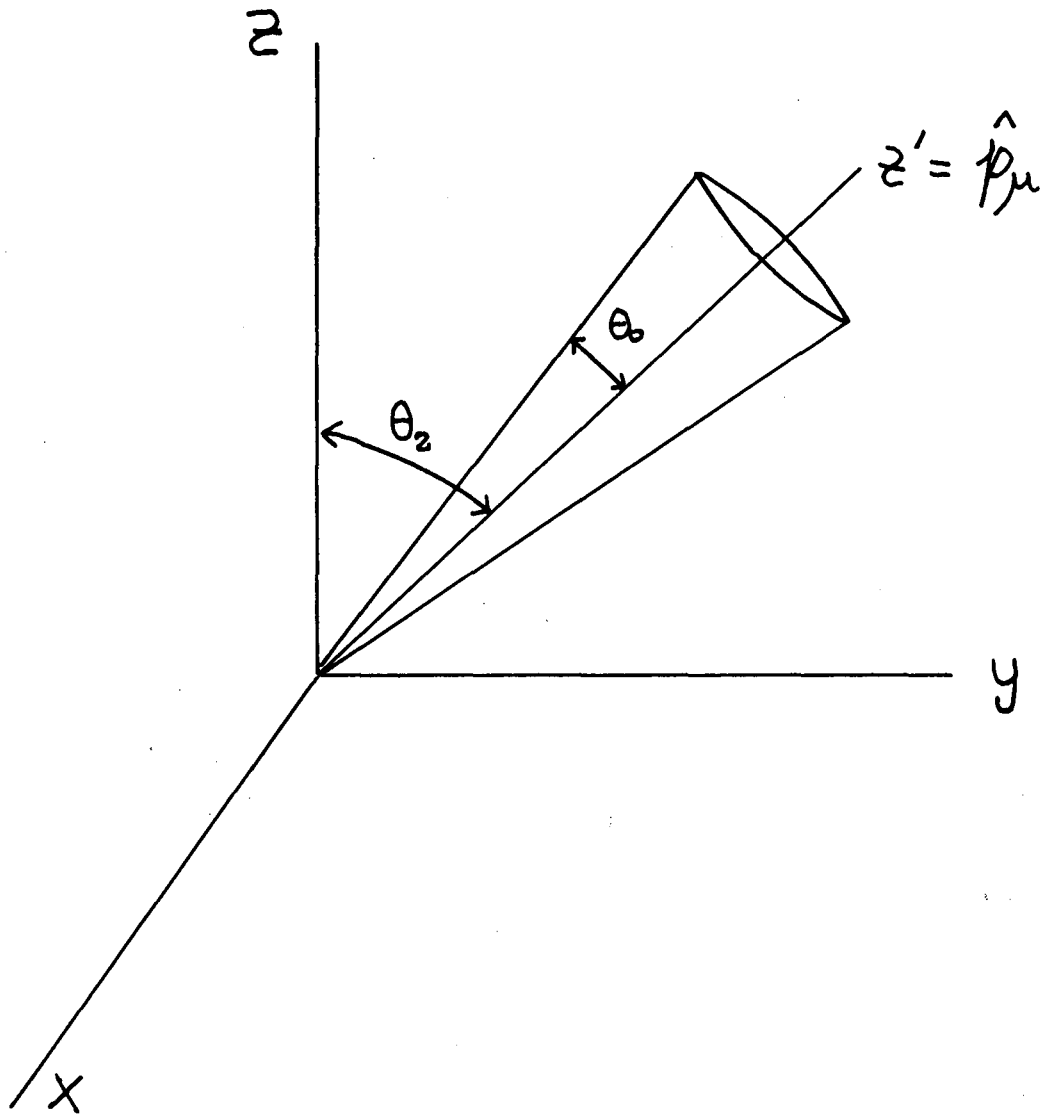

XBL 686-1049

Fig. 25. Calculation of likelihood normalizations.

so that the normalization condition is

$$\frac{1}{2\pi}\int_0^{2\pi}\int_\theta^{\pi}\frac{1}{c}[1+\frac{P}{3}(\cos\theta_2\cos\theta' - \sin\theta_2\sin\theta'\sin\varphi')]$$

$$\cdot\ \sin\theta' d\theta' d\varphi' = 1 \qquad \text{(B-1)}$$

Solving Eq. (B-1) for the normalization factor c, we find

$$c = (1+\cos\theta_o)[1 - \frac{P\cos\theta_2}{6}(1-\cos\theta_o)]. \qquad \text{(B-2)}$$

In the analysis for the parameter ξ we assume the muon to be fully polarized $(P = 1)$, and observe the distribution of the electron decay direction with respect to the predicted polarization directions, $\hat{\sigma}_\mu(\xi)$. In this case we have

$$c_i(\xi) = (1+\cos\theta_o)[1 - \frac{1}{6}(1-\cos\theta_o)(\hat{p}_e\cdot\hat{\sigma}_\mu(\xi))_i].$$

Having found ξ we use the likelihood to measure the magnitude P of polarization along the predicted direction. From Eq. (B-2) we then have

$$c_i(P) = (1+\cos\theta_o)[1 - \frac{P}{6}(1-\cos\theta_o)(\hat{p}_e\cdot\hat{\sigma}_\mu(\xi))_i]$$

In determining the average muon polarization components in the K-decay rest frame we define for each event orthogonal axes $\hat{\epsilon}_L$, $\hat{\epsilon}_T$, $\hat{\epsilon}_\perp$. For the longitudinal component,

$$\cos\theta_2 = \hat{p}_\mu\cdot\hat{\epsilon}_L = 1,$$

so that

$$c_i(P_L) = (1 + \cos\Theta_o)[1 - \frac{P_L}{6}(1 - \cos\Theta_o)].$$

The transverse and perpendicular axes are orthogonal to the muon direction,

$$\cos\Theta_2 = \hat{p}_\mu \cdot \hat{\epsilon}_T = \hat{p}_\mu \cdot \hat{\epsilon}_\perp = 0$$

and we have

$$c_i(P_T) = c_i(p_\perp) = (1 + \cos\Theta_o) \ .$$

C. Comparison of Prompt/Delayed $K_{\mu 3}$ Data

We studied $K_{\mu 3}$ events, observing the μ^+ and its subsequent decay, provided the μ-e decay came within a given time from the initial K^+ decay. We obtained data from two different values of this waiting period: the $K_{\mu 3}$ data subjected to the polarization analysis, for which we observed μ-e decays up to a time t_d, and a smaller amount of "prompt" data, with decays observed to time t_p. The fraction of muons which decay within a time t is given by

$$f = 1-e^{-t/\tau}$$

where τ is the muon lifetime. Defining R as the ratio of the fraction of decays in the prompt data to the fraction of decays in the delayed data, we have

$$R = \frac{f_p}{f_d}$$

so the predicted value of R is

$$R_T = \frac{1-e^{-t_p/\tau}}{1-e^{-t_d/\tau}} \qquad \text{(C-1)}$$

The data consists of events with μ-e decays and events without decays, "stops" as called by the scanner. From the observed number of events, we calculate

$$R_T = \left(\frac{D_p}{D_p+S_p}\right) \Big/ \left(\frac{D_d}{D_d+S_d}\right) \qquad \text{(C-2)}$$

where D_p, S_p are the numbers of decay events and of "stops" in the prompt data; D_d, S_d are the corresponding numbers for the delayed data. In addition to these numbers of true $K_{\mu 3}$ events, there may be backgrounds which can be interpreted as $K_{\mu 3}$ events with μ-e decays. From sources such as $K_{\pi 2}$ decays with a π^+ interaction in the range chamber, the frequency of these background events will be independent of the time allowed for the μ-e decay, but proportional to the number of actual $K_{\mu 3}$ events. If we define B as the number of events in the delayed data due to such backgrounds, then the experimental value of R is

$$R_E = \frac{D_p + B\left(\frac{D_p + S_p}{D_d + S_d}\right)}{D_p + S_p + B\left(\frac{D_p + S_p}{D_d + S_d}\right)} \Bigg/ \left(\frac{D_d + B}{D_d + S_d + B}\right)$$

which reduces with Eq. (C-2) to:

$$f_B = \frac{B}{D_d} = \frac{(R_E - R_T)}{(1 - R_E)} \quad .$$

From the observed value R_E and the theoretical value R_T calculated with Eq. (C-1), we can calculate f_B, the fraction of background "decays" in the delayed $K_{\mu 3}$ data.

D. Depolarization by a Magnetic Field

Our method of measuring muon polarization required that the magnetic field be small in the region of the μ-e decays. We delayed firing the range chamber for 3.5 μsec, about 1-1/2 muon lifetimes, so that the decay electron track would be frequently observed. For each event we did not know the time after the muon came to rest that the decay took place. Significant procession of the muon spin during the time the apparatus was sensitive to a decay would have affected the polarization measurement. We enclosed the range chamber in a double walled iron box to reduce the magnetic field in the decay region. The residual field was less than 200 milligauss.

To estimate the actual depolarization in our data due to the magnetic field, consider a muon at time $t=0$ with polarization of magnitude P_o along some axis. The spin is processed with frequency Ω so that at time t the observed polarization P will be

$$P = P_o \cos \Omega t \quad ,$$

where $\Omega = \omega_o |\hat{\sigma} \times \vec{B}| ; \omega_o = 8.51 \times 10^4$ radians/gauss-sec.

If we measure the muon polarization by observing all decays from time $t=0$ to $t=t_1$ then

$$P = P_o \frac{\int_o^{t_1} \cos \Omega t \; e^{-t/\tau} \frac{dt}{\tau}}{\int_o^{t_1} e^{-t/\tau} \frac{dt}{\tau}}$$

which becomes

$$\frac{P}{P_o} = \frac{1-e^{-t1/\tau}(\cos \Omega\tau \sin \Omega t_1)}{(1-e^{-t_1/\tau})(1+\Omega^2 \tau^2)}$$

The muon lifetime, τ, is 2.2 μsec[10] and t_1 was 3.5 μsec. The fraction of remaining polarization, P/P_o, as a function of a magnetic field transverse to the polarization direction is shown in Fig. 26. We measured all components of the field throughout the decay region under magnet and accelerator conditions similar to those during the data collection. The largest component observed was less than 200 milligauss, a value indicated by the arrow in Fig. 26. From magnetic fields of this magnitude there is no significant depolarization.

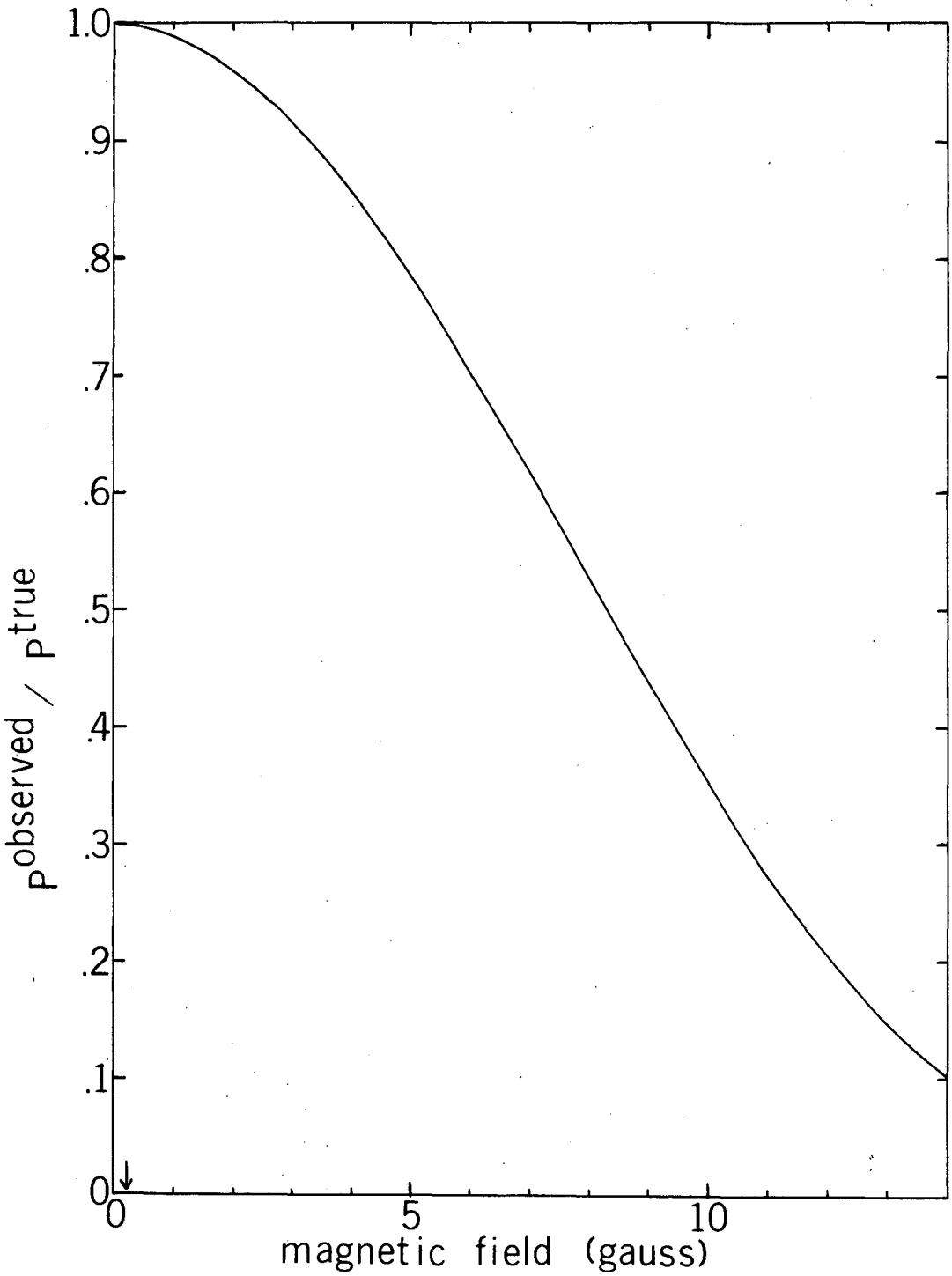

XBL 685-881

Fig. 26. Apparent muon polarization as a function of magnetic field transverse to the polarization direction.

REFERENCES

1. E. S. Ginsberg, Phys. Rev. 142, 1035 (1966).
2. S. W. McDowell, Nuovo Cimento 9, 258 (1958).
3. J. Werle, Nucl. Phys. 6, 1 (1958).
4. N. Cabibbo and A. Maksymowicz, Phys. Letters 9, (1964).
5. C. Bouchiat and L. Michel, Phys. Rev. 106, 170 (1957).
6. T. D. Lee and C. S. Wu, Ann. Rev. Nucl. Sci. 15, 381 (1965).
7. H. Rudloe, M. Deutsch, and T. Marill, Commun. Assoc. Computing Machinery 6, 332 (1963).
8. D. J. Hudson, CERN report 64-18, 1964.
   J. Orear, UCRL-8417, 1958.
9. P. Dennery and H. Primakoff, Phys. Rev. 131, 1334 (1963).
10. Data compilation of A. H. Rosenfeld et al., Rev. Mod. Phys. 40, 77 (1968).
11. M. P. Baladin et al., DUBNA report JINR-P-1286, 1963.
12. B. Rossi, High Energy Particles, p. 35, Prentice-Hall, 1952.
13. See summary of G. H. Trilling in Proceedings of the International Conference on Weak Interactions, report NAL-7130, 1965.
14. J. D. Good, Phys. Rev. 113, 352 (1959).
15. T. D. Lee and C. S. Wu, Ann. Rev. Nucl. Sci., 16, 471 (1966).
16. R. Peierls, Proc. Roy. Soc. A149, 467 (1935).
17. A. C. Callahan et al., Phys. Rev. 150, 1153 (1966).
18. V. Bisi et al., Phys. Rev. 139, B1068 (1965).
19. G. L. Jensen et al., Phys. Rev. 138, B1507 (1965).
20. G. Giacomelli et al., Nuovo Cimento 34, 1134 (1964).

21. J. L. Brown et al., Phys. Rev. Letters 8, 450 (1962).

22. D. Cutts et al., Phys. Rev. 138, B969 (1965).

23. V. A. Smirnitski, Phys. Rev. Letters 12, 233 (1964).

24. T. H. Groves et al., Phys. Rev. 135, B1269 (1964).

25. G. Borreanni, Phys. Rev. 140, B1686 (1965).

26. D. Bartlett et al., Phys. Rev. Letters 16, 282 (1966).

27. F. R. Eisler et al., Phys. Rev. 169, 1090 (1968).

28. D. W. Carpenter et al., Phys. Rev. 142, 871 (1966).

29. L. B. Auerbach et al., Phys. Rev. Letters 17, 980 (1966).

30. K. K. Young et al., Phys. Rev. Letters 18, 806 (1967).

31. J. Bettels et al., private communication. We thank these authors for sending us their results prior to publication.

32. A Brief account of this experiment is given in D. Cutts et al., Phys. Rev. Letters 20, 955 (1968).

33. R. F. Stiening, UCRL-18231 (1968).

LEGAL NOTICE

This report was prepared as an account of Government sponsored work. Neither the United States, nor the Commission, nor any person acting on behalf of the Commission:

A. Makes any warranty or representation, expressed or implied, with respect to the accuracy, completeness, or usefulness of the information contained in this report, or that the use of any information, apparatus, method, or process disclosed in this report may not infringe privately owned rights; or

B. Assumes any liabilities with respect to the use of, or for damages resulting from the use of any information, apparatus, method, or process disclosed in this report.

As used in the above, "person acting on behalf of the Commission" includes any employee or contractor of the Commission, or employee of such contractor, to the extent that such employee or contractor of the Commission, or employee of such contractor prepares, disseminates, or provides access to, any information pursuant to his employment or contract with the Commission, or his employment with such contractor.

TECHNICAL INFORMATION DIVISION
LAWRENCE RADIATION LABORATORY
UNIVERSITY OF CALIFORNIA
BERKELEY, CALIFORNIA 94720